School of Science
Department of Imaging & Applied Physics

Detection of Trojan Asteroids in the Orbits of Earth and Mars

Michael Anthony Todd

This thesis is presented for the Degree of
Doctor of Philosophy
of
Curtin University

January 2014

To the best of my knowledge and belief this thesis contains no material previously published by any other person except where due acknowledgement has been made. This thesis contains no material which has been accepted for the award of any other degree or diploma in any university.

Michael A. Todd

15 January 2014

Astronomy compels the soul to look upwards
and leads us from this world to another.

– Plato, The Republic, 360 BCE

Acknowledgements

While there is always just one name on the cover of a work such as this, there are so many people who contribute in so many ways in taking an idea and developing it into something that fills a hundred-and-something pages.

Life is more than just eating, sleeping and working. It is also about having fun, learning something new, being challenged to rise above what you thought you could do and learning to fly on your own. I am thankful for everyone that I had the pleasure of meeting, who challenged me, who supported me, who dragged me onto the sports fields and who helped me moving houses.

Without the people in my life that supported me both during this project and before, I would never have reached this point. In particular I am very thankful for having in my life:

Heidi, my soulmate, who has encouraged me, helped me, worked through the nights with me, kept going and kept me going, provided a reality check when I needed it and occasionally sprayed water when I didn't although she would say that I did.

My children, Jessica and Cory, who often led me to see the world again through new eyes and to marvel at what I saw as if it was for the first time.

My parents, who have always believed in me and supported me in whatever I attempted.

My supervisors, Mario and David, for their constant encouragement, support and advice.

My fellow students, colleagues and others who have been around during this journey to share some laughter and fun and, of course, a bit of work here and there.

Thank you all!

Abstract

The European Space Agency's *Gaia* space mission is the next-generation astrometry mission following *Hipparcos*. *Gaia* will perform a systematic survey of the whole sky down to magnitude $V = 20$, about one billion stars and 300,000 Solar System objects, with unprecedented astrometric precision. In the process it will completely survey the regions of Earth's and Mars' orbits where Trojan asteroids may be found, something that has never been able to be done with ground-based telescopes.

This work describes probability distributions and constrains the sky search areas for Trojan asteroids in the orbits of Earth and Mars. It proposes search strategies using ground-based telescopes and predicts outcomes from the *Gaia* mission for the detection of Earth and Mars Trojans. It also describes the role of the Zadko Telescope, in Western Australia, as part of the *Gaia* Follow-Up Network for Solar System Objects and the development of the High Efficiency Image Detection & Identification (HEIDI) pipeline software to rapidly analyse time series image data.

Trojan asteroids (or Trojans) share the orbit of a planet about the Sun and librate around the L4 or L5 Lagrangian points. Trojan appear to be stable on long timescales, on the order of the age of the Solar System, and are therefore important Solar System fossils as they provide insight into the evolution of the Solar System. Discovery and study of Trojans in the orbits of Earth and Mars will help constrain models for the distribution and interactions of bodies in the inner Solar System.

The Earth Trojan regions occupy sky areas on the order of 1,500 square degrees and hence are too large to be fully surveyed using ground-based telescopes in the limited time imposed by the observing geometry. The optimal strategy for a ground-based telescope is to systematically survey these regions over an extended period, observing each region for a few minutes per day, twice per week, for one year. The total time commitment of this strategy is a few tens of hours spread over the year.

The Mars Trojan regions are large and have sky areas which vary from about 2,000 square degrees at a solar elongation of 60 degrees to between 11,000 square degrees and 17,000 square degrees at opposition due to Mars' orbit eccentricity. A consequence of the size of the Trojan regions is that at solar elongations greater than 150 degrees the sky area becomes too large to be surveyed in a single night by any existing wide-field ground-based telescope. Adopting the strategy proposed

for the Earth Trojan regions reduces the time requirement to only a few minutes per night at intervals of 3 to 4 days.

Although the Earth and Mars Trojan regions occupy large sky areas, *Gaia* will survey these regions multiple times during its mission. Simulations for the detection of Earth and Mars Trojans show that *Gaia* will not detect the Earth Trojan 2010 TK_7. Although it is very close to Earth and crosses *Gaia*'s field of view in almost every scan cycle, it is too small and hence too faint to be detected by *Gaia*. The smallest Earth Trojan that *Gaia* can detect will have a diameter of about 600 m. The implication of this is that *Gaia* is unlikely to discover any additional Earth Trojans.

The simulations also show that *Gaia* will detect Mars Trojans with diameters larger than 800 m, hence *Gaia* will detect all of the known Mars Trojans. The starting conditions and orbit parameters have a significant impact on the detection of smaller bodies. *Gaia* may detect Mars Trojans as small as 400 m depending on the starting conditions and the orbit of the Trojan. The implication is that *Gaia* could discover more than 100 new Mars Trojans.

Since *Gaia*'s mission is to perform an all-sky survey, its orbit does not allow targeted follow-up studies. Consequently, it is necessary to use ground-based optical telescopes to follow up on *Gaia* detections. The *Gaia* Data Processing and Analysis Consortium (DPAC) has established a network of ground-based telescopes, the *Gaia* Follow-Up Network for Solar System Objects (*Gaia* FUN-SSO). The Zadko Telescope, in Western Australia, has been flagged as an important site because of its location, automated scheduling system and sensitivity.

As a node in the *Gaia* FUN-SSO, it has participated in campaigns to observe Solar System objects prior to the launch of *Gaia*. During the campaign to observe the Potentially Hazardous Asteroid 2005 YU_{55} the Zadko Telescope contributed one of the longest observing periods of all the participating telescopes and was the only Southern Hemisphere telescope to make a contribution. The residual astrometric errors for the Zadko Telescope observations were typically better than 0.20 arcsec in both right ascension and declination, compared to the mean residual error for this *Gaia* FUN-SSO test of 0.30 arcsec. During the *Gaia* mission the Zadko Telescope will assist in validating new Solar System objects discovered by *Gaia* and provide astrometry and photometry for these targets.

Analysing images to extract astrometric and photometric data is often largely a manual process. However, the newly developed HEIDI software provides the ability to rapidly process sets of astronomical images. This will be a useful tool for identifying Solar System objects detected by *Gaia* and providing astrometric

and photometric data to the *Gaia* FUN-SSO.

HEIDI is implemented in the programming language Python, runs on a Linux platform and has minimal hardware requirements. By automatically selecting calibration sources, applying corrections to compensate for variations between images in a time series and identifying known Solar System objects, HEIDI has many applications in producing astrometric and photometric results. These include photometric light curves for asteroid rotation measurements and shape modelling, determining the type of a supernova and measuring the decay rate of a gamma-ray burst optical afterglow. HEIDI thus fills a need in providing rapid analysis of time series image data.

Publications included as part of this thesis

(Listed in order as found in this thesis)

Todd, M., D. M. Coward, M. G. Zadnik. 2012. "Search strategies for Trojan asteroids in the inner Solar System." *Planetary and Space Science* 73 (1): 39-43. doi:10.1016/j.pss.2011.11.002.

Todd, M., P. Tanga, D. M. Coward, M. G. Zadnik. 2012. "An optimal Earth Trojan asteroid search strategy." *Monthly Notices of the Royal Astronomical Society Letters* 420 (1): L28-L32. doi:10.1111/j.1745-3933.2011.01186.x.

Todd, M., P. Tanga, D. M. Coward, M. G. Zadnik. 2012. "An optimal Mars Trojan asteroid search strategy." *Monthly Notices of the Royal Astronomical Society* 424 (1): 372-376. doi:10.1111/j.1365-2966.2012.21204.x.

Todd, M., P. Tanga, D. M. Coward, M. G. Zadnik. 2012. "Detection of inner Solar System Trojan Asteroids by Gaia." *Proceedings of Gaia-FUN-SSO-2 International Workshop, Institut de Mécanique Céleste et de Calcul des Éphémérides, Paris Observatory, France, 19-21 September 2012.*

Todd, M., P. Tanga, D. M. Coward, M. G. Zadnik. 2014. "Predictions for the detection of Earth and Mars Trojan asteroids by the Gaia satellite." *Monthly Notices of the Royal Astronomical Society* 437 (4): 4019-4026. doi:10.1093/mnras/stt2223.

Todd, M., D. M. Coward, P. Tanga, W. Thuillot. 2013. "Australian participation in the Gaia Follow-Up Network for Solar System Objects." *Publications of the Astronomical Society of Australia* 30: 14-18. doi:10.1017/pasa.2012.014.

Todd, M., H. U. Wallon Pizarro, P. Tanga, D. M. Coward, and M. G. Zadnik. 2014. HEIDI: An Automated Process for the Identification and Extraction of Photometric Light Curves from Astronomical Images. *Monthly Notices of the Royal Astronomical Society* (submitted). arXiv:1401.2593 [astro-ph.IM]

Statement of contribution of others

Michael A. Todd's input into this project and the associated papers included the execution of all the experimental work and a dominant contribution to the intellectual input involved in the project. As is almost always the case in the physical sciences, other scientists made contributions to the work that were significant enough to warrant co-authorship on the resulting journal articles. These are specified below.

D. M. Coward and M. G. Zadnik provided manuscript editing and project supervision.

P. Tanga provided technical knowledge on the operation of the telescopes and focal plane array of the European Space Agency's *Gaia* spacecraft as well as operating the *Gaia* simulator.

W. Thuillot provided technical knowledge on the operation of the Gaia Follow-Up Network for Solar System Objects.

H. U. Wallon Pizarro provided advice on transcribing software algorithms into mathematical notation.

Michael A. Todd

Assoc. Prof. Marjan G. Zadnik (Supervisor)

Copyright declaration

I warrant that I have obtained, where necessary, permission from the copyright owners to use any third-party copyright material reproduced in the thesis, or to use any of my own work in which copyright is held by another party.

Michael A. Todd

15 January 2014

Additional publications by Michael A. Todd relevant to this thesis but not forming part of it

Todd, M. 2013. "Trojan Asteroids in the Inner Solar System." In *Asteroids. Prospective Energy and Material Resources*, edited by Viorel Badescu, 35-44. Berlin: Springer-Verlag.

Mignard, F., P. Tanga, M. Todd. 2011. "Observing Earth Trojans with Gaia?" *Gaia DPAC Technical Note GAIA-C4-TN-FM-051-1.*

Coward, D., M. Laas-Bourez, M. Todd. 2011. "The Zadko Telescope: the Australian Node of a Global Network of Fully Robotic Follow-up Telescopes." *Proceedings of Gaia FUN-SSO International workshop, Institut de Mécanique Céleste et de Calcul des Éphémérides, Paris Observatory, France, 29 November - 1 December 2010.*

Coward, D. M., A. Heary, G. Venville, M. Todd, M. Laas-Bourez, M. Zadnik, A. Klotz, M. Boer, N. Longnecker. 2011. "The Zadko Telescope: A resource for science education enrichment." *Advances in Space Research* 47 (11): 1922-30. doi:10.1016/j.asr.2011.01.005

Coward, D. M., M. Todd, T.P. Vaalsta, J. Zadko, P. Luckas, A. Imerito, D. Blair, R. Burman, S. Gordon, A. Fletcher, A. Ahmet, J. Moore, M. Zadnik, M. Boer, A. Klotz, L. Yan, S. Kumar, and J. Patel. 2010. "The Zadko Telescope: A Southern Hemisphere Telescope for Optical Transient Searches, Multi-Messenger Astronomy and Education." *Publications of the Astronomical Society of Australia* 27 (3): 331-339. doi:10.1071/AS09078

Contents

Acknowledgements **iv**

Abstract **v**

Publications included as part of this thesis **viii**

Statement of contribution of others **ix**

Copyright declaration **x**

Additional publications relevant to this thesis but not forming part of it **xi**

List of figures **xv**

List of tables **xvi**

1 Introduction **1**

1.1 Overview 1

1.2 Trojan asteroids 1

1.3 Earth Trojans 4

1.4 Mars Trojans 8

1.5 Asteroid brightness measurements 12

1.6 This research 21

2 Search strategies for Trojan asteroids in the inner Solar System **25**

3 An optimal Earth Trojan asteroid search strategy **31**

4 An optimal Mars Trojan asteroid search strategy 37

5 Detection of inner Solar System Trojan Asteroids by Gaia 43

6 Predictions for the detection of Earth and Mars Trojan asteroids by the Gaia satellite 48

7 Australian participation in the Gaia Follow-Up Network for Solar System Objects 57

8 HEIDI: An Automated Process for the Identification and Extraction of Photometric Light Curves from Astronomical Images 63

9 Conclusions and further work 71

9.1 Conclusions 71

9.1.1 Introduction 71

9.1.2 Search strategies for Trojan asteroids in the inner Solar System 73

9.1.3 An optimal Earth Trojan asteroid search strategy 74

9.1.4 An optimal Mars Trojan asteroid search strategy 75

9.1.5 Detection of inner Solar System Trojan Asteroids by Gaia 77

9.1.6 Predictions for the detection of Earth and Mars Trojan asteroids by the Gaia satellite 78

9.1.7 Australian participation in the Gaia Follow-Up Network for Solar System Objects 79

9.1.8 HEIDI: An Automated Process for the Identification and Extraction of Photometric Light Curves from Astronomical Images 81

9.1.9 Summary 82

9.2 Further Work 83

9.2.1 Earth coorbital asteroids 83

9.2.2 Inner Earth Objects 83

9.2.3 HEIDI pipeline software 84

A Statements of contributions of others **86**

A.1 Statements of contributions of others for "Search strategies for Trojan asteroids in the inner Solar System" 87

A.2 Statements of contributions of others for "An optimal Earth Trojan asteroid search strategy" 90

A.3 Statements of contributions of others for "An optimal Mars Trojan asteroid search strategy" 94

A.4 Statements of contributions of others for "Detection of inner Solar System Trojan Asteroids by Gaia" 98

A.5 Statements of contributions of others for "Predictions for the detection of Earth and Mars Trojan asteroids by the Gaia satellite" 102

A.6 Statements of contributions of others for "Australian participation in the Gaia Fol-low-Up Network for Solar System Objects" 106

A.7 Statements of contributions of others for "HEIDI: An Automated Process for the Identification and Extraction of Photometric Light Curves from Astronomical Images" 110

B Copyright forms **115**

B.1 Elsevier journal articles 116

B.2 Oxford University Press journal articles 118

B.3 Cambridge University Press journal articles 120

B.4 Institut de Mécanique Céleste et de Calcul des Éphémérides Press articles 122

List of figures

1.1 The gravitational field of the Sun–Earth system with the five Lagrangian points. 2
1.2 Inclinations of known asteroids with semimajor axes of $a \approx 1$ au. . 7
1.3 Inclinations of known asteroids with semimajor axes of $a \approx 1.52$ au. 11
1.4 The Kirkwood gaps in the main asteroid belt. 13
1.5 An Earth Trojan asteroid at one of the equilateral L4 or L5 Lagrangian points. 14
1.6 Light curves for asteroid 939 Isberga. 15
1.7 Light curves of the main supernova types. 16
1.8 Aladin field showing the position of asteroid 939 Isberga on 22 November 2011. 17
1.9 Aladin field showing the position of asteroid 939 Isberga on 25 November 2011. 18

List of tables

1.1 Calculated temperatures for the selected Sun-like stars in Figures 1.8 and 1.9. 19

Chapter 1

Introduction

1.1 Overview

Asteroids are abundant in the inner Solar System, i.e. the region of space that is smaller than the radius of Jupiter's orbit around the Sun. More than 600,000 asteroids are currently known to exist (Minor Planet Center 2013a). The vast majority of these asteroids reside in the main asteroid belt between the orbits of Mars and Jupiter. A small fraction of the known asteroids (about 10,000) have orbits that take them close to Earth's orbit, i.e. within 0.3 au. These number represents about half of the predicted population of near-Earth asteroids (about 20,000) Mainzer et al. (2012). These asteroids are of interest for the dynamical evolution of their orbits and the gravitational interactions that may have precipitated them to migrate from the main belt into near-Earth orbits.

1.2 Trojan asteroids

Trojan asteroids (or Trojans) are another category of great interest for both the evolution of their orbits and their gravitational interactions. In the restricted three-body problem there are five points where an object can exist in a stable 1:1 mean motion resonance (i.e. coorbital) with the other two bodies (Murray and Dermott 1999). These points are known as the Lagrangian points (Figure 1.1).

An object can only be in 1:1 mean motion resonance with a given planet if the semimajor axis of the object is very similar to that of the planet. How similar the object's semimajor axis needs to be to the semimajor axis of the planet depends on the relative masses of the two major bodies, i.e. the planet and the Sun. If μ is the planet–Sun mass ratio, then the semimajor axis of the object (a) and

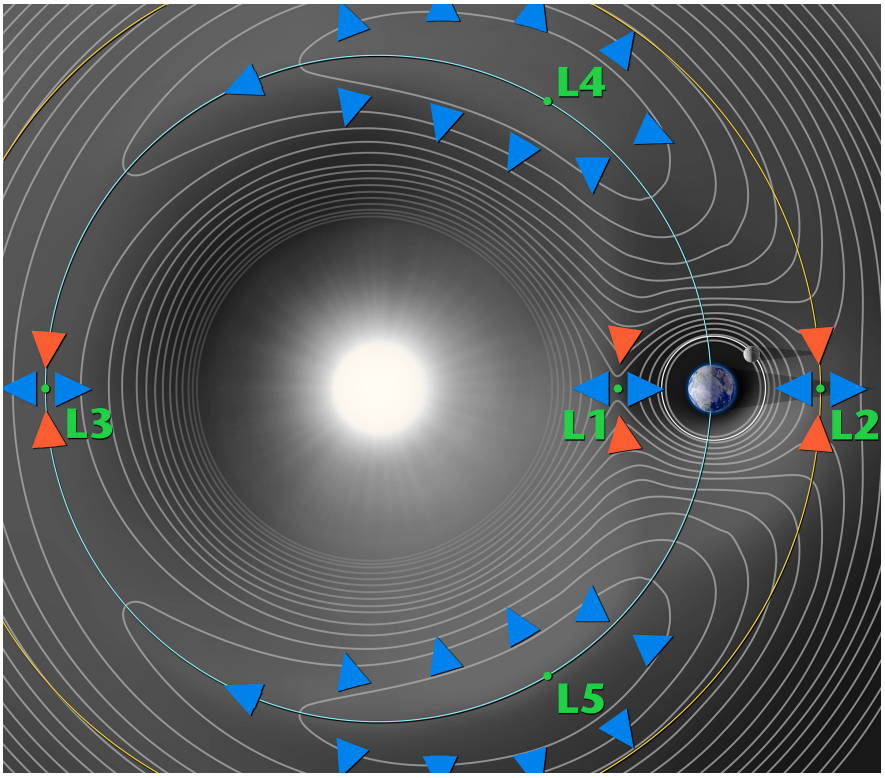

Figure 1.1: The gravitational field of the Sun–Earth system with the five Lagrangian points where an object of negligible mass can exist in a stable 1:1 mean motion resonance (NASA/WMAP Science Team 2012).

the semimajor axis of the planet (a_1) need to fulfil the following relation for the object to be coorbital (Morais and Morbidelli 2002):

$$|a - a_1| < \left(\frac{\mu}{3}\right)^{\frac{1}{3}} a_1. \tag{1.1}$$

For the Earth–Sun system the ratio is $\mu = 3.0044 \cdot 10^{-6}$ and thus:

$$|a - a_1| < 0.00694 \cdot a_1.$$

Given that Earth's semimajor axis is 1.0000 au, for a body to be in 1:1 mean motion resonance the semimajor axis of that body must be within the range $0.9931 < a < 1.0069$ au.

Performing the same calculation for the Mars–Sun system, the ratio is $\mu = 3.2276 \cdot 10^{-7}$ and thus:

$$|a - a_1| < 0.00476 \cdot a_1.$$

With Mars' semimajor axis being 1.5237 au, a body in 1:1 mean motion resonance has a semimajor axis in the range $1.5165 < a < 1.5309$ au.

Various artificial satellites have been positioned in the stable zones near the L1 and L2 Lagrangian points. These include the *Solar and Heliospheric Observatory (SOHO)* near L1 and *Gaia* near the L2 point. In the N-body case of the Solar System the L1, L2 and L3 Lagrangian points are typically subject to perturbation by other bodies. Thus although the L1 and L2 Lagrangian points are used to position spacecraft in stable orbits about the Sun, the mechanics are usually more complex. The spacecraft, as is the case with *Gaia*, may be in a Lissajous orbit around the Lagrangian point. It may also employ some form of propulsion to maintain the stability of its orbit.

Only the L4 and L5 Lagrangian points have been found to be stable with respect to external perturbations. Objects in the stable zones near the L4 and L5 Lagrangian points are referred to as "Trojan asteroids" or "Trojans". Trojan asteroids represent the solution to Lagrange's famous triangular problem and appear to be stable on long timescales (100 Ma to 4.5 Ga) (Pilat-Lohinger, Dvorak, and Burger 1999; Scholl, Marzari, and Tricarico 2005) in the N-body case of the Solar System. This raises the question whether they formed with the planets from the Solar nebula or were captured in the Lagrangian regions by gravitational effects. Study of Trojan asteroids therefore provides insight into the early evolution of the Solar System.

While about 6,000 Trojan asteroids have been discovered in the orbit of Jupiter as a result of both systematic searches and accidental discoveries, only a few systematic searches have been conducted for Trojan asteroids in the orbits of Earth and Mars. The limitation in both cases is that of available observing time although the specific restrictions are quite different.

A systematic search for Earth Trojans suffers from having only a small amount of viewing time available. This is a result of the geometry of the Earth–Sun–asteroid relative positions. Searching for Earth Trojans necessitates observing low to the horizon just after sunset or just before sunrise at an angle less than about 60 degrees from the Sun.

In contrast, a systematic search for Mars Trojans has most of the night available for observing, depending on the relative positions of Earth and Mars. Mars' orbital period is 1.88 years and so the intervals between search programmes can be about 2 years, if searches are only conducted near opposition. However, the spatial separation between the regions can allow the L5 (trailing) region to be surveyed as Mars approaches opposition and the L4 (leading) region to be surveyed after Mars has passed opposition. This provides a period of several months during which each of these regions can be fully surveyed.

The predicted number of Trojan asteroids in the inner Solar System is much greater than the number yet discovered. These predictions have evolved over time based on the results of observational analyses as well as computer modelling and simulations. The development of survey telescopes such as Catalina and Pan-STARRS and space-based survey instruments such as the European Space Agency's *Gaia* satellite will lead to the discovery of additional Trojan asteroids in the inner Solar System. The probability of discovery can be maximised by determining the sky areas most likely to contain these asteroids and devising appropriate strategies for search campaigns. The results of surveys will also refine the limits for predictions about the Trojan asteroid population.

1.3 Earth Trojans

Dunbar and Helin (1983) analysed 18 photographic plates taken at the 1.2-m Palomar Schmidt telescope in California during a survey for Earth Trojans between 1978 and 1982. Based on the detection limits, sky coverage and a hypothetical distribution model they estimated an upper limit on the Earth Trojan population. Their conclusion was that the Earth Trojan population in the L4 region is less than 7.0 ± 3.5 asteroids with diameters larger than 250 m. They also noted poor statistics for the L5 region but that the results were consistent with those obtained for the L4 region.

The advent of modern computing enabled extensive modelling and simulations for stable Trojan orbits. For example, the stability of Trojan orbits in the inner Solar System was examined by Mikkola and Innanen (1990, 1992, 1994, 1995) and further explored by P. A. Wiegert, Innanen, and Mikkola (1997), Tabachnik and N. W. Evans (1999, 2000), Morais and Morbidelli (2002), and Scholl, Marzari, and Tricarico (2005) and others.

Mikkola and Innanen (1990) modelled Earth Trojan orbits starting with particles near the triangular (L4 and L5) Lagrangian points of the Earth. The initial values were produced simply by rotating Earth's position and velocity by 60 degrees in the ecliptic plane. As well as studying coplanar orbits they also studied inclined orbits and varied the starting values for the semimajor axes. They found that stable orbits persisted for tens of thousands of years provided that the semimajor axes were similar to Earth's semimajor axis and that the inclinations were not too large. For larger inclinations, greater than about 70 degrees, the eccentricities quickly destabilised. A key result from this modelling was that asteroids

can exist in stable orbits in a 1:1 mean motion resonance with Earth and that those orbits can be inclined to the plane of Earth's orbit.

Mikkola and Innanen (1992) extended their modelling to integrations over about 2 Ma. They noted that the integrated orbits remained stable without any significant evolution over that period. Their conclusion was that stable Trojan orbits existed in the inner Solar System on million-year timescales.

Mikkola and Innanen (1995) extended the study of Mars Trojan orbits (Mikkola and Innanen 1994) to Earth Trojan orbits. They modelled the evolution of Trojan orbits with particles that started at the classical L4 Lagrangian point and extended the period to 6 Ma. As in Mikkola and Innanen (1990), the initial values were produced by rotating the position and velocity of Earth by 60 degrees in the ecliptic plane. The effects of rotating the inclinations of the orbits in one degree increments up to inclinations of 40 degrees were also studied. They concluded that small inclinations were stable and that the most likely orbits for Earth Trojans had inclinations smaller than about six degrees.

The first coorbital asteroid to be discovered was 3753 Cruithne in 1986. Although not a Trojan, a study of the mechanics of asteroid 3753 Cruithne by P. A. Wiegert, Innanen, and Mikkola (1997) demonstrated that coorbital asteroids do exist. 3753 Cruithne has an orbit with a high eccentricity ($e \approx 0.51$) and is inclined to the plane of the ecliptic by about 19.8 degrees. P. A. Wiegert, Innanen, and Mikkola (1997) commented that although the horseshoe orbit of 3753 Cruithne may not be stable on long timescales, the very low a priori probability of an object being injected into such an unusual orbit makes a recent origin seem equally unlikely.

Whiteley and Tholen (1998) conducted a search of Earth's L4 and L5 Lagrangian regions with the University of Hawaii 2.24-m telescope. This search used a CCD which subtended a field of 7.5×7.5 arcmin and had a limiting sensitivity of $R \approx 22.8$. This limit corresponds to C-type asteroids of about 350 m in diameter or S-type asteroids of about 175 m in diameter. The search covered a sky area of 0.35 square degrees without resulting in a discovery. From this they estimated an upper limit of about three objects per square degree.

Later modelling by Tabachnik and N. W. Evans (2000) on inner Solar System coorbital asteroids found stable zones for Earth Trojan orbits. They ran simulations on two sets of data. The first simulation consisted of test particles in the plane of the ecliptic, with the same orbit parameters as Earth but with the arguments of perihelion varied through 360 degrees. This simulation was run over 50 Ma. The result was that about 64% of the test particles survived until

the end of the 50 Ma simulation. About 19% of the survivors were in the Trojan regions while the remainder were on horseshoe orbits. The second simulation was similar to the first but with various orbit inclinations. This simulation was run over 25 Ma with the result that only about 18% of the test particles survived until the end. However almost of the survivors were in the Trojan regions. Tabachnik and N. W. Evans (2000) found two bands of stability for the orbits: inclinations of less than about 16 degrees and between 24 and 34 degrees.

Building on previous modelling, Morais and Morbidelli (2002) estimated the population of Earth coorbitals. They projected the evolution of test bodies with eccentricities and inclinations according to the near-Earth asteroid model of Bottke et al. (2002), taking the origin of the coorbitals to be those near-Earth asteroids with semimajor axes between 1.1 and 1.2 au. Although none of the test bodies survived in 1:1 mean motion resonance for longer than 1 Ma they concluded that a steady state scenario existed. From their modelling, Morais and Morbidelli (2002) predicted a coorbital population of 0.65 ± 0.12 asteroids with a diameter larger than 1 km and 16.3 ± 3.0 asteroids with diameters between 100 m and 1 km.

A comparison of the inclinations of 55 known asteroids with semimajor axes of about 1 au with the prediction for stable inclinations for coorbitals from Morais and Morbidelli (2002) shows that most of these have low inclinations (Figure 1.2). Since every asteroid will pass through the ecliptic at each node of its orbit, an observer's best chance of detecting a near-Earth asteroid is to search near the ecliptic. As this approach has been the most common practice (Stokes, J. B. Evans, and Larson 2002) and because the Earth–Sun–Trojan geometry requires observations at low elevations above the horizon with limited observing time, it has most likely produced a selection bias.

As of today only one Earth Trojan (2010 TK_7) has been discovered (Connors, P. Wiegert, and Veillet 2011). The inclinations of the Earth Trojan 2010 TK_7 ($i = 20.9°$) and of the coorbital asteroid 3753 Cruithne ($i = 19.8°$) lie deep within the modelled range of stable inclinations. This demonstrates that Earth Trojans do exist and suggests the possibility that additional Trojans may be waiting to be discovered. The prospect of discovering these is limited by the restrictions imposed by the geometry.

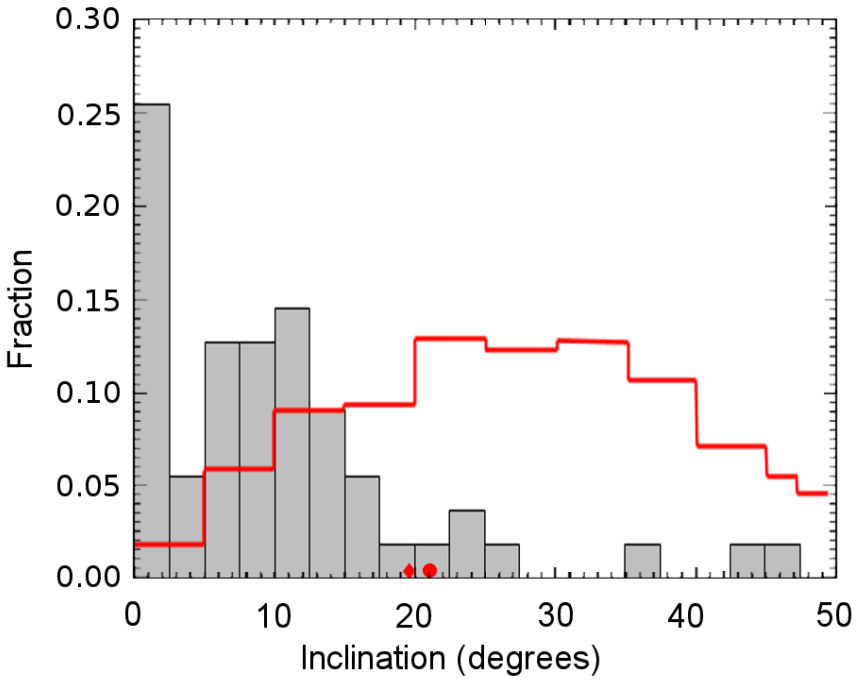

Figure 1.2: Inclinations of 55 known asteroids with semimajor axes of about 1 au (bars) compared to the prediction for stable inclinations for coorbitals (red line) from Morais and Morbidelli (2002). The inclination of the Earth Trojan 2010 TK_7 is indicated by the red dot. The inclination of the coorbital asteroid 3753 Cruithne is indicated by the red diamond.

1.4 Mars Trojans

A similar scarcity exists for Mars Trojans; the prediction is that there are about 50 Mars Trojans with diameters larger than 1 km (Tabachnik and N. W. Evans 1999). However, as of today only five Mars Trojans are known, and three additional asteroids have been proposed as Mars Trojans by C. de la Fuente Marcos and R. de la Fuente Marcos (2013).

In 1974, Weissman and Wetherill (1974) stated that, "there must be no large objects in Mars Trojan orbit or [Weissman and Wetherill] would expect them to have been found in random searches for minor planets." History shows the first Mars Trojan to have been found in 1990 with the discovery of asteroid 5261 Eureka during the course of the Mars and Earth-Crossing Asteroid and Comet Survey conducted by E. M. and C. S. Shoemaker at Palomar Observatory (Bowell et al. 1990). It can thus be asserted that any argument that Trojans would have already been found accidentally is based on assumption.

Following the discovery of 5261 Eureka, Mikkola and Innanen (1994) performed numerical integrations for Mars Trojan orbits for periods in excess of 4 Ma. The primary study concerned the dependence of the stability of the motion on the orbital inclination. They found that long-term stability only occurred in specific inclination ranges with respect to Jupiter's orbit. As Jupiter is the major perturbing planet the angular orbital elements of the test particles were calculated with respect to Jupiter's orbit, with the x-axis directed to Jupiter's osculating perihelion and the z-axis perpendicular to the osculating orbital plane. The elements could also be defined with respect to the ecliptic plane. Jupiter's orbit has a low inclination (1.3°) so the inclination ranges are comparable. Mikkola and Innanen (1994) found the stable inclination intervals (with respect to Jupiter's orbit) to be between 15 and 30 degrees, and between 32 and 44 degrees. They attribute the instability for inclinations between 30 and 32 degrees to a secular resonance with Jupiter.

Tabachnik and N. W. Evans (1999) subsequently performed integrations for Mars Trojan orbits over much greater periods and obtained very similar results. They modelled the evolution of the Trojan orbits for periods between 25 and 60 Ma. The modelled orbits included a range of inclinations near the Mars L4 and L5 Lagrangian points. Tabachnik and N. W. Evans (1999) found that long-term stability was almost identical between L4 and L5 in terms of orbit inclinations but that there were some differences in stable longitudes. The stable inclination intervals were between 15 and 30 degrees and between 32 and 40 degrees for L4

and between 15 and 40 degrees for L5. They noted that the instability band found by Mikkola and Innanen (1994) between 30 and 32 degrees was found to exist in the L4 region but not in the L5 region. Tabachnik and N. W. Evans (1999) commented that L5 Trojans with starting inclinations in that range seem to be stable and that the existence of L5 Mars Trojan 1998 VF_{31}, which has an inclination of about 31.3 degrees, was evidence of stability.

Tabachnik and N. W. Evans (1999) also reported on the stable ranges of longitudes found for the Mars Trojans in their simulations. They found that the L4 and L5 Lagrangian regions were similar in extent but not symmetric either side of Mars. The probability densities peaked at longitudes of about 60 degrees (L4) and 300 degrees (L5), consistent with the classical Lagrangian points, but were quite widely distributed either side of these points. The stable Mars L4 region spanned 95 degrees, with longitudes between 25 and 120 degrees. The stable L5 region was slightly smaller, spanning 90 degrees, with longitudes between 240 and 330 degrees.

The results from Tabachnik and N. W. Evans (1999) confirmed the findings of Mikkola and Innanen (1994) but constrained the upper limit on the range of inclinations to 40 degrees. They found limits on the ranges of stable longitudes for the Mars Trojan regions, determining that Mars Trojans may not be clustered near the classical Lagrangian points but that they could be distributed up to 60 degrees away in longitude. They noted that both 5261 Eureka and 1998 VF_{31} lie deep within one of the stable zones, that their orbits remain Trojan-like for durations of at least 50 Ma and hence suggested that they may be of primordial origin. Furthermore, Tabachnik and N. W. Evans (1999) estimated there to be about 50 Mars Trojans with diameters larger than 1 km.

Following this work, Tabachnik and N. W. Evans (2000) modelled coorbital asteroids for Mars. Simulations for orbits in the plane of Mars' orbit showed only one remaining test particle after 50 Ma and none after 60 Ma, confirming the suspicion of Mikkola and Innanen (1994) that such orbits are not stable on long timescales. They also found that low-inclination orbits are not stable as the inclinations quickly increase until the effects of a secular resonance with Jupiter cause destabilisation. On timescales of 25 Ma the simulations of inclined orbits showed stable zones for inclinations between 14 and 40 degrees although they found a resonance with Jupiter that destabilised inclinations at about 29 degrees. Further simulations on timescales of 100 Ma for test particles located at the classical L4 and L5 Lagrangian points showed the same stable inclination ranges although they noted a trend that inclinations larger than about 35 degrees tended to be

less stable. Tabachnik and N. W. Evans (2000) concluded that the two known Mars Trojans of that time (5261 Eureka and 1998 VF_{31}), with orbit inclinations of 20.3 and 31.3 degrees respectively, may be of primordial origin as they lie deep within the stable zones. The additional three Mars Trojans that are currently known (1999 UJ_7, 2007 NS_2 and 2001 DH_{47}) have inclinations of 16.7, 18.6 and 24.4 degrees, respectively, which also places them within these stable zones. The three asteroids proposed as Mars Trojans by C. de la Fuente Marcos and R. de la Fuente Marcos (2013) (2011 SC_{191}, 2011 SL_{25} and 2011 UN_{63}) also reside within these stable zones, having inclinations of 18.7, 21.5 and 20.4 degrees, respectively.

Later modelling by Scholl, Marzari, and Tricarico (2005) revised the ranges of stable inclinations to between 15 and 28 degrees and between 30 and 35 degrees. They integrated the motion of test bodies in Trojan orbits and measured their diffusion, finding that the most stable inclinations were between about 15 and 30 degrees and that these were stable over the age of the Solar System. They found that orbits with inclinations smaller than 15 degrees and with inclinations at about 30 degrees were destabilised by secular resonances within a few Ma. Orbits with inclinations larger than 35 degrees were rapidly destabilised by the Kozai resonance with Jupiter.

Scholl, Marzari, and Tricarico (2005) also found that the dynamical lifetimes of the four known Mars Trojans of that time (5261 Eureka, 1998 VF_{31}, 1999 UJ_7 and 2001 DH_{47}) were of the order of the age of the Solar System. They concluded that all four bodies may have resided in the Trojan region since the formation of the Solar System, with the caveat that when integrating clones of these bodies a few clones always became unstable before reaching 4.5 Ga. They also noted that these four Trojans are kilometre-sized bodies and thus their orbits are, a priori, affected by the Yarkovsky force. However their results indicated that the Trojan resonance locking prevails against the Yarkovsky force for bodies larger than a few metres in diameter.

In comparing the inclinations of 72 known asteroids that have semimajor axes of about 1.52 au (similar to that of Mars) with the modelled stable inclinations for coorbitals from Morais and Morbidelli (2002) a bias towards low inclinations is evident (Figure 1.3). This bias is most likely a selection effect as discussed in Section 1.3. The inclinations of all of the known Mars Trojans lie deep within the modelled range of stable inclinations.

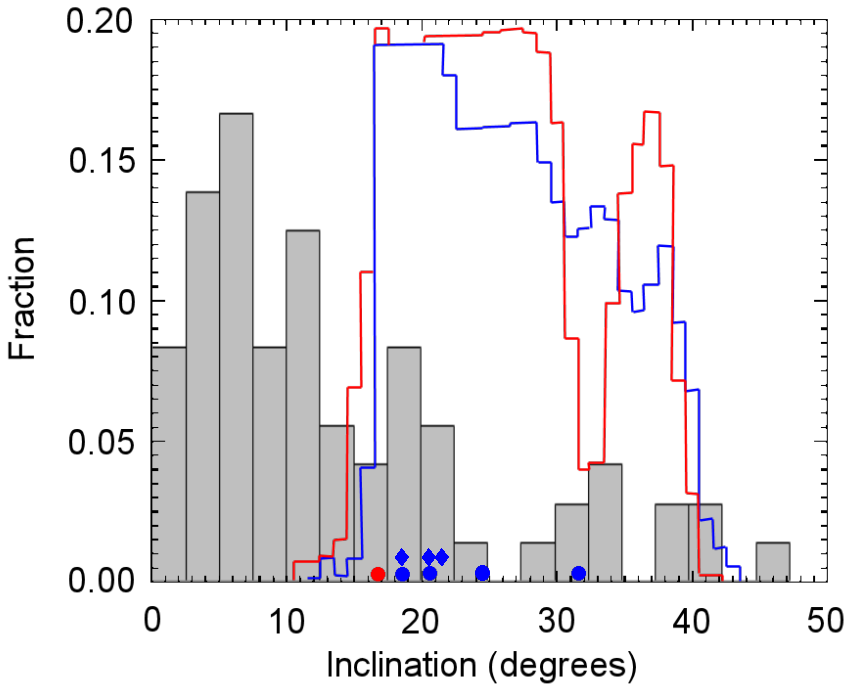

Figure 1.3: Inclinations of 72 known asteroids (bars) that have semimajor axes of about 1.52 au compared to the prediction for stable inclinations for Mars coorbitals in the L4 (red) and L5 (blue) regions from Morais and Morbidelli (2002). The inclinations of the known Mars Trojans are indicated by the red and blue dots. The inclinations of the proposed Trojans from C. de la Fuente Marcos and R. de la Fuente Marcos (2013) are indicated by blue diamonds.

1.5 Asteroid brightness measurements

Asteroids do not emit any light of their own in the visible spectrum hence their apparent brightness is a product of reflected sunlight. The brightness is usually stated as visual (V) magnitude, from the Johnson-Morgan UBV photometric system (Johnson and Morgan 1953). The passband of a V filter has an equivalent wavelength of 550 nm (Roy and Clarke 2003).

As the brightness is a product of reflected sunlight, this depends on the position of the asteroid relative to the Sun and the Earth and the properties of the asteroid. The V magnitude of an asteroid with a phase angle less than 120 degrees is calculated by (Morbidelli et al. 2002):

$$V = 5\log_{10}(r\Delta) + H - 2.5\log_{10}\left[(1-G)\,\phi_1 + G\phi_2\right], \tag{1.2}$$

where r and Δ are the heliocentric and geocentric distances respectively, H is the absolute magnitude, G is the slope parameter and ϕ_1 and ϕ_2 depend on the phase angle α through the relationships:

$$\phi_1 = exp\left\{-\left[3.33\tan\frac{\alpha}{2}\right]^{0.63}\right\}, \tag{1.3}$$

$$\phi_2 = exp\left\{-\left[1.87\tan\frac{\alpha}{2}\right]^{1.22}\right\}. \tag{1.4}$$

The slope parameter G determines how the apparent brightness of the object decays with increasing phase angle. Bodies with a large slope parameter are brighter than bodies with a small slope parameter for the same values of absolute magnitude, phase angle and heliocentric distance (Morbidelli et al. 2002).

The absolute magnitude H can be used to derive an effective diameter. Effective diameter is the diameter of a hypothetical spherical asteroid that would provide the same apparent brightness as the observed asteroid irrespective of the actual shape. The relationship between diameter and absolute magnitude is given by:

$$\log_{10} D = 3.1235 - 0.2H - 0.5\log_{10} p_v, \tag{1.5}$$

where D is the diameter in kilometres, H is the absolute magnitude and p_v is the albedo (Warner, Harris, and Pravec 2009).

The albedo of an asteroid depends on its composition. However, rather than classifying asteroids by composition as this cannot be directly ascertained, asteroids are classified by spectral class. The most widely used taxonomies for asteroids are currently the Tholen (1984), the Bus and Binzel (2002) and the

Bus–DeMeo et al. (2009) spectral taxonomies. The Bus and Binzel (2002) visible wavelength taxonomy was built upon the Tholen (1984) system. The Bus–DeMeo et al. (2009) spectral taxonomy extended the Bus and Binzel (2002) taxonomy into the near-infrared. Consequently, there are multiple taxonomic classes.

In the absence of spectral data a strict classification cannot be performed. A spectral survey of main belt asteroids showed that the majority of asteroids in the inner part of the main belt are silicaceous (S type) while asteroids in the outer part are predominantly carbonaceous (C type) (P. Wiegert et al. 2007). Asteroids are thus often assumed to be S type if they are near-Earth asteroids or they reside in the inner part of the main belt and C type if they reside in the outer part of the main belt. This division between the inner and outer parts of the main belt occurs at a distance of about 2.5 au from the Sun, i.e. the 3:1 Kirkwood gap (Figure 1.4). The populations of asteroids in the inner Solar System, i.e. the

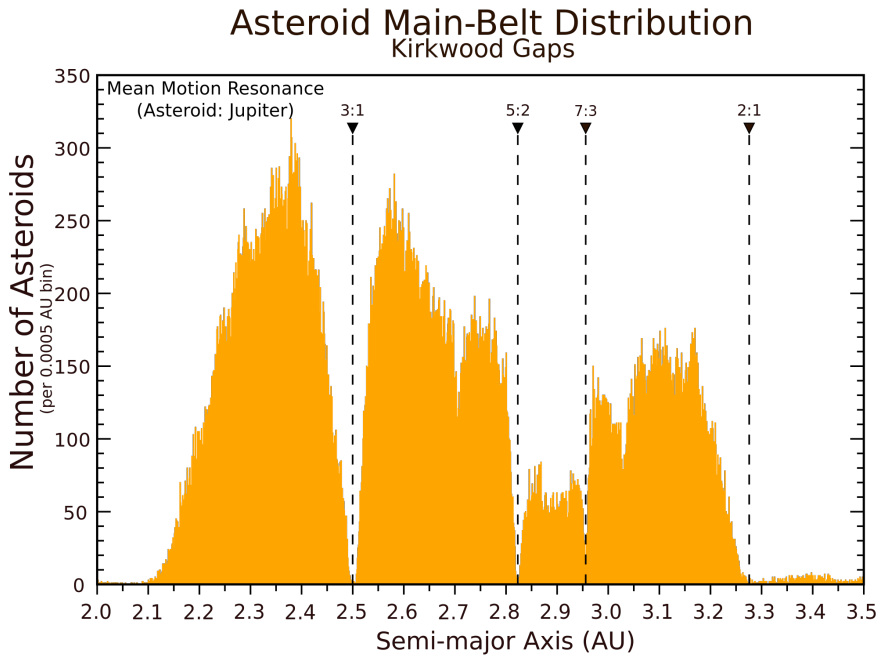

Figure 1.4: The Kirkwood gaps in the main belt are caused by mean motion resonances with Jupiter (Alan Chamberlain, NASA/JPL-Caltech 2007).

Apollos, Amors, Atens and Atiras, are also predominantly S type. This suggests that they originated from the inner part of the main belt (D. F. Lupishko and T. A. Lupishko 2001; Binzel et al. 2004; Stuart and Binzel 2004; D. F. Lupishko, Martino, and Binzel 2007).

Pravec et al. (2012) determined the mean albedos from a sample of 583 main

belt asteroids to be 0.197±0.051 and 0.057±0.013 for the Bus–DeMeo S/A/L and C/G/B/F/P/D types, respectively. When the albedo is unknown an assumed mean albedo is substituted. Since the albedo for near-Earth asteroids and for asteroids in the inner part of the main belt is about 0.2 and for asteroids in the outer part of the main belt is about 0.06, the mean albedo typically used is 0.14. The size is thus based on an assumption made about the composition which is in turn based on the orbit of the asteroid. Hence an absolute magnitude of $H = 17.75$ and an assumed albedo of $p_v = 0.14$ represents an assumed effective diameter of 1 km.

Using these formulae (Equations 1.2 - 1.5) the V magnitude of an asteroid 1 km in diameter ($H = 17.75$) at a phase angle of 60 degrees and at a distance of 1 au from the Earth, as may be the case for an Earth Trojan, is calculated to be $V = 19.3$, assuming a slope parameter of 0.15 and distance of about 1 au from the Sun, as illustrated in Figure 1.5.

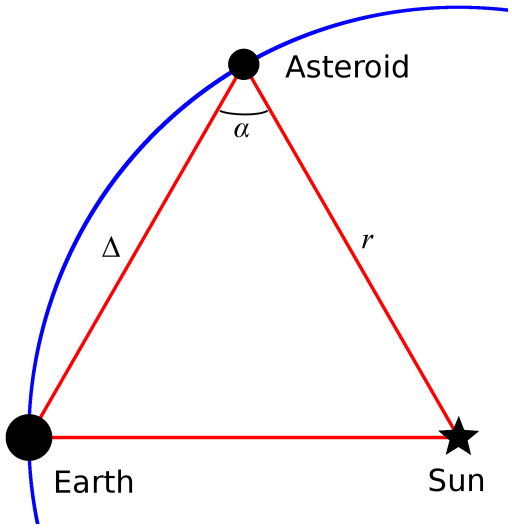

Figure 1.5: An Earth Trojan at one of the equilateral L4 or L5 Lagrangian points would have a phase angle of $\alpha = 60°$ and be at a distance of $\Delta = 1$ au from the Earth and $r = 1$ au from the Sun.

This calculated V magnitude represents the mean brightness. On short time-scales the brightness varies about this mean. This is due to the rotation of the asteroid as it tumbles through space in its orbit about the Sun. As the asteroid rotates its orientation changes with respect to an observer. A rocky body smaller than about 600 km in size is not massive enough to have accreted into a spheroid (Lineweaver and Norman 2010) thus most asteroids have irregular shapes. Hence

the surface area presented to the observer changes, as does the amount of reflected sunlight.

The rotation changes the amount of light reflected from the surface in a periodic fashion. Thus frequent observations of an asteroid can reveal a regular periodic variation in the apparent brightness (Figure 1.6). This regular periodic

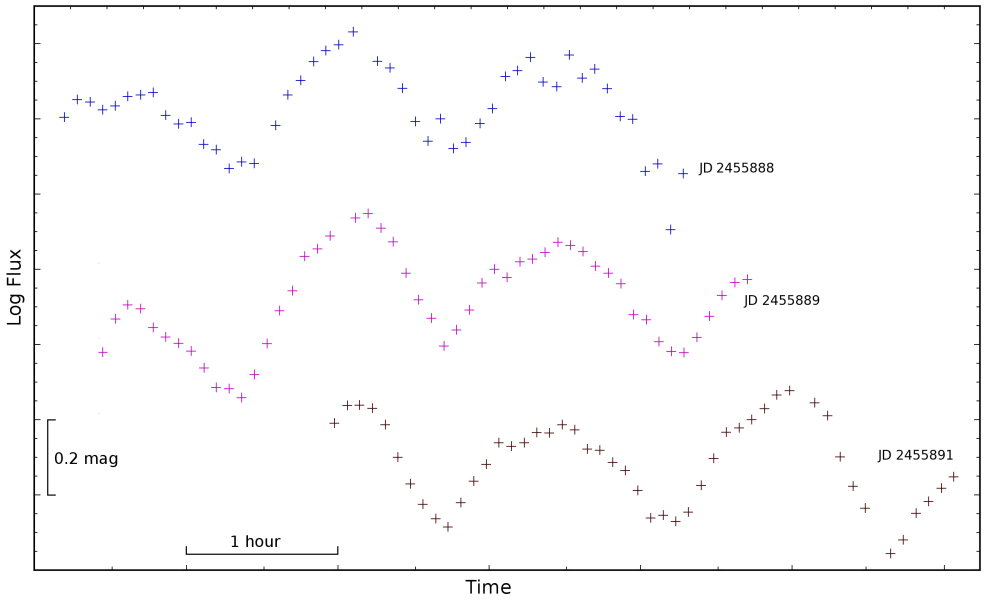

Figure 1.6: Light curves for asteroid 939 Isberga using time series that were obtained on three separate dates. A primary periodicity consistent with the expected rotation period of 2.9173 h is evident (Todd, Wallon Pizarro, et al. 2014).

variation is commonly known as a light curve. The light curve of an asteroid can be used to derive a model for its shape. This shape model can be constructed without specific knowledge of the size of the asteroid.

Light curves can be obtained for more than just asteroid rotations. Other optical transient events such as supernovae, gamma-ray burst optical afterglows and occultations and exoplanet studies all have characteristic light curves. An accurate light curve allows modelling of the key characteristics of the transient object or event. For example, different supernova types can be identified from the shape of the light curve (Figure 1.7), much of what is known about gamma-ray bursts comes from studying the afterglows, and the duration of the event when an asteroid or exoplanet passes in front of a star provides information on the size of the object.

The analysis of a time series of astronomical images to produce a light curve is very time-consuming. The process is often quite similar regardless of the type

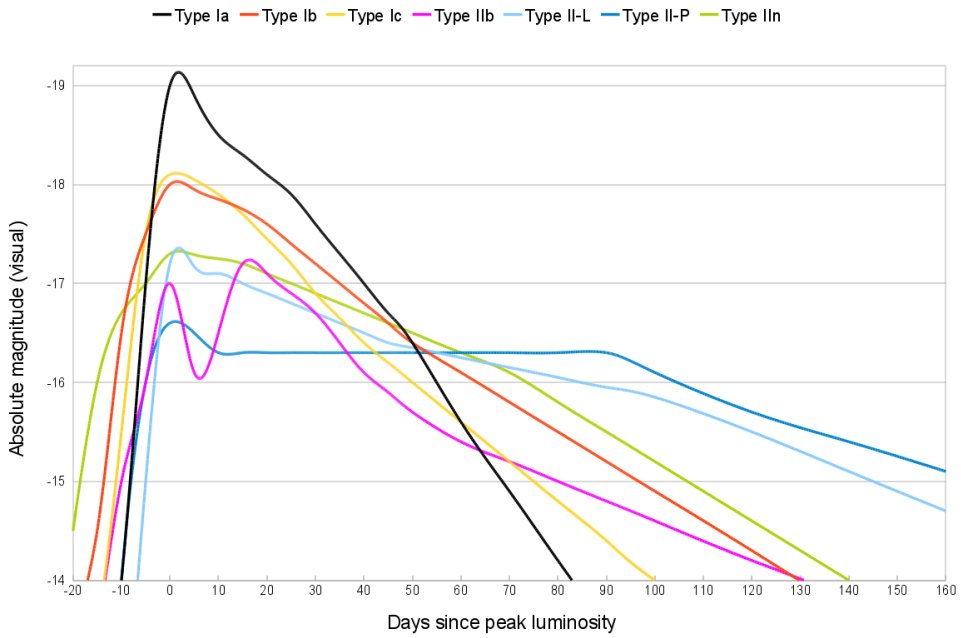

Figure 1.7: Light curves of the main supernova types, representative of peak brightness and rise and decay times (Lithopsian 2012).

of object whether it is an asteroid tumbling through space, a supernova, etc. The brightness of the target must be measured for each image over the time series. A suitable reference source must also be selected and measured for each image. When possible, this reference source should be the same for each image in the time series. Corrections also need to be made to compensate for any changes in observing conditions from one image to the next.

In some processes the reference source needs to have particular characteristics. The reference source may need to be within a specific brightness range relative to the target, be of a specific spectral class or be suitable for use as a photometric standard e.g. Landolt (1992). In the case of asteroid light curves it is common to use a Sun-like (i.e. G-type) star located as near as possible to the asteroid as a reference (F. Vachier, personal communication 22 February 2011). In the cases where more than one calibration source is available the measurement precision can be improved; however, this is also much more time-consuming.

In some cases the choice of suitable calibration sources is sparse. Observations of asteroid 939 Isberga were made by the author on 22, 23 and 25 November 2011 using the Zadko Telescope near Gingin, north of Perth in Western Australia (Coward et al. 2010). The software sky atlas Aladin (Bonnarel et al. 2000) was used to identify suitable G-type stars for use as reference stars in the field. Equa-

tions 1.7 and 1.8 were applied to photometric data obtained from the NOMAD catalogue (Zacharias et al. 2004). The result identified suitable reference stars, fitting the $B - V$ and $V - K$ criteria described in Equation 1.6.

The ALADIN field for 22 November 2011 is shown in Figure 1.8 and the field for 25 November 2011 in Figure 1.9. It was found that there were four potential reference stars in the field for both 22 November (Figure 1.8) and 25 November (Figure 1.9). Due to the short arc length over this span of four days, the same

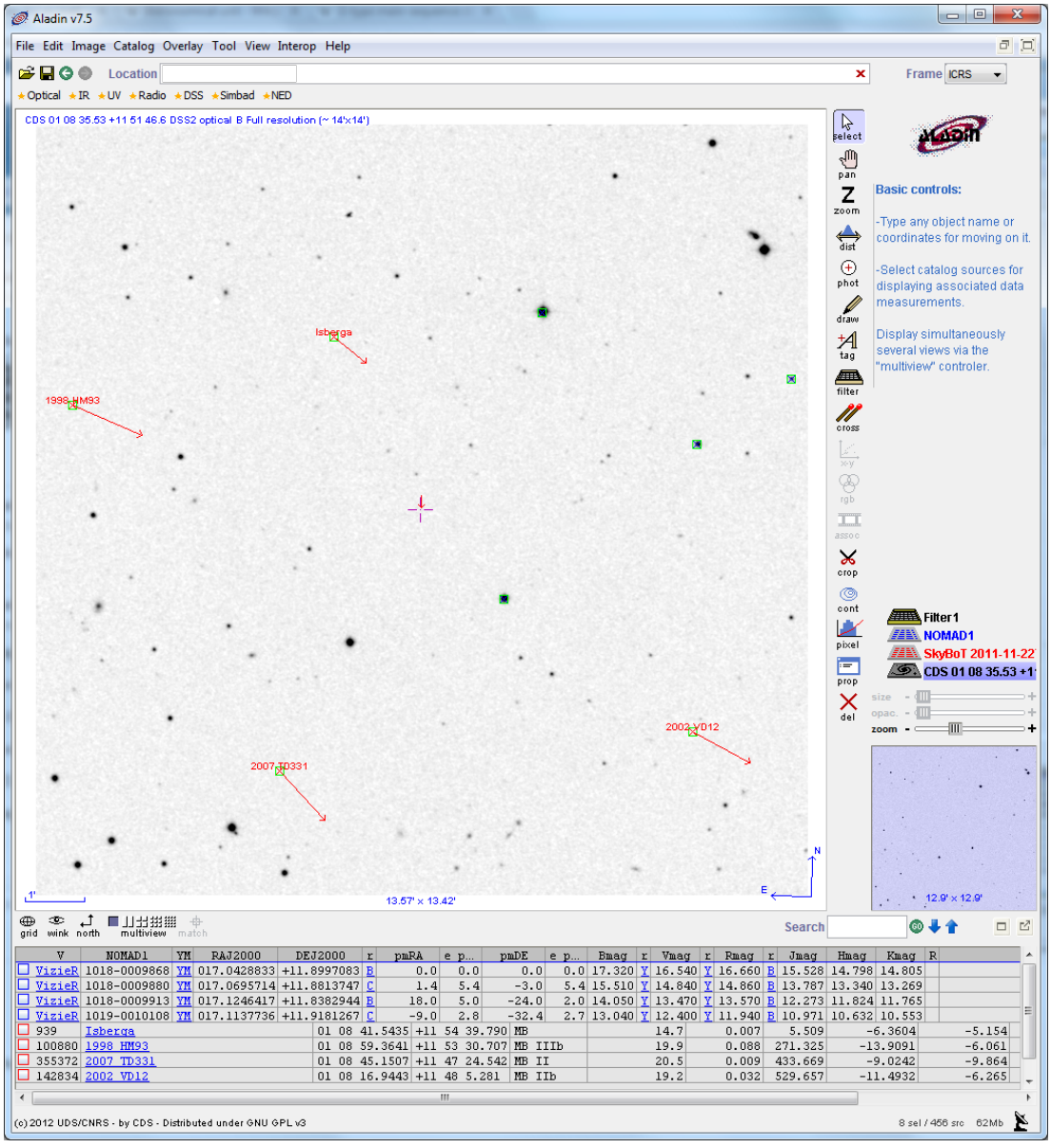

Figure 1.8: ALADIN field showing the position of asteroid 939 Isberga on 22 November 2011. Potential reference stars are indicated by a cross (×) within a green box (□).

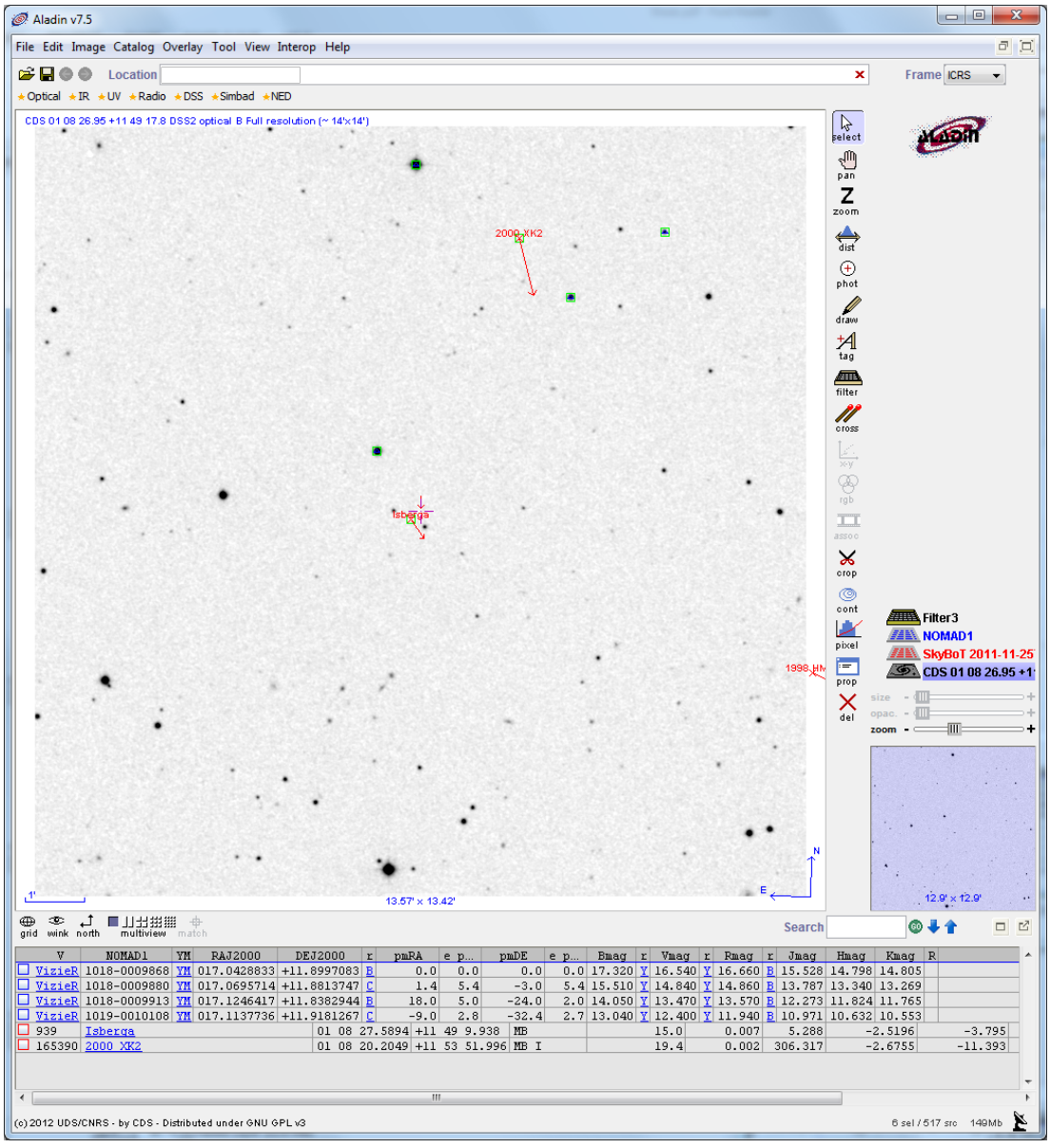

Figure 1.9: ALADIN field showing the position of asteroid 939 Isberga on 25 November 2011. Potential reference stars are indicated by a triangle (△) within a green box (□).

four stars appeared in both fields.

A filter was applied in ALADIN to identify potential reference stars. These were selected using the criteria (F. Vachier, personal communication 22 February 2011):

$$0.5 < B - V < 1.0 \quad \text{and} \quad 1.4 < V - K < 2.0, \tag{1.6}$$

where B, V and K are the magnitude values in the respective filter bands.

The Sun has a surface temperature of about 5800 K, a $B - V$ value of about 0.65 (Gray 1995) and a $V - K$ value of about 1.5 (Bessell, Castelli, and Plez 1998). Applying the $B - V$ (Equation 1.7) and $V - K$ (Equation 1.8) colour-temperature relations from Boyajian et al. (2012):

$$\begin{aligned} \log_{10} T_{EFF} = {} & 3.9680 \pm 0.0025 - 0.2633 \pm 0.0876(B-V) - \\ & 3.2195 \pm 1.3407(B-V)^2 + 15.3548 \pm 6.8551(B-V)^3 - \\ & 27.2901 \pm 15.7373(B-V)^4 + 19.9193 \pm 16.8465(B-V)^5 - \\ & 4.5127 \pm 6.8539(B-V)^6, \end{aligned} \tag{1.7}$$

$$\begin{aligned} \log_{10} T_{EFF} = {} & 3.9685 \pm 0.0034 + 0.0830 \pm 0.0570(V-K) - \\ & 1.8948 \pm 0.2874(V-K)^2 + 4.0799 \pm 0.5438(V-K)^3 - \\ & 3.7353 \pm 0.4739(V-K)^4 + 1.5651 \pm 0.1936(V-K)^5 - \\ & 0.2472 \pm 0.0301(V-K)^6, \end{aligned} \tag{1.8}$$

where T_{EFF} is the effective temperature of the star, to the photometric magnitudes for the selected stars we see that these are a close fit to the Sun (Table 1.1).

Table 1.1: Calculated temperatures for the selected Sun-like stars in Figures 1.8 and 1.9.

NOMAD ID	B	V	K	T_{EFF}	
				$(B-V)$	$(V-K)$
1018-0009868	17.43	16.54	14.805	5835.3	5404.7
1018-0009880	15.51	14.84	13.269	5576.9	5617.4
1018-0009913	14.05	13.47	11.765	5963.4	5438.6
1019-0010108	13.04	12.40	10.553	5703.5	5271.8

The method that was employed to obtain the brightness measurements and calculate V magnitudes used the open source astronomical software package AUDELA (Klotz et al. 2012). Specifically:

- The nearest candidate star to the target was selected as the reference star.

- The catalogue V magnitude for that star (V_{star}) was recorded (from ALADIN).
- The integrated flux of the star (φ_{star}) was measured (using AUDELA).
- The integrated flux of the asteroid ($\varphi_{asteroid}$) was measured.
- The V magnitude of the asteroid ($V_{asteroid}$) was calculated using the standard formula:

$$V_{asteroid} = V_{star} - 2.5 \log_{10} \left(\frac{\varphi_{asteroid}}{\varphi_{star}} \right). \tag{1.9}$$

This process was repeated for each image in the time series.

The nearest candidate star for 22 November 2011 differed from the nearest candidate star for 25 November. The nearest candidate star for 22 November was 1019-0010108 whereas for 25 November it was 1018-0009913. Comparison measurements were made using the alternative reference star 1018-0009880 ($V = 14.84$) as it was similar in brightness to Isberga ($V = 15.0$). It was found that some differences existed between the calculation results with the different reference stars. It was also found that differences existed between the calculated V magnitudes of these stars when using one star as a basis for measuring the other.

While not considered significant in the context of obtaining relative photometry for the rotation period of the asteroid, this led to considering the implications of using as many stars as possible as calibration sources. Using multiple stars allows cross-referencing of the flux measurements over the span of observations. This in turn enables selection of stable sources, i.e. not varying over the span of observations. Such an approach requires automation as the time requirement to process this manually would be prohibitive.

The facility to be able to quickly analyse a set of images and produce a light curve is particularly valuable on automated telescopes, e.g. the Zadko Telescope near Gingin, Western Australia (Coward et al. 2010). As it is possible to load an observing programme that will acquire a large number of images in a comparatively short period of time, the ability to analyse the data almost immediately to obtain even a preliminary result can be of great benefit. It has become common that robotic telescopes are used in programmes requiring rapid response to a trigger event such as the detection of gamma-ray bursts, gravity waves, neutrino emissions etc. The Zadko Telescope is actively engaged in such programmes (Coward et al. 2010; Branchesi et al. 2011; Ageron et al. 2012) as part of the

TAROT[1] network as well as being a participant in the Gaia Follow-Up Network for Solar System Objects (*Gaia* FUN-SSO[2]) (Todd, Coward, Tanga, et al. 2013). Consequently, there is a high potential for the creation of data sets containing transient sources that need rapid analysis.

1.6 This research

Trojan asteroids are of great interest for both the evolution of their orbits and their gravitational interactions. The predicted numbers of Trojan asteroids in the orbits of Earth and Mars are much greater than the number yet discovered. Survey telescopes such as Catalina and Pan-STARRS and space-based survey instruments such as the European Space Agency's *Gaia* satellite will lead to the discovery of additional Trojan asteroids. The probability of discovery can be maximised by determining the sky areas most likely to contain these asteroids and devising appropriate strategies for search campaigns. The results of surveys will also refine the limits for predictions about the Trojan asteroid population.

The European Space Agency's *Gaia* space mission is the next-generation astrometry mission following *Hipparcos*. *Gaia* will perform a systematic survey of the whole sky down to a magnitude of $V = 20$, about one billion stars and 300,000 Solar System objects. This survey will determine the positions of stars with unprecedented astrometric precision due to *Gaia* having a limiting accuracy of 10^{-5} arcseconds (Mignard 2011). In the process it will completely survey the regions of Earth's and Mars' orbits where Trojan asteroids may be found, something that has not been able to be accomplished with ground-based telescopes.

As of today only one Earth Trojan (2010 TK_7) has been discovered (Connors, P. Wiegert, and Veillet 2011). The inclination of the Earth Trojan 2010 TK_7 (20.9 degrees) lies deep within the modelled range of stable inclinations. This demonstrates that Earth Trojans do exist, and the population prediction by Morais and Morbidelli (2002) suggests the possibility that more may be waiting to be discovered. The prospect of discovering these is limited by the restrictions imposed by the geometry.

The number of predicted Mars Trojans is also much greater than the number of known Trojans. As of today only five Mars Trojans are known, and three additional asteroids have been proposed as Mars Trojans by C. de la Fuente Marcos

1. Télescope à Action Rapide pour les Objets Transitoires
2. http://www.imcce.fr/gaia-fun-sso

and R. de la Fuente Marcos (2013). The population prediction by Tabachnik and N. W. Evans (1999) for the number of Trojan asteroids in Mars' orbit suggests that these known Trojans constitute only about one-tenth of the population.

Todd, Coward, and Zadnik (2012) presents models that constrain optimal search areas for Trojan asteroids in the orbits of Earth and Mars. Based on these models, this paper examines strategies for survey telescopes that optimise observing patterns and cadences to maximise the probability of detection. This paper also considers implications for detection of Trojan asteroids with respect to the *Gaia* satellite and limitations of *Gaia*'s observing geometry. This paper is included as Chapter 2 of this thesis.

Todd et al. (2012a) elaborates on the model described in Todd, Coward, and Zadnik (2012) for Earth Trojans. This paper considers the apparent brightness of an Earth Trojan depending upon its position within the limits of the region. It describes imaging cadences for narrow and wide-field survey telescopes, including the *Gaia* satellite, for the most efficient use of telescope time to maximise the probability of detecting additional Earth Trojans. This paper is included as Chapter 3 of this thesis.

Todd et al. (2012b) elaborates on the model described in Todd, Coward, and Zadnik (2012) for Mars Trojans. This paper considers the apparent brightness of Mars Trojans depending on their positions relative to Earth. It describes the differences in the apparent sky area of the Mars Trojan regions depending upon the relative geometries of the Earth, the Sun and these regions. This paper also proposes a strategy for the most efficient use of telescope survey time to maximise the probability of detecting Mars Trojans. The implications for the *Gaia* mission are that *Gaia* could detect any Mars Trojans larger than 1 km in diameter, provided the relative motion perpendicular to *Gaia*'s CCD array is less than 0.40 arcsec/s. This paper is included as Chapter 4 of this thesis.

Todd et al. (2013) focuses on the implications of the *Gaia* mission for the discovery of Earth and Mars Trojan asteroids. This paper presents the initial results of simulations for the detection of Trojan asteroids in the orbits of Earth and Mars by *Gaia*. It predicts that any undiscovered Earth Trojans are likely to be too small and hence too faint for *Gaia* to detect. This paper also predicts that *Gaia* is likely to detect any additional Mars Trojans which are of sizes comparable to those already known. This paper is included as Chapter 5 of this thesis.

Todd et al. (2014) presents the detailed results of simulations for the detection of the known Trojan asteroids in the orbits of Earth and Mars by *Gaia*. This paper predicts that *Gaia* will not detect the Earth Trojan 2010 TK_7 but that

it will detect any Earth Trojans with diameters larger than 600 m. This paper also predicts that *Gaia* will detect the currently known Mars Trojans and could discover more than 100 new Trojans as small as 400 m in diameter thereby testing the estimates of the Mars Trojan asteroid population. This paper is included as Chapter 6 of this thesis.

Todd, Coward, Tanga, et al. (2013) describes the involvement of the Zadko Telescope in preliminary tests of the *Gaia* Follow-Up Network for Solar System Objects. Due to orbital constraints, detections by *Gaia* of Solar System objects will require follow-up observations from ground-based telescopes for discovery confirmations and to enable orbit computations. A programme to identify ground-based optical telescopes for a *Gaia* follow-up network for Solar System Objects was initiated by the *Gaia* Data Processing and Analysis Consortium (DPAC) in 2010 (Thuillot, Hestroffer, and Tanga 2011). The purpose of this network is to perform the critical tasks of identifying the object, providing confirmation of the discovery and tracking the object to constrain its orbit. The Zadko Telescope in Western Australia was flagged as an important node in this network due to its southern location, longitude and automated scheduling system. This paper describes the results obtained by the Zadko Telescope during a test of this network that used the fast moving Potentially Hazardous Asteroid 2005 YU_{55} as the target. This paper is included as Chapter 7 of this thesis.

Todd, Wallon Pizarro, et al. (2014) describes the operation and software algorithms of the High Efficiency Image Detection & Identification (HEIDI) pipeline software. As part of this research the author has developed a software package for rapidly processing time series containing optical transient sources. HEIDI rapidly processes images and analyses the variations in brightness of optical transients such as asteroids, gamma-ray burst optical afterglows and *Gaia* transient candidates.

Taking the approach that all sources in an image are potential reference sources, the variations in the brightness of those sources are assessed automatically across the time series. Corrections are made to compensate for these variations while also taking into account that some sources may intrinsically vary on short time scales (e.g. short period variable stars). As the concept originated from observing asteroids and producing light curves, Solar System objects are identified automatically during the image processing. HEIDI rapidly processes sets of astronomical images, taking only a few minutes compared to the many hours required by the method described in Section 1.5. This allows prompt analysis and rapid dissemination of results for time critical events such as gamma-ray

burst optical afterglows and follow-up of *Gaia* detections. This paper is included as Chapter 8 of this thesis.

This research describes probability distributions and constrains the sky search areas for Trojan asteroids in the orbits of Earth and Mars. It proposes search strategies for ground-based telescopes which optimise observing patterns and cadences to maximise the probability of detecting Earth and Mars Trojans. It describes the characteristics of these Trojan asteroids and assesses the implications for their detection by the *Gaia* satellite, including predictions for the number of expected discoveries.

This work also describes the role of the Zadko Telescope, in Western Australia, as part of the *Gaia* Follow-Up Network for Solar System Objects which will provide confirmations for *Gaia* detections.

Finally, the development of the HEIDI software will be of great benefit to this and other programmes. This ability to quickly analyse a set of images and produce high quality results is particularly valuable on automated or robotic telescopes such as the Zadko Telescope. An increasing number of programmes require prompt follow-up and rapid analysis of time series data. With potential application to the prompt analysis and rapid issuing of results for programmes such as the prompt follow-up of gamma-ray burst alerts for the detection of transient optical emissions, HEIDI addresses a need in providing rapid analysis of time series image data.

Chapter 2

Search strategies for Trojan asteroids in the inner Solar System

Todd, M., D. M. Coward, M. G. Zadnik. 2012. "Search strategies for Trojan asteroids in the inner Solar System." *Planetary and Space Science* 73 (1): 39-43. doi:10.1016/j.pss.2011.11.002.

Planetary and Space Science 73 (2012) 39–43

Contents lists available at SciVerse ScienceDirect

Planetary and Space Science

journal homepage: www.elsevier.com/locate/pss

Search strategies for Trojan asteroids in the inner Solar System

M. Todd [a,*], D.M. Coward [b], M.G. Zadnik [a]

[a] Department of Imaging and Applied Physics, Bldg 301, Curtin University, Kent St, Bentley, WA 6102, Australia
[b] School of Physics, M013, The University of Western Australia, 35 Stirling Hwy, Crawley, WA 6009, Australia

ARTICLE INFO

Article history:
Received 22 July 2011
Received in revised form
2 November 2011
Accepted 3 November 2011
Available online 18 November 2011

Keywords:
Numerical methods
Observational methods
Minor planets
Asteroids
Planets
Satellites
Celestial mechanics
Solar System

ABSTRACT

Trojan asteroids are minor planets that share the orbit of a planet about the Sun and librate around the L4 or L5 Lagrangian points of stability. They are important because they carry information on early Solar System formation, when collisions between bodies were more frequent. Discovery and study of terrestrial planet Trojans will help constrain models for the distribution of bodies and interactions in the inner Solar System.

We present models that constrain optimal search areas, and strategies for survey telescopes to maximize the probability of detecting inner planet Trojans. We also consider implications for detection with respect to the Gaia satellite, and limitations of Gaia's observing geometry.

1. Introduction

Trojan asteroids are minor planets that share the orbit of a planet about the Sun, and librate around the Lagrangian points of stability that lie 60° ahead of (L4), or behind (L5), the planet in its orbit. Trojans represent the solution to Lagrange's famous triangular problem and appear to be stable on long time-scales (100 Myr to 4.5 Gyr) (Pilat-Lohinger et al., 1999; Scholl et al., 2005) in the N-body case of the Solar System. This raises the question whether the Trojans formed with the planets from the Solar nebula or were captured in the Lagrangian regions by gravitational effects. Study of the Trojans therefore provides insight into the early evolution of the Solar System.

About 5000 Jupiter Trojans are currently known to exist. Some searches have been conducted for Earth Trojans (ET) (Dunbar and Helin, 1983; Whiteley and Tholen, 1998; Connors et al., 2000). A search covering approximately 0.35 deg^2 by Whiteley and Tholen (1998) resulted in a crude upper population limit of fewer than three objects per square degree, down to $R=22.8$. A subsequent search by Connors et al. (2000) covering about nine square degrees, down to $R=22$, failed to discover any ETs. Recent examination of data from the WISE satellite has resulted in the discovery of the first known ET (Connors et al., 2011). Among the other terrestrial planets, four Trojans have been discovered in the orbit of Mars. Current models (Mikkola and Innanen, 1990; Tabachnik and Evans, 2000a) suggest that this represents less than a tenth of the Mars Trojan population.

This paper describes probability distributions synthesized from existing models. This allows us to constrain optimal search areas and examine strategies to maximize the probability of detecting Trojans. We also examine the possibility of detection of Trojans by the Gaia satellite.

2. Models

2.1. Earth Trojans

A synthesis of a stable orbit inclination model (Morais and Morbidelli, 2002) and heliocentric longitude model (Tabachnik and Evans, 2000b) was used to identify probability regions for existence of bodies (Fig. 1). With limits established for the regions of interest the sky area in the heliocentric frame can be easily determined using the standard solid angle integral $\int\int_S(\mathbf{r}\cdot\mathbf{n})/r^3\,dS$ (where $\mathbf{r}$ is the radius vector, $\mathbf{n}$ is the unit normal vector, and $r=|\mathbf{r}|$). Calculation of the geocentric solid angle, necessary for Earth-based observations, requires a transformation from the heliocentric reference. A numerical integration is performed with which we can calculate the sky area presented by any region from any position. This enables determination of the sky area for an Earth-based observer, or a space-based instrument such as the Gaia satellite which will be positioned at Earth's L2 Lagrangian point.

* Corresponding author. Tel.: +61 407089308.
E-mail address: michael.todd@icrar.org (M. Todd).

0032-0633/$ - see front matter © 2011 Elsevier Ltd. All rights reserved.
doi:10.1016/j.pss.2011.11.002

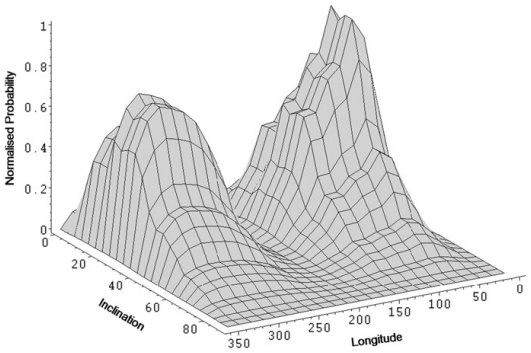

Fig. 1. Normalised probability contour for Earth Trojan bodies by inclination and Heliocentric longitude (degrees). The figure shows peak detection probabilities for longitudes consistent with the classical Lagrangian points but that bodies, while co-orbital with Earth, are unlikely to be co-planar.

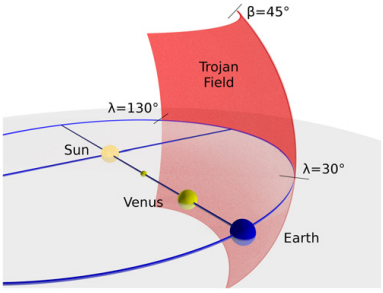

Fig. 2. Perspective illustration of Earth Trojan (L4) field. The field is bounded by Heliocentric longitude limits $30^\circ \leq \lambda \leq 130^\circ$ and inclination limit $\beta \leq 45^\circ$. A complementary field exists in the trailing Lagrangian L5 region.

The ET fields (Fig. 2) are bounded by the upper inclination limit (FWHM) of $\sim 45^\circ$ (Morais and Morbidelli, 2002) and heliocentric longitude limits (FWHM) of $30^\circ \lesssim \lambda \lesssim 130^\circ$ (L4 region) and $240^\circ \lesssim \lambda \lesssim 340^\circ$ (L5 region) (Tabachnik and Evans, 2000b). The heliocentric solid angle of each of these regions is 2.468 sr (8100 deg^2). The geocentric solid angle[1] of the L4 ET field is 1.066 sr (3500 deg^2). The time required to completely survey this area, several hours even for widefield survey telescopes (see Table 1), is greater than the amount of time the field is visible per day.

Selecting inclination limits of $10^\circ \lesssim \beta \lesssim 45^\circ$ (Fig. 3), based on the FWHM of the binned inclination distribution in Morais and Morbidelli (2002), reduces the sky area of the field to about 1300 deg^2 and includes $\sim 74\%$ of those simulated bodies. A widefield telescope can survey this field in a single session of about 1.5 hours (Table 2). A second set of observations is normally necessary for moving object detection. These paired sessions should be repeated at intervals of no more than three months since the field spans 100° longitude. Such a programme will take one year to complete. This strategy requires a significant amount of telescope time on these nights. This is not considered an optimal strategy as one aim is to have minimal impact on other activities.

[1] The Python code used to calculate these areas is available from the first author on request.

Table 1
Comparison of survey telescopes showing the required time to survey the entire field.

Telescope	Limiting mag.	Exposure (s)	FOV (deg^2)	Entire field		Instrument capabilities
				FOVs	Time (h)	
Catalina	$V \sim 20$	30	8.0	437	3.6	Drake et al. (2003)
Pan-STARRS	$R \sim 24$	30	7.0	499	4.2	Jedicke et al. (2007)
LSST[a]	$r \sim 24.7$	30	9.6	364	3.0	Jones et al. (2009)
Gaia[b]	$V \sim 20$		0.69	63		Mignard et al. (2007)

[a] The Large Synoptic Survey Telescope (LSST) is still in the development phase (www.lsst.org).

[b] Gaia will operate in a continuous scanning mode where the CCD array will be read out at a rate corresponding to the angular rotation rate of the satellite (6 h period). The FOV value represents the number of rotations by Gaia. Gaia's specific precession parameters are not considered so values should be considered as representative.

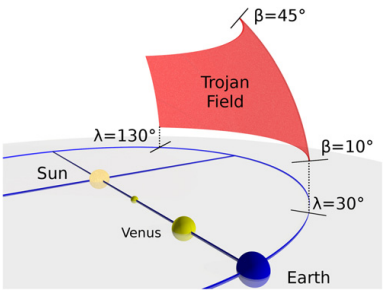

Fig. 3. The Earth Trojan (L4) target field ranges from Heliocentric longitude $30^\circ \leq \lambda \leq 130^\circ$ and latitude $10^\circ \leq \beta \leq 45^\circ$. A complementary field exists in the trailing Lagrangian L5 region. This illustration represents the search field in which a body will be observable some time during its orbit.

Table 2
Comparison of survey telescopes showing the required time for different survey strategies.

Telescope	Entire field		Restricted field		Ecliptic region		10° swath	
	FOVs	Time (h)	FOVs	Time (h)	FOVs	Time (min)	FOVs	Time (min)
Catalina	437	3.6	163	1.4	112	56	18	9
Pan-STARRS	499	4.2	186	1.6	128	64	20	10
LSST	364	3.0	136	1.2	94	47	15	8

A strategy which further reduces the per-session time is to survey a region bounded by the longitude limits and lower inclination limits to detect ETs as they cross the ecliptic. This reduces the sky area of the region to 900 deg^2 and results in a corresponding decrease in telescope time per-session (Table 2). The duration of this programme is six months as any Trojans detected in that six-month period would be crossing either to the North or to the South. However, the observations must be repeated at more frequent intervals since, in this region, the ET will have a higher apparent motion than at the highest or lowest points in its orbit, as indicated in Morais and Morbidelli (2002). As a consequence it will cross this region relatively quickly.

The result is that the total time requirement for the programme is not significantly reduced.

Gaia will operate in a continuous scanning mode and survey the whole sky, by rotating and precessing at a predetermined rate, to a limiting magnitude of $V \sim 20$ many times during its mission (Mignard et al., 2007). Without considering the precession rate, or its effect on Gaia's coverage of the Trojan regions, we reduce the calculation to consider only the minimum possible number of rotations to survey the entire field (Table 1). In this context the FOVs and time are incompatible to comparison because the operation is unalterable. Also, Gaia will effectively survey each field twice per cycle, taking narrow, slightly overlapping, swaths of the sky with each rotation.

Examination of Gaia's mode of operation leads us to the concept of surveying a swath and using Earth's revolution about the Sun to sweep out the field described in Fig. 3. This greatly reduces the time requirement per session as indicated in Table 2. A swath 10° wide reduces the per-session sky area to about 140 deg^2, reducing the imaging time to a few minutes. This strategy requires paired observing sessions on a weekly basis. The field is redefined at monthly intervals to repeat the survey of the target field. The length of this programme is one year, however, this programme has the advantage of minimal time per session. These observations can be conducted at the end of twilight, with the primary science missions continuing as normal during the night. We consider this strategy could be employed for an extended period with minimal impact on regular activities.

2.2. Mars Trojans

Similar problems exist in planning observations to search for additional Mars Trojans (MT). The MT fields are bounded by the upper inclination limit (FWHM) of 35° (Scholl et al., 2005) and heliocentric longitude limits (FWHM) of $50^\circ \lesssim \lambda \lesssim 80^\circ$ and $290^\circ \lesssim \lambda \lesssim 315^\circ$ (Tabachnik and Evans, 2000b) for the L4 and L5 regions, respectively. A synthesis of these models identifies probability regions for existence of bodies (Fig. 4). These regions each define a sky area (Fig. 5) of about 9500 deg^2 at opposition, almost three times larger than ET field. The changing geometry between Earth and Mars complicates a comprehensive analysis. At this time we examine the strategy considered optimal for the ET search, that of taking swaths of the field and using Earth's revolution about the Sun to sweep out the entire region, in the case of the MT field at opposition. A detailed study will be the subject of future work in this area.

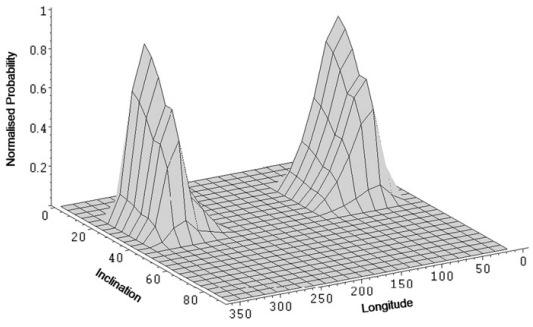

Fig. 4. Normalised probability contour for Mars Trojan bodies by Inclination and Heliocentric longitude (degrees). The figure shows peak detection probabilities for longitudes consistent with the classical Lagrangian points but that bodies, while co-orbital with Mars, are unlikely to be co-planar.

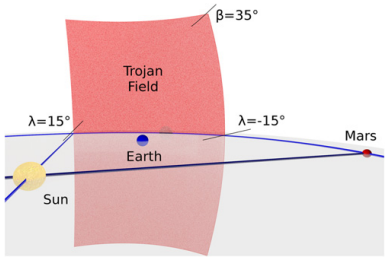

Fig. 5. Mars Trojan (L4) target field is bounded by Heliocentric longitudes $50^\circ \lesssim \lambda \lesssim 80^\circ$ and inclination limit $\beta \lesssim 45^\circ$. A complementary field exists in the trailing Lagrangian L5 region.

We find that, at opposition, it is still most efficient to take swaths of the MT field as Earth revolves past the field in its orbit. The sky area surveyed per-day can be the same as that for the ET field. The geocentric latitudes are greater than for the ET field, but the longitude range can be reduced accordingly. The major difference to be noted is that the range in Right Ascension and Declination can be redefined for each pair of observations to survey regions at opposition. Before and after opposition, when the relative position of Earth results in a smaller sky area for the MT fields, other strategies for surveying this region could be employed. This will be the subject of future investigation.

2.3. Telescope surveys

For ground-based telescopes, geographic location is a consideration. Observing with a telescope in a particular hemisphere increases the observing window in that hemisphere. This is at the expense of the complementary field, i.e. Northern Hemisphere sites have fields at Northern latitudes visible for a greater duration at the expense of the amount of time for which a Southern latitude field is visible due to Earth's axial inclination. Gaia, at the L2 Lagrangian point, will spend equal amounts of time surveying both Northern and Southern latitude fields.

The limitation in observable longitudes must also be considered. If observing begins when the Sun's altitude is 20° below the local horizon, a minimum observing altitude of 20° will survey longitudes with a Solar elongation of 40°. This still permits the greater part of the ET field, at greater elongations (Fig. 6), to be surveyed although low altitudes will be subject to greater atmospheric extinction.

Despite the small FOV of the Gaia satellite it has been included for comparison. Gaia does not suffer the limitation of local horizon and airmass affecting the available observing time. However, this advantage is mitigated by its limiting magnitude of $V=20$. Gaia has a defined orbit which prevents it observing targets of opportunity, however, its primary mission is to perform an all-sky survey. A similar observing restriction exists for Gaia where, by design, it is limited to a minimum Solar elongation of 45°. This corresponds to an elongation of $\sim 48^\circ$ for a ground-based telescope.

Observations of ETs are time-limited by the Earth–Sun-object geometry. This geometry also causes them to appear to be slow-moving but repeat imaging can be performed on subsequent days. MTs are less problematic for the obvious reason that observing opportunities do not have the same time constraints that are imposed by the specific geometry for ET observations.

While this delay between follow-up images introduces other variations due to such things as change in atmospheric conditions, seeing etc this could be compensated for by some image convolution. Some telescopes are implementing image processing

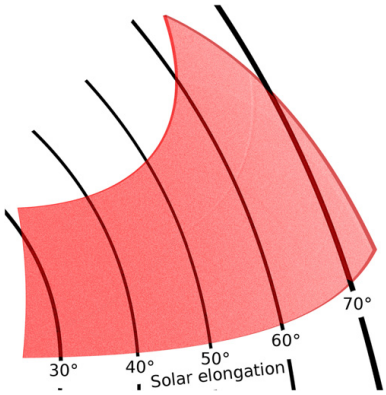

Fig. 6. Solar elongation across the Earth Trojan field ranges from 25° to 75°. This illustration represents the field from a geocentric perspective.

systems designed specifically for asteroid detection (e.g. Pan-STARRS+MOPS—Moving Object Processing System) where the asteroid is an apparently stationary transient because it is a very distant slow moving object (Jedicke et al., 2007). This method could be applied to nearer objects which are apparently slow moving as a result of the particular Earth–Sun-object positions at the time of observation.

3. Results

Surveys of the entire ET field within the chosen limits are impractical. The sky area of each field is too great to cover in the available time with current survey telescopes. However, it is possible to survey a region restricted by the upper and lower inclination limits. These surveys can be conducted at the beginning (L5 region) and end (L4 region) of the night. However, while possible, it may be impractical as this occupies a significant amount of telescope time on those nights. As the field spans $\sim 90^\circ$ in longitude the intervals between surveys would nominally be three months. This bears the risk of missing low-inclination ETs completely through not having yet entered the field or of having just exited the field. It also bears the risk of detecting ETs shortly before exiting the field towards the ecliptic, possibly requiring follow-up observations in a less favourable orientation to the local horizon. Reducing the intervals to two months results in a small amount of oversampling, reducing the risk of missing an ET. Assuming that only the Northern or Southern field could be surveyed depending on the location of the telescope, the programme length would be 1 year, the orbital period of an ET.

It is possible to conduct a survey in the ecliptic plane between latitude 0 and the lower limit of the field to search for ETs as they cross the ecliptic. This reduces the necessary time to survey the region as the ecliptic region is smaller. The time saving per session is about 30%. In addition the length of the programme is reduced to six months, as any Trojans detected in that period would be crossing either to the North or to the South. In this region the ET will have a higher apparent motion, crossing the region relatively quickly, and more frequent sampling is required. This outweighs the benefit of the shorter programme as the total time requirement is not significantly different to that required to survey the entire field over the period of one year.

Attempting to survey the entire ET field in a single session is challenging. However, observing a swath of sky in a particular range of Right Ascension and Declination and using Earth's revolution about the Sun to survey the field as it crosses the observed region requires minimal time each session, i.e. two sessions per week for one year. The observed region is redefined at monthly intervals so that the field is imaged again. This results in some oversampling of the field but has the benefit that lost nights due to adverse weather conditions become less critical to the overall programme.

Surveys of the MT field are only possible when the Sun–Earth–Mars geometry permits observations. A detailed study will be the subject of future work. In our initial assessment we find that surveys of the MT field at opposition are, in many ways, more difficult than the ET field as it occupies a much larger sky area. However, the field can be surveyed using the method of observing a swath of sky. As Earth passes the field during its revolution about the Sun the observations will progressively image the entire field. The range in Right Ascension and Declination must be redefined for each pair of observations so that the imaged region progresses across the MT field with Earth's revolution.

We note that Gaia's precession cycle, which limits observations to Solar elongations $>45^\circ$ (Mignard et al., 2007), also prevents observations at Solar elongations $>135^\circ$. This restricts Gaia from observing at opposition, hence such observations can only be made by other telescopes. The possibility of Gaia detecting MTs within its observable region will be addressed in future work.

4. Summary and future work

Despite the thousands of known Jupiter Trojans very few inner planet Trojans have been discovered. Simulations (Morais and Morbidelli, 2002) have predicted the existence of a number of Earth Trojans, but currently only one is known to exist (Connors et al., 2011). We note that this object, 2010 TK_7, would pass through the region described in this paper during its orbit. The prospect of detecting additional ETs is limited by the small amount of time available each day due to the Earth–Sun-ET geometry.

This paper has identified the region of highest probability for detection of ETs. We suggest an optimal strategy of observing a sub-region of the ET field and using Earth's revolution about the Sun to progressively survey the field. This approach takes only a few minutes per session, two days per week, and is readily achievable by a survey telescope such as Catalina or Pan-STARRS. While this method requires a programme of continued observations for one year, the total time commitment for the programme is a few tens of hours spread throughout that year.

A similar observing strategy is also suggested for the Mars Trojan field during its passage through opposition. The different, and changing, geometry of Earth with respect to MTs makes a detailed study more involved than the relatively static geometric condition of the ETs. Mars is our nearest planetary neighbour with known Trojans, with many more MTs predicted to exist (Tabachnik and Evans, 1999). The peculiarities of the changing geometry and the implications for a search for additional Mars Trojans will be explored in greater depth in the future.

The specific observing geometry of the Gaia satellite and its position at Earth's L2 Lagrangian point will be examined in more detail in future work. Gaia will not share the limitations of ground-based telescopes of atmosphere and local horizon. The primary limitations identified for Gaia are the limiting magnitude ($V \sim 20$) and its precession cycle which restricts observations to Solar elongations between 45° and 135° (Mignard et al., 2007). Results of detailed simulations for detection of Earth Trojans, with

particular regard to the detection limits and observational mode of operation of Gaia, will be reported in the future.

Follow-up after any initial detection by additional observations or other actions may be necessary to enable orbit computations and confirmations of discovery. Some of these tasks may be best handled by telescopes other than the survey telescope which made the initial detection. In the case of Gaia, a number of ground-based telescopes as a follow-up network for Solar System object detection is being developed (Thuillot et al., 2010).

Acknowledgments

The authors would like to thank the anonymous referees whose comments and suggestions significantly improved the final version of this manuscript. M. Todd thanks the organisers of the Gaia workshop (Pisa 2011) for providing a fertile environment for discussing Gaia science. D.M. Coward is supported by an Australian Research Council Future Fellowship.

References

Connors, M., et al., 2000. Bulletin of the American Astronomical Society 32, 1019.
Connors, M., Wiegert, P.,Veillet, C., 2011. Nature 475, 481.
Drake, A.J., et al., 2003. First results from the Catalina real-time transient survey. Astrophysical Journal 696, 870.
Dunbar, R.S., Helin, E.F., 1983. Estimation of an upper limit on the Earth Trojan asteroid population from Schmidt Survey Plates. Bulletin of the American Astronomical Society 15, 830.
Jedicke, R., Magnier, E.A., Kaiser, N., Chambers, K.C., 2007. The next decade of Solar System discovery with Pan-STARRS. In: Milani, A., Valsecchi, G.B., Vokrouhlický, D. (Eds.), Proceedings of the IAU Symposium 236, Near Earth Objects, Our Celestial Neighbours: Opportunity and Risk. , Kluwer, Dordrecht, pp. 341.
Jones, R.L., et al., 2009. Solar System Science with LSST. Earth, Moon, and Planets 105, 101.
Mignard, F., et al., 2007. The Gaia Mission: expected applications to asteroid science. Earth, Moon, and Planets 101, 97.
Mikkola, S., Innanen, K.A., 1990. Studies on solar system dynamics. II—the stability of Earth's Trojans. Astronomical Journal 100, 290.
Morais, M.H.M., Morbidelli, A., 2002. The population of near-Earth asteroids in coorbital motion with the Earth. Icarus 160, 1.
Pilat-Lohinger, E., Dvorak, R., Burge, C., 1999. Trojans in stable chaotic motion. Celestial Mechanics and Dynamical Astronomy 73, 117.
Scholl, H., Marzari, F., Tricarico, P., 2005. Dynamics of Mars Trojans. Icarus 175, 397.
Tabachnik, S., Evans, N.W., 1999. Cartography for Martian Trojans. Astrophysical Journal 517, L63.
Tabachnik, S., Evans, N.W., 2000a. Asteroids in the inner Solar system—I. Existence. Monthly Notices of the Royal Astronomical Society 319, 63.
Tabachnik, S., Evans, N.W., 2000b. Asteroids in the inner Solar system—II. Observable properties. Monthly Notices of the Royal Astronomical Society 319, 80.
Thuillot, W., Hestroffer, D., Tanga, P., 2010. Complementary ground-based observations for Solar System applications. EAS Publications Series 45, 237–242.
Whiteley, R.J., Tholen, D.J., 1998. A CCD Search for Lagrangian Asteroids of the Earth–Sun System. Icarus 136, 154.

Chapter 3

An optimal Earth Trojan asteroid search strategy

Todd, M., P. Tanga, D. M. Coward, M. G. Zadnik. 2012. "An optimal Earth Trojan asteroid search strategy." *Monthly Notices of the Royal Astronomical Society Letters* 420 (1): L28-L32. doi:10.1111/j.1745-3933.2011.01186.x.

Monthly Notices of the ROYAL ASTRONOMICAL SOCIETY LETTERS

Mon. Not. R. Astron. Soc. **420,** L28–L32 (2012) doi:10.1111/j.1745-3933.2011.01186.x

An optimal Earth Trojan asteroid search strategy

M. Todd,[1⋆] P. Tanga,[2] D. M. Coward[3] and M. G. Zadnik[1]

[1] *Department of Imaging and Applied Physics, Bldg 301, Curtin University, Kent St, Bentley, WA 6102, Australia*
[2] *Laboratoire Cassiopée, Observatoire de la Côte dAzur, BP 4229, 06304 Nice Cedex 04, France*
[3] *School of Physics, M013, The University of Western Australia, 35 Stirling Highway, Crawley, WA 6009, Australia*

Accepted 2011 November 3. Received 2011 November 3; in original form 2011 August 1

ABSTRACT

Trojan asteroids are minor planets that share the orbit of a planet about the Sun and librate around the L4 or L5 Lagrangian points of stability. They are important solar-system fossils because they carry information on early Solar system formation, when collisions between bodies were more frequent. Discovery and study of terrestrial planet Trojans will help constrain models for the distribution of bodies and interactions in the inner Solar system. Since the discovery of the first outer planet Trojan in 1906, several thousand Jupiter Trojans have been found. Of the terrestrial planets, there are four known Mars Trojans, and one Earth Trojan has been recently discovered. We present a new model that constrains optimal search areas, and imaging cadences for narrow and wide-field survey telescopes including the *Gaia* satellite for the most efficient use of telescope time to maximize the probability of detecting additional Earth Trojans.

Key words: methods: numerical – methods: observational – celestial mechanics – minor planets, asteroids: general – planets and satellites: general.

1 INTRODUCTION

Trojan asteroids are minor planets that share the orbit of a planet about the Sun and librate around the L4 and L5 Lagrangian points of stability. The L4 and L5 points are 60° ahead and behind, respectively, the planet in its orbit. Trojans represent the solution to Lagrange's famous triangular problem and appear to be stable on long time-scales (100 Myr–4.5 Gyr) (Pilat-Lohinger, Dvorak & Burger 1999; Scholl, Marzari & Tricarico 2005) in the *N*-body case of the Solar system. This raises the question whether the Trojans formed with the planets from the Solar nebula or were captured in the Lagrangian regions by gravitational effects. Studying the Trojans provides insight into the early evolution of the Solar system.

Since the discovery of the first Trojan in 1906 (Nicholson 1961), several thousand more have been found in the orbit of Jupiter. Of the terrestrial planets, four Trojans have been discovered in the orbit of Mars. There have been some attempts at searching for Earth Trojans (ET) (Dunbar & Helin 1983; Whiteley & Tholen 1998; Connors et al. 2000). Examination of a sky area of approximately 0.35 deg^2 by Whiteley & Tholen (1998) resulted in a crude upper limit on population estimates of ∼3 objects deg^{-2}, down to $R = 22.8$. The subsequent search by Connors et al. (2000) covered ∼9 deg^2, down to $R = 22$, with no ETs detected. Recent examination of data from the WISE satellite has resulted in the discovery of the first known ET (Connors, Wiegert & Veillet 2011).

⋆E-mail: michael.todd@icrar.org

The earlier non-discovery may be attributed to a lack of observations targeting regions in which ETs could be found. For example, the programmes to search for near-Earth asteroids (NEAs) generally employ observation strategies which survey regions having a higher probability of containing potential Earth impactors. Typically, these regions are near the plane of the ecliptic and do not specifically target the entire region of stability for ETs. The Earth–Sun–ET geometry requires observations at low altitudes with limited observing time, restricting the ability to make multiple or follow-up observations. This geometry also results in low apparent motion relative to field stars as the orbit arc is at an oblique angle to an observer on Earth. Other reasons for non-detection include small population and orbital inclinations outside the plane of the ecliptic. Asteroids which could be Trojan candidates would not be flagged for further study by routine surveys because their apparent motions would not match the parameters of the survey for follow-up.

Models (Mikkola & Innanen 1990; Tabachnik & Evans 2000a) indicate that ET-stable orbits have some inclination to the plane of the ecliptic, in the range of 10°–45°. Subsequent simulations (Morais & Morbidelli 2002) predict 0.65 ± 0.012 ETs with diameter >1 km and 16.3 ± 3.0 asteroids with diameter >100 m. The existence of the co-orbital asteroid 3753 Cruithne (Wiegert, Innanen & Mikkola 1997), and the recent discoveries of the horseshoe orbiter 2010 SO_{16} (Christou & Asher 2011) and L4 Trojan 2010 TK_7 (Connors et al. 2011), confirm the possibility of objects orbiting the Sun in 1:1 mean motion resonance with Earth. The question is how many and what size are the bodies that share Earth's orbit as Trojan asteroids.

Assuming Trojans are approximately evenly distributed between the L4 and L5 regions, then just one of these fields could be examined with the expectation that the other region would yield a similar result. However, it should be considered that, given the short window of opportunity for making ground-based optical observations near morning (L4 region) and evening twilight (L5 region), both regions should be surveyed. With this in mind, it is important to find the optimal strategy to maximize sky coverage and probability of detection given those time constraints.

This Letter employs a model probability distribution which we use to constrain optimal search areas and imaging cadences for efficient use of telescope time while maximizing the probability of detecting ETs.

2 MODEL

Existing models for ETs provide estimates on populations but not composition. This is an important factor considering that albedo depends on composition. In the most likely case, ETs may be of S-type (silicaceous) similar to NEAs and inner main-belt asteroids, or they may be of C-type (carbonaceous). This influences the detection limit as S-types have an albedo $p_v = 0.20$ and C-types have an albedo $p_v = 0.057$ (Warner, Harris & Pravec 2009). Calculations of absolute and apparent magnitudes for the classical L4 and L5 Lagrangian points, from Tedesco, Cellino & Zappala (2005) and Morais & Morbidelli (2002), are shown in Table 1, neglecting atmospheric extinction. Assuming S-types as the dominant class in the inner Solar system the apparent magnitude for an ET of 1-km diameter varies between $V = 17.9$ and 19.5 (Fig. 1), depending on the geometry across the field (Fig. 2). An ET of 100-m diameter varies in magnitude between $V = 22.9$ and 24.5 across the field in the same fashion.

A synthesis of the stable orbit inclination model (Morais & Morbidelli 2002) and heliocentric longitude model (Tabachnik & Evans 2000b) was used to identify probability regions where bodies are most likely to be (Fig. 3). The ET fields (Fig. 2) bounded by upper and lower inclination limits (full width at half-maximum, FWHM) of $10^\circ \lesssim \beta \lesssim 45^\circ$ include ∼74 per cent of bodies (Morais & Morbidelli 2002). The heliocentric longitude limits (FWHM) of

Table 1. Absolute and apparent magnitudes at the classical L4 and L5 Lagrangian points.

Type	Albedo	Diameter	Abs. mag. (H)	App. mag. (V)
S-type	0.20	1.0 km	17.37	18.9
		100 m	22.36	23.9
C-type	0.057	1.0 km	18.73	20.3
		100 m	23.73	25.3

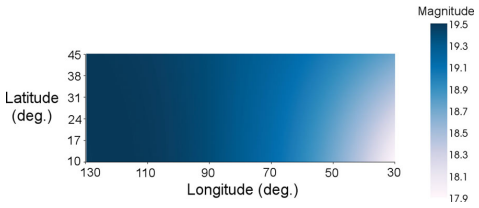

Figure 1. Apparent magnitude of a 1 km Earth Trojan by heliocentric longitude and latitude. The figure shows variation from $V = 17.9$ at the nearest part of the field (to Earth) to $V = 19.5$ at the farthest part.

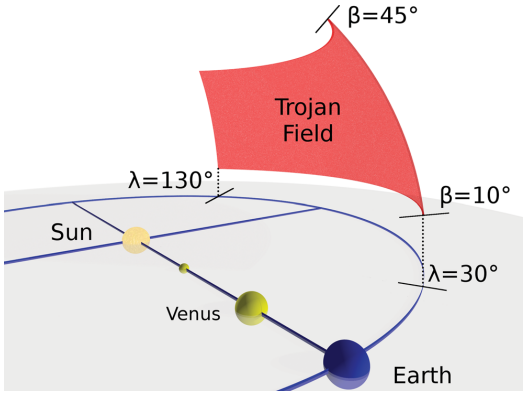

Figure 2. Perspective illustration of the Earth Trojan (L4) target field. The field ranges from heliocentric longitude (λ) 30° to 130° and latitude (β) 10° to 45°. A complementary field exists in the trailing Lagrangian L5 region. This illustration represents the field through which a body will pass during its orbit.

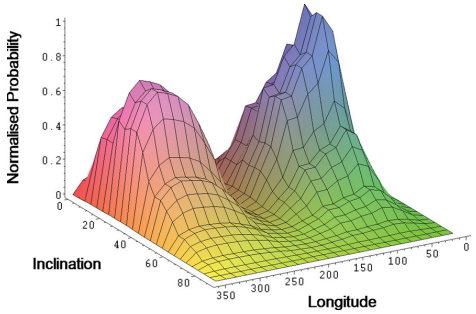

Figure 3. Normalized probability contour for Earth Trojan bodies by inclination and heliocentric longitude (degrees). The figure shows peak detection probabilities for longitudes consistent with the classical Lagrangian points but that bodies, while co-orbital with Earth, are unlikely to be co-planar.

$30^\circ \lesssim \lambda \lesssim 130^\circ$ (L4 region) and $240^\circ \lesssim \lambda \lesssim 340^\circ$ (L5 region) include ∼45 and 40 per cent of bodies, respectively (Tabachnik & Evans 2000b). The regions bounded by these limits enclose ∼63 per cent of projected bodies. The recently-discovered ET, 2010 TK_7 (Connors et al. 2011), has inclination $i = 20.^\circ88$ and mean longitude within the limits for the L4 region.

The heliocentric solid angle of each region is 0.931 sr (3056 deg^2). Calculation of the geocentric solid angle, necessary for Earth-based observations, requires a transformation from the heliocentric reference. A numerical integration is performed using the standard solid angle integral $\iint_S (\boldsymbol{r} \cdot \boldsymbol{n}) / r^3 \mathrm{d}S$ (where $\boldsymbol{r}$ is the distance vector from the geocentre to the surface $\mathrm{d}S$, $\boldsymbol{n}$ is the unit vector normal to that surface, and $r = |\boldsymbol{r}|$) to determine the solid angle subtended at points other than the centre. This integration enables the calculation of sky area[1] for the heliocentric surface, from the geocentre either for an Earth-based observer or for a space-based instrument such as the *Gaia* satellite, which will be located near the Earth's L2

[1] The PYTHON code used to calculate these solid angles is available from the author on request.

Lagrangian point (Mignard et al. 2007). The calculated geocentric solid angles are 0.3948 sr (1296 deg^2) and 0.4451 sr (1461 deg^2) for the L4 and L5 regions, respectively. From the L2 Lagrangian point, for the *Gaia* satellite, the solid angles are 0.3855 sr (1265 deg^2) and 0.4310 sr (1415 deg^2). The variation between regions is due to the slight differences in positions relative to Earth.

2.1 Telescope surveys

Having identified the ET fields, we consider the ability of current and proposed wide-field telescopes to survey these regions. It is clear from the size of the regions (>1000 deg^2) that a wide-field survey telescope would be needed for any attempt at surveying the entire region. However, even existing telescopes with the widest fields of view (FOVs) would barely be able to survey the entire region once in a single day due to observing constraints imposed by the Earth–Sun–ET geometry.

We also consider the implications for a space-based telescope with the impending launch of the *Gaia* satellite. *Gaia* will not be subject to the same constraints as ground-based telescopes. Although *Gaia* has a relatively small FOV, it will operate in a continuous scanning mode. It will image all of the sky down to a solar elongation of 45° (Mignard et al. 2007), but without the observational limitation of local horizon and airmass. However, this advantage is mitigated by its limiting magnitude of $V = 20$.

The continuous-scanning operation mode of *Gaia* leads to the concept of a strategy of observing a swath of the region, a range in right ascension and declination defining a particular subregion. Observations can be made of that defined region, repeated twice per week, and making use of Earth's revolution about the Sun to progressively survey the target field. A 10°-wide swath (Fig. 4) would be imaged in minutes by a survey telescope, as shown in Table 2. The region is redefined at monthly intervals to recommence the survey. Thus, each month the target field passes through the observed region. In this fashion, the entire field is resampled over a period of 1 year. This can be done at the beginning and end of the night, requiring minimal telescope time, before and after the primary science missions.

Observations of ETs are time-limited by the geometry of the Earth–Sun–ET positions. There exist specific constraints particular to the geographic location of a telescope. For example, Northern hemisphere telescopes will have access to the entire northern part of the ET region described in Fig. 2, while Southern hemisphere telescopes will have access to only that portion visible above the local horizon. Some seasonal variation will occur with the change in relative orientations throughout the year, as noted in Whiteley & Tholen (1998). The amount of variation will depend on geographic location.

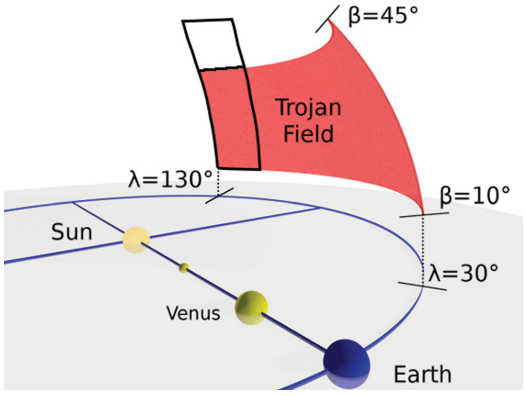

Figure 4. Observing a defined range in right ascension and declination, with Earth's revolution about the Sun, results in the entire field being imaged as it passes across the observed region.

By the end of evening twilight when it becomes possible to survey the L5 region, assuming (for convenience) the Sun's altitude is −20°, the classical Lagrangian point has an altitude of about 40°. Hence, atmospheric extinction on detection limits must be considered. Because there are many contributing factors to atmospheric extinction, reference to the 'average' approximation given by Green (1992) suggests the extinction at 40° altitude is 0.44 mag and at 25° altitude is 0.66 mag for a site at sea level.

The stable orbits of the ETs have been modelled to have an inclination range of 10°–45° (Morais & Morbidelli 2002). The heliocentric longitude ranges (FWHM) are 30°–130° and 240°–340° for L4 and L5, respectively (Tabachnik & Evans 2000b). Since the modelled orbits are inclined at some angle to the ecliptic, the survey could be carried out in the upper or lower ecliptic latitudes (β) at $10° \leq \beta \leq 45°$ and $-10° \leq \beta \leq -45°$. By surveying fields in those latitudes the transverse motion per unit time is reduced. To an Earth-based observer an ET will appear to oscillate in an up-and-down motion about the plane of the ecliptic during its orbit about the Sun. The exhibited transverse motion will appear sinusoidal, with the apparent transverse motion reaching minimum at the extremes of its heliocentric latitude and reaching maximum when crossing the ecliptic plane.

It is impossible, a priori, to predict the direction of motion for the ET. Consequently, it is not possible to apply a tracking offset for the apparent motion to increase the detection limit. A suitable alternative is to observe with the intention of imaging the ET at maximum heliocentric latitude when the apparent motion is at minimum. As it will then appear to be a slow-moving object, follow-up becomes difficult in the same night. However, repeat imaging can be performed on subsequent days rather than trying to acquire follow-up images during the same session. This approach also has the advantage of increasing the available observing time for a target field, if necessary.

While this delay between follow-up images introduces other variations from such things as changes in atmospheric conditions and seeing, this could be compensated for by image convolution. Some telescopes are implementing image processing systems designed specifically for asteroid detection (e.g. Pan-STARRS+MOPS – Moving Object Processing System) where the asteroid is an apparently stationary transient because it is a very distant slow-moving object (Jedicke et al. 2007). This method can be applied to nearer objects which are apparently slow moving as a result of the particular Earth–Sun–MP positions at the time of observation.

3 RESULTS

Surveys of the entire field within the chosen limits are impractical on telescopes with small FOV but are reasonable on survey telescopes with sufficient FOV to accomplish the task in a single night, such as Catalina or the Large Synoptic Survey Telescope (LSST).[2] In these cases, it may be possible to survey the regions defined by the inclination limits at intervals of approximately 2 months. This

[2] The LSST is still in the development phase (www.lsst.org).

Table 2. Comparison of different survey telescopes showing the required time to survey the entire field compared to an optimal strategy of observing a 10° swath and using Earth's revolution to sweep across the field.

Telescope	Limiting mag.	Exposure (s)	FOV	Entire field		10° swath		Instrument capabilities
				FOVs	Time	FOVs	Time (min)	
Catalina	$V \sim 20$	30	8.0 deg^2	162/183	1.35 h/1.5 h	12–18	6–9	Drake et al. (2003)
PTF 1.2 m	$R \sim 20.6$	60	8.1 deg^2	160/180	2.7 h/3 h	12–18	12–18	Law et al. (2009)
Pan-STARRS	$R \sim 24$	30	7.0 deg^2	185/209	1.5 h/1.7 h	13–20	7–10	Jedicke et al. (2007)
LSST	$r \sim 24.7$	30	9.6 deg^2	135/152	1.1 h/1.3 h	10–15	5–8	Jones et al. (2009)
Gaia	$V \sim 20$	39.6[a]	0.69°	63/74	378 h/444 h[b]			Mignard et al. (2007)

[a] *Gaia* will operate in a continuous scanning mode where the CCD array will be read out at a rate corresponding to the angular rotation rate of the satellite (6-h period). The FOV value represents the number of rotations by *Gaia*. *Gaia*'s specific precession parameters are not considered, so values should be considered as representative.
[b] Approximate time to complete sufficient rotations to scan across the entire field. The actual time spent scanning within the field will be a fraction of this value.

requires the fields to be surveyed twice within a few days. These surveys can be conducted at the beginning (L5 region) and end (L4 region) of the night. Although this is possible, it may be impractical as this occupies a significant amount of telescope time on those nights.

As the field spans 90° in longitude, the intervals could nominally be 3 months. This increases the risk of missing low-inclination ETs completely through not having yet entered the field or of having just exited the field. It also increases the risk of detecting ETs shortly before exiting the field towards the ecliptic, possibly requiring follow-up observations in a less favourable orientation to the local horizon. By observing at intervals of 2 months, a small amount of oversampling is introduced and the risk of missing an ET is reduced. On the assumption that only the northern or southern field could be surveyed depending on the location of the telescope, the programme length would be 1 year, the length of the orbital period of a Trojan as it would pass through this field once per revolution.

It is possible to conduct a survey in the ecliptic plane between latitude 0 and the lower limit of the field to search for Trojans as they cross the ecliptic. This reduces the necessary time per session to survey the region as the ecliptic region is smaller than the ET field. The length of this programme is reduced, requiring six months. Any Trojans detected in that 6-month period would be crossing either to the north or to the south. However, the time saving per session is only about 30 per cent and requires more frequent sampling since, in this region, the ET will have a higher apparent motion. This could outweigh any benefit in the reduced per-session length as the total time requirement is not significantly different to that required to survey the entire field over the period of 1 year.

Attempting to survey the entire field in a single session is challenging. The desirability of minimizing the time per session is our key objective. Observing a swath of sky in a particular range of right ascension and declination, and using Earth's revolution about the Sun to survey the field as it crosses the observed region, achieves this aim. This approach requires minimal time each session, i.e. two sessions per week during the course of 1 year. The observed region is redefined at monthly intervals to recommence sampling of the field. Some oversampling will occur as the field crosses the observed region. This results in nights lost due to adverse weather conditions becoming less critical to the overall programme.

4 SUMMARY AND FUTURE WORK

Despite the thousands of known Jupiter Trojans, of the terrestrial planets a mere handful of Trojans have been discovered. There are only four known Mars Trojans, and the first ET has only been very recently discovered (Connors et al. 2011). Simulations (Morais & Morbidelli 2002) have predicted the existence of a number of ETs. The prospect of detecting these is limited by the small amount of time available per day due to the Earth–Sun–ET geometry. This implies that the conventional approach to detecting asteroids by repeated observations of a field must have cadence times in days rather than hours.

Surveys of the entire ET field are impractical due to the observational limits imposed by the geometry, and the many hours it would take to conduct such a survey. This Letter has identified the region of highest probability for detection, in the inclination range of 10°–45° and heliocentric longitude range of 30°–130° (L4) and 240°–340° (L5). The sky area for Earth-based observers has been determined using numerical integrations. A strategy has been proposed for observing a sub-region of the ET field and using Earth's revolution about the Sun to progressively survey the field as it crosses this subregion. This approach takes only a few minutes per session, two days per week, and is readily achievable by a survey telescope before or after the primary science mission. While this method requires a programme of continued observations for 1 year, the total time commitment for the programme is a few tens of hours spread throughout that year. We note that the only known ET, 2010 TK_7, would pass through this region during its orbit.

The specific observing geometry of the *Gaia* satellite and its position at Earth's L2 Lagrangian point will be examined in more detail in future work. Initial simulations for the detection of Trojans by *Gaia* show promise (Mignard, private communication). Results of detailed simulations will be reported with particular regard to the detection limits and observational mode of operation of *Gaia*.

The different, and changing, geometry of the Earth–Mars Trojan relationship makes a detailed study more involved than the relatively static geometric condition of the ETs. As our nearest planetary neighbour with known Trojans, and the prediction that many more should exist in Mars' orbit (Tabachnik & Evans 1999), a similar modelling exercise is in progress. The peculiarities of the changing geometry and the implications for a search for additional Mars Trojans will be explored in greater depth.

The search area defined for ETs may also result in the detection of inner-Earth objects (IEOs), asteroids with orbits interior to Earth's orbit about the Sun, as they pass across the field. To date, there have been nine IEOs discovered; however, the predicted number is 36 ± 26 with diameter >1 km and 530 ± 240 with diameter >250 m (Zavodny et al. 2008). Further work is required to examine the potential for discovery of these IEOs during an ET search.

ACKNOWLEDGMENTS

The authors would like to thank the anonymous referee whose comments and suggestions significantly improved the final version of this manuscript. MT thanks the organizers of the *Gaia* workshop (held in Pisa, Italy, 2011) for providing a fertile environment for discussing *Gaia* science. DMC is supported by an Australian Research Council Future Fellowship.

REFERENCES

Christou A. A., Asher D. J., 2011, MNRAS, 414, 2965
Connors M. et al., 2000, BAAS, 32, 1019
Connors M., Wiegert P., Veillet C., 2011, Nat, 475, 481
Drake A. J. et al., 2003, ApJ, 696, 870
Dunbar R. S., Helin E. F., 1983, BAAS, 15, 830
Green D. W. E., 1992, Int. Comet Q., 14, 55
Jedicke R., Magnier E. A., Kaiser N., Chambers K. C., 2007, in Milani A., Valsecchi G. B., Vokrouhlický D., eds, Proc. IAU Symp. 236, Near Earth Objects, Our Celestial Neighbours: Opportunity and Risk. Kluwer, Dordrecht, p. 341
Jones R. L. et al., 2009, Earth Moon Planets, 105, 101
Law N. M. et al., 2009, PASP, 121, 1395
Mignard F. et al., 2007, Earth Moon Planets, 101, 97
Mikkola S., Innanen K. A., 1990, AJ, 100, 290
Morais M. H. M., Morbidelli A., 2002, Icarus, 160, 1
Nicholson S. B., 1961, Astron. Soc. Pac. Leaflets, 8, 239
Pilat-Lohinger E., Dvorak R., Burge Ch., 1999, Celest. Mech. Dyn. Astron., 73, 117
Scholl H., Marzari F., Tricarico P., 2005, Icarus, 175, 397
Tabachnik S., Evans N. W., 1999, ApJ, 517, L63
Tabachnik S., Evans N. W., 2000a, MNRAS, 319, 63
Tabachnik S., Evans N. W., 2000b, MNRAS, 319, 80
Tedesco E. F., Cellino A., Zappala V., 2005, AJ, 129, 2869
Warner B. D., Harris A. W., Pravec P., 2009, Icarus, 202, 134
Whiteley R. J., Tholen D. J., 1998, Icarus, 136, 154
Wiegert P. A., Innanen K. A., Mikkola S., 1997, Nat, 387, 686
Zavodny M., Jedicke R., Beshore E. C., Bernardi F., Larson S., 2008, Icarus, 198, 284

This paper has been typeset from a TEX/LATEX file prepared by the author.

Chapter 4

An optimal Mars Trojan asteroid search strategy

Todd, M., P. Tanga, D. M. Coward, M. G. Zadnik. 2012. "An optimal Mars Trojan asteroid search strategy." *Monthly Notices of the Royal Astronomical Society* 424 (1): 372-376. doi:10.1111/j.1365-2966.2012.21204.x.

Monthly Notices
of the
ROYAL ASTRONOMICAL SOCIETY

Mon. Not. R. Astron. Soc. **424,** 372–376 (2012) doi:10.1111/j.1365-2966.2012.21204.x

An optimal Mars Trojan asteroid search strategy

M. Todd,[1⋆] P. Tanga,[2] D. M. Coward[3] and M. G. Zadnik[1]

[1]*Department of Imaging and Applied Physics, Building 301, Curtin University, Kent Street, Bentley, WA 6102, Australia*
[2]*Laboratoire Cassiopée, Observatoire de la Côte dAzur, BP 4229, 06304 Nice, Cedex 04, France*
[3]*School of Physics, M013, The University of Western Australia, 35 Stirling Highway, Crawley, WA 6009, Australia*

Accepted 2012 April 27. Received 2012 April 10

ABSTRACT

Trojan asteroids are minor planets that share the orbit of a planet about the Sun and librate around the L4 or L5 Lagrangian points of stability. Although only three Mars Trojans have been discovered, models suggest that at least 10 times this number should exist with diameters $\geq$1 km. We derive a model that constrains optimal sky search areas and present a strategy for the most efficient use of telescope survey time that maximizes the probability of detecting Mars Trojans. We show that the *Gaia* space mission could detect any Mars Trojans larger than 1 km in diameter, provided the relative motion perpendicular to *Gaia's* CCD array is less than 0.40 arcsec s^{-1}.

Key words: methods: numerical – methods: observational – celestial mechanics – minor planets, asteroids: general – planets and satellites: general.

1 INTRODUCTION

Trojan asteroids are minor planets that share the orbit of a planet about the Sun and librate around the L4 and L5 Lagrangian points of stability. The L4 and L5 points are 60° ahead and behind, respectively, the planet in its orbit. Trojans represent the solution to Lagrange's famous triangular problem and appear to be stable on long time-scales (100 Myr to 4.5 Gyr) (Pilat-Lohinger, Dvorak & Burger 1999; Scholl, Marzari & Tricarico 2005) in the *N*-body case of the Solar system. This raises the question whether the Trojans formed with the planets from the solar nebula or were captured in the Lagrangian regions by gravitational effects. Studying the Trojans provides insight into the early evolution of the Solar system.

Since the discovery of the first Trojan in 1906 (Nicholson 1961) several thousand more have been found in the orbit of Jupiter. Among the terrestrial planets only Earth and Mars are known to have Trojans. While Earth has only a single known Trojan (2010 TK_7) which was discovered through examination of data from the *WISE* satellite (Connors, Wiegert & Veillet 2011), Mars presently has three known Trojans (5261 Eureka, 1998 VF_{31} and 1999 UJ_7) listed by the Minor Planet Center. Previous modelling (Tabachnik & Evans 1999, 2000a,b) suggests that this number represents less than one-tenth of the Mars Trojan (MT) population with diameter $\geq$1 km and that there may be in excess of 100 with diameter $\geq$100 m.

Non-discovery of additional MTs may be attributed to a lack of observations targeting regions in which MTs could be found, or their apparent motion being similar to inner main belt objects. Programmes to search for near-Earth asteroids (NEA) may flag objects with high apparent motion for further study, while slower moving objects are noted but may not be specifically followed up. NEA search regions are near the plane of the ecliptic and do not specifically target the entire region of stability for MTs. Observations are also limited to periods when the MT regions are visible from Earth. Other reasons for non-detection include the relatively small population and orbital inclinations outside the plane of the ecliptic. Asteroids which could be Trojan candidates would not be flagged for further study by routine surveys because their apparent motions would not match the parameters of the survey for follow-up.

The spatial separation between the regions allows the L5 (trailing) region to be surveyed while Mars approaches opposition, and the L4 (leading) region surveyed when Mars has passed opposition. This affords a period of several months during which these regions could each be fully surveyed. Even with such relative flexibility in the available observing period, in contrast to searching for Earth Trojans (Todd et al. 2012b), it is still important to find the optimal strategy for efficient use of telescope time while maximizing sky coverage and probability of detection.

This paper employs a model probability distribution which we use to constrain optimal search areas and imaging cadences for efficient use of telescope time while maximizing the probability of detecting MTs. We examine in greater depth the case of detecting MTs from the initial study of inner planet Trojans (Todd, Coward & Zadnik 2012a).

2 MODEL

Existing models (Tabachnik & Evans 1999, 2000a,b) provide estimates of MT populations, and some studies of the composition of known MTs have been made. Rivkin et al. (2003) found that (5261) Eureka and (101429) 1998 VF_{31} are most likely Sa- or A-class asteroids and that (121514) 1999 UJ_7 may be of X-class. This is an

⋆E-mail: michael.todd@icrar.org

Table 1. Absolute and apparent magnitudes at opposition, with apparent magnitudes for objects at perihelion and aphelion assuming eccentricity similar to that of Mars.

Class	Albedo	Diameter	Abs. mag. (H)	App. mag. (V) Peri.	Aph.
S-class	0.203	1.0 km	17.35	16.2	17.4
		100 m	22.35	21.2	22.4
C-class	0.057	1.0 km	18.73	17.6	18.8
		100 m	23.73	22.5	23.8

important consideration since albedo can vary greatly depending on composition. It is likely that other MTs will be relatively high albedo S-class (silicaceous) asteroids similar to NEAs and inner main belt asteroids, although there may be C-class (carbonaceous) asteroids. This affects the detection limit as S-class asteroids have a typical albedo of $p_v = 0.203$, X-class asteroids have $p_v = 0.174$ and C-class asteroids have $p_v = 0.057$ (Warner, Harris & Pravec 2009). In this paper calculations are made using these albedo values for S- and C-class asteroids to set limits on calculated magnitudes.

Calculations of absolute and apparent magnitudes at opposition using the methods described in Tedesco, Cellino & Zappala (2005) and Morais & Morbidelli (2002) are shown in Table 1, neglecting atmospheric extinction. Assuming S-class as the dominant class in the inner Solar system, and that an MT has an eccentricity similar to that of Mars, the apparent magnitude for an MT of 1-km diameter varies between $V = 16.2$ at opposition to $V = 20.7$ at a solar elongation of 60° (Fig. 1) with the field at perihelion. An MT of 100-m diameter varies in magnitude between $V = 21.2$ and 25.7 across this elongation range in the same fashion. If the field is at aphelion the brightness ranges from $V = 17.4$ to 20.3 (1-km diameter) and $V = 22.4$ to 25.3 (100-m diameter).

Mikkola & Innanen (1994) found that MT orbits are only stable within the inclination ranges of $15^\circ \lesssim i \lesssim 30^\circ$ and $32 \lesssim i \lesssim 44^\circ$ over an integration period of 4 Myr. Tabachnik & Evans (1999) mapped stable inclinations, finding that inclinations of $15^\circ \lesssim i \lesssim 30^\circ$ were more favourable. Scholl et al. (2005) refined this result, finding that objects with inclinations $\gtrsim 35^\circ$ become destabilized over longer periods. These orbit inclination models, and the heliocentric longitude model of Tabachnik & Evans (2000b), were used to identify regions where bodies are most likely to exist (Fig. 2).

The MT fields (Fig. 3) are bounded by the upper inclination limit of 35° and heliocentric longitude limits (full width at half-maximum) of $40^\circ \lesssim \lambda \lesssim 90^\circ$ (L4 region) and $270^\circ \lesssim \lambda \lesssim 320^\circ$ (L5 region). About ~69 per cent of the projected bodies exist within these regions. We assume the distribution of bodies between the L4 and L5 regions is approximately equal.

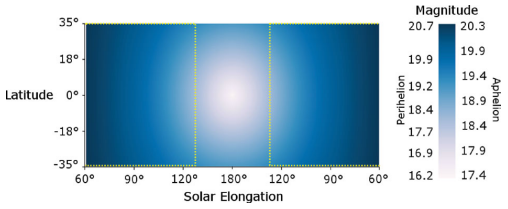

Figure 1. Apparent magnitude of a 1-km MT by solar elongation and heliocentric latitude. Brightness ranges from $V = 17.4$ at opposition (180°) to $V = 20.3$ at a solar elongation of 60° when the field is at aphelion, and ranges from $V = 16.2$ to 20.7 when the field is at perihelion. Elongations ≤135° lie within *Gaia*'s scanning limit (yellow dotted line).

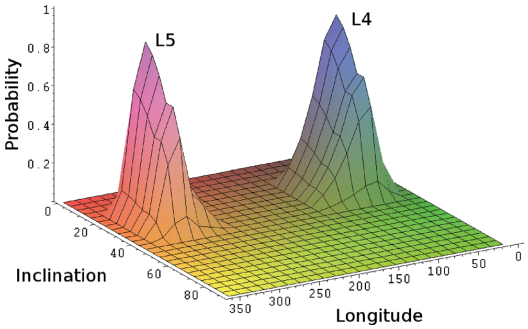

Figure 2. Probability distribution for MT bodies by inclination and heliocentric longitude (degrees). The figure shows peak detection probabilities for longitudes consistent with the classical Lagrangian points, but that bodies, while co-orbital with Mars, are unlikely to be coplanar.

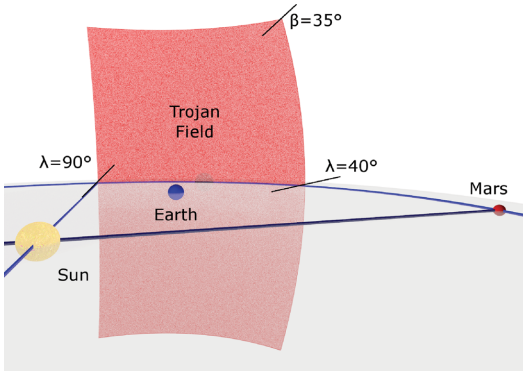

Figure 3. Perspective illustration of MT (L4) target field. The field ranges from heliocentric longitude (λ) 40° to 90° and latitude (β) −35° to 35°. A complementary field exists in the trailing Lagrangian L5 region. This illustration represents the region in which Trojans are expected to be found, with the classical Lagrangian point at opposition.

The heliocentric solid angle of each MT field is 1.0 sr (3280 deg^2). Calculation of the geocentric solid angle, necessary for Earth-based observations, requires a transformation from the heliocentric reference. A numerical integration is performed using the solid angle integral described in Todd et al. (2012b) to determine the sky area for an Earth-based observer or a space-based instrument such as the *Gaia* satellite,[1] which will be located near the Earth's L2 Lagrangian point (Mignard et al. 2007), for the observer's position relative to the field.

Calculations are made for Earth's longitude corresponding to the aphelion and perihelion longitudes of Mars' orbit to determine the upper and lower limits on maximum sky area. The calculated geocentric solid angles are 3.32 sr (10 900 deg^2) and 5.14 sr (16 900 deg^2) for the fields at opposition at aphelion and perihelion, respectively. With the field centres at a solar elongation of 60° the fields are 0.68 sr (2240 deg^2) and 0.62 sr (2040 deg^2) for Earth at

[1] http://gaia.esa.int

Mars' aphelion and perihelion longitudes, respectively. For *Gaia*, at the L2 Lagrangian point, these values differ by less than 1.5 per cent from the values calculated for Earth. Although *Gaia's* orbit prevents observing regions at opposition, it will survey elongations from 45° to 135°.

3 TELESCOPE SURVEYS

The ability of current and proposed wide-field survey telescopes to survey the regions where Trojans are likely to be found in the orbits of Earth and Mars was first examined in Todd et al. (2012a). It was found that the large sky area, particularly when the region is at opposition, would require a wide-field telescope to survey the entire region. Attempting to complete such a survey in a single day was found to be time consuming and inefficient.

Table 2 compares the relative capabilities of selected survey telescopes to cover the entire MT region at opposition and at a solar elongation of 60°. We show that there exists up to eightfold difference in area, and hence time required, between the region at opposition and at 60° elongation. Although the *Gaia* satellite has a narrow field of view (FOV), it has been included since it will operate in a continuous scanning mode and its orbit will enable it to image all of the sky to a solar elongation of 45° (Mignard et al. 2007). *Gaia* will not be affected by the constraints of local horizon and airmass experienced by ground-based telescopes; however, this advantage is mitigated by its limiting magnitude of $V = 20$.

The strategy of observing a swath of the region and progressively imaging the entire field over a period of time (Todd et al. 2012b) is suggested as an optimal method of searching for MTs. By imaging a swath of sky between the upper and lower latitude limits, the entire field can be surveyed over time as Earth (and Mars) revolves about the Sun. A single FOV-wide swath would be imaged in minutes by a survey telescope, as shown in Table 3. Whether the traditional approach of comparing images for moving object detection or flagging uncatalogued sources, the cadence is determined by the telescope FOV.

The relative geometry of Earth and Mars means that in a 2-yr period Mars is not visible for about 3 months either side of conjunction. The same applies to the MT fields, but it also means the when the L4 field is at conjunction, the L5 field is at least partly visible. This allows the fields to be surveyed over an extended period, or at different elongations in a synodic period. Defining specific regions and progressively observing the field over an extended period allows the entire field to be surveyed with efficient use of telescope time, and the observations accommodated around the primary science missions.

On approach to the trailing edge of the L5 MT region, observations can be made in the morning before sunrise. Thus end-of-night observations could be set to image across L5 on approach. When Mars is near opposition, morning observations can be made of the L4 region and evening observations can be set up to re-cover the L5 region. After the L4 region has passed opposition evening observations can be made to re-cover that region. Morning observations will

Table 2. Comparison of different survey telescopes showing the required time to survey the entire field at opposition and at a solar elongation of 60°. At opposition the sky area ranges from 10 900 deg^2 (aphelion) to 16 900 deg^2 (perihelion), while at an elongation of 60° it ranges from 2240 deg^2 (aphelion) to 2040 deg^2 (perihelion).

Telescope	Limiting mag.	Exposure (s)	FOV	Opposition		60° elongation		Instrument capabilities
				FOVs	Time (h)	FOVs	Time (h)	
Catalina	$V \sim 20$	30	8.0 deg^2	1360–2110	11.3–17.6	280–255	2.3–2.1	(Drake et al. 2009)
PTF 1.2 m	$R \sim 20.6$	60	8.1 deg^2	1345–2085	22.4–34.8	277–252	4.6–4.2	(Law et al. 2009)
Pan-STARRS	$R \sim 24$	30	7.0 deg^2	1555–2415	13.0–20.1	320–292	2.7–2.4	(Jedicke et al. 2007)
LSST	$r \sim 24.7$	30	9.6 deg^2	1135–1760	9.5–14.7	234–213	2.0–1.8	(Jones et al. 2009)
Gaia	$V \sim 20$	39.6[a]	0.69° wide	160–195[b]		55–50[b]	330–300[c]	(Mignard et al. 2007)

[a] *Gaia* will operate in a continuous scanning mode where the CCD array will be read out at a rate corresponding to the angular rotation rate of the satellite (6-h period).
[b] *Gaia*'s orbit parameters prevent observations within 45° of opposition. These values represent how many rotations it would take for *Gaia* to survey a region of this size. *Gaia*'s specific precession parameters are not considered, so values should be considered as representative.
[c] Approximate time to complete sufficient rotations to scan across the entire field. The actual time spent scanning within the field will be a fraction of this value.

Table 3. Comparison of different survey telescopes showing the required time to survey a single swath of one CCD width or detector width of the field at opposition compared to a solar elongation of 60°. At opposition, the height of the field ranges from 66° (aphelion) to 83° (perihelion) above the ecliptic plane, while at an elongation of 60° the height is ∼30°.

Telescope	Opposition		120° elongation		60° elongation	
	FOVs	Time (min)	(FOVs)	(Time)	(FOVs)	(Time)
Catalina	47–59	23.5–29.5	37–46	18.5–23	21–22	10.5–11
PTF 1.2 m	47–59	47–59	37–46	37–46	21–22	21–22
Pan-STARRS	50–63	25–31.5	40–49	20–24.5	22–23	11–11.5
LSST	43–54	21.5–27	34–42	17–21	19–20	9.5–10
Gaia[a]		131–166[b]		104–130		60–61

[a] *Gaia* will operate in a continuous scanning mode where the CCD array will be read out at a rate corresponding to the angular rotation rate of the satellite (6-h period). *Gaia*'s specific precession parameters are not considered, so values should be considered as representative.
[b] *Gaia*'s orbit parameters prevent observations within 45° of opposition.

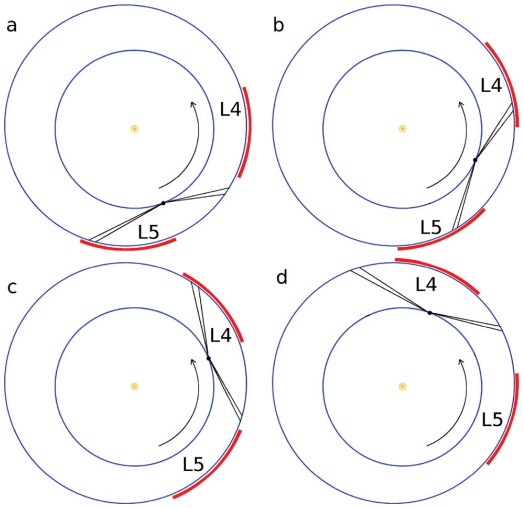

Figure 4. Observing a defined region of the sky, with Earth's orbit about the Sun, implies the entire field can be imaged. The passage of time between each position from 4(a) to 4(d) is about 1.5 months.

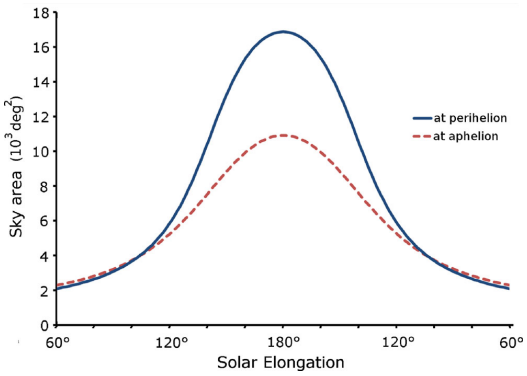

Figure 5. The sky area of each region varies from ∼2000 deg^2 at a solar elongation of 60° to 11 000–17 000 deg^2 at opposition (180°). The change in distance between Earth's and Mars' orbit, primarily due to Mars' eccentricity, significantly affects the sky area when the field is near opposition.

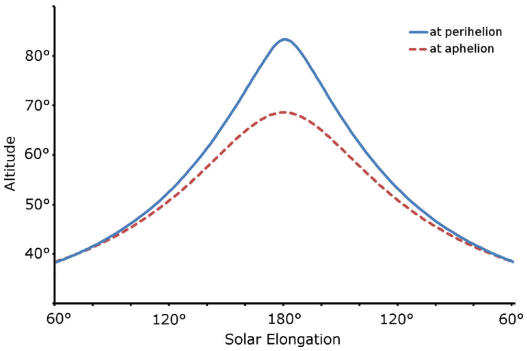

Figure 6. The angular height of the MT field above (and below) the ecliptic plane from the geocentre at opposition ranges from 66° at aphelion, or 83° at perihelion, to ∼30° at a solar elongation of 60°.

have ceased. The progression in Fig. 4 shows how the MT regions might be surveyed as Earth passes by in its orbit.

Observations of MTs are time limited only by the relative orbits of Earth and Mars. There will exist specific constraints particular to the geographic location of a telescope, depending on the relative positions of Earth and the MT field. For example some Northern hemisphere telescopes may not have access to the entire southern part of the MT region described in Fig. 3 when the field is near opposition, and the converse will apply to some Southern hemisphere telescopes.

The limit adopted in this paper is that of solar elongation of 60°, but with the MT regions each being visible for several months as Earth passes by, it is possible to survey the fields at a wide range of solar elongations. If the observations are made at small elongations, the available time is limited, whereas at (or near) opposition the amount of sky area can be the limiting factor. Fig. 5 shows the difference in sky area of the field between opposition and 60° elongation, and Fig. 6 shows the difference in height.

While a delay between follow-up images introduces other variations from such things as changes in atmospheric conditions and seeing, this could be compensated for by image convolution. Some telescopes are implementing image processing systems designed specifically for asteroid detection (e.g. Pan-STARRS+MOPS – Moving Object Processing System) (Jedicke et al. 2007). Depending on the relative positions of Earth and the MT field, the apparent motion will vary with distance and direction.

Gaia's orbit dictates that it will scan narrow strips of the sky. As it will be a scanning instrument that performs a continuous scan by smooth and regular rotation of the spacecraft, follow-up observations for any object must be made by another instrument. Consequently a network of ground-based telescopes, the *Gaia* Follow Up Network for Solar System Objects (Gaia-FUN-SSO),[2] is being established to provide follow-up observations after detection of Solar system objects.

The scanning law governing *Gaia's* operation and the way the CCDs will operate (Tanga et al. 2008; Mignard 2010) limits the detection of Solar system objects as they cross the CCD array. With the 106.°5 separation between lines of sight, motion in the 'across-scan' (AC) direction of 0.40 arcsec s^{-1} will cause an object to traverse one FOV width and so have passed out of the FOV between the first and second observations of the field, even if starting at the edge of the CCD array on the first pass. An AC motion greater than 0.040 arcsec s^{-1} is larger than the pixel size in the AC direction and will cause smearing across pixels. Similarly, an 'along-scan' (AL) motion greater than 0.013 arcsec s^{-1} is larger than the pixel size in the AL direction. Since the motion of a Solar system object across the CCD depends on the relative positions of the object and *Gaia*, and the particular scanning orientation of *Gaia* at that time, these are important considerations for the design of the algorithms for detection of Solar system objects.

[2] http://www.imcce.fr/gaia-fun-sso/

4 SUMMARY

Despite the thousands of known Jupiter Trojans, a mere handful of terrestrial Trojans have been discovered. There are only three known MTs, and the first Earth Trojan has only been very recently discovered (Connors et al. 2011). Simulations (Tabachnik & Evans 1999, 2000a,b) predict that this number constitutes about one-tenth of the MT population with diameter $\geq$1 km. The prospect of detecting this population is limited by the size of the stable regions in which MTs can exist. However, the Earth–Mars geometry offers an extended period over which a survey could be conducted. The conventional method of detecting asteroids by repeated observations of a field can be used with a systematic approach to survey the entire MT field during a synodic period.

This study has identified the region of highest probability for detection, with an inclination $\leq 35^\circ$ and heliocentric longitude range of 40°–90° (L4) and 270°–320° (L5). Surveys of the entire field within the chosen limits are impractical on telescopes with small FOV but are possible on survey telescopes with sufficient FOV to accomplish the task in a single night, such as Catalina and the Large Synoptic Survey Telescope (LSST),[3] when the field is at a solar elongation $\lesssim 150^\circ$. In these cases, it may be possible to survey the regions defined by the inclination limits. This would require the fields to be surveyed twice within a few days, as is common for main belt asteroids. Although possible, it is rather impractical as this occupies a significant amount of telescope time. When the field is at a solar elongation $>150^\circ$, the sky area becomes too large to be able to be surveyed in a single night by any existing wide-field telescope.

Given the challenges involved in attempting to survey the entire field in a single session, we aimed to minimize the time requirement. Observing a swath of sky each session and progressively sampling the entire field over a synodic period achieves this aim. This approach requires minimal time each session by making a single pass across the field. By repeating this at intervals which provides an overlap of the telescope FOV from one pass to the next, the common regions of consecutive images can be compared.

The sky areas for Earth-based observers at different solar elongations have been determined using the numerical integrations described in Todd et al. (2012b). A strategy has been proposed for observing a subregion of the MT field and, as Earth revolves about the Sun, redefining this region and progressively surveying the entire field during a synodic period. This approach takes only a few minutes per night at intervals of 3–4 d. This approach requires the observed region to be redefined at intervals to progressively observe the entire field over those months when the field is visible from Earth.

Since the field is visible during the majority of one synodic period (about 2 years), nights lost due to adverse weather conditions can be rescheduled without critically impacting the timing of the programme. The flexibility in the timing allows such a programme to be more readily accommodated alongside the primary science mission, and is readily achievable by a survey telescope. While this method requires a programme of continued observations over several months, the total time commitment for the programme is a few tens of hours spread over that period.

The *Gaia* satellite, at Earth's L2 Lagrangian point, will survey the MT fields as part of its larger mission to survey the whole sky. With a detection limit of $V = 20$, *Gaia* can be expected to detect MTs larger than 1-km diameter, provided the lateral motion across the CCD array is less than 0.40 arcsec s^{-1}. As with any uncatalogued Solar system object detected by *Gaia*, these would need to be followed up by ground-based telescopes.

The specific observing geometry of the *Gaia* satellite at Earth's L2 Lagrangian point will be examined in more detail in future work. Initial simulations for *Gaia's* detection of inner Solar system Trojans in the orbits of Earth and Mars show promise. Results of detailed simulations will be reported with particular regard to the detection limits and observational mode of operation of *Gaia*.

[3] The LSST is still in the development phase (www.lsst.org).

ACKNOWLEDGMENTS

MT thanks the organizers of the *Gaia* Solar System Science workshop (held in Pisa, Italy, 2011) for providing a fertile environment for discussing *Gaia* science. DMC is supported by an Australian Research Council Future Fellowship.

REFERENCES

Connors M., Wiegert P., Veillet C., 2011, Nat, 475, 481
Drake A. J. et al., 2009, ApJ, 696, 870
Jedicke R., Magnier E. A., Kaiser N., Chambers K. C., 2007, in Milani A., Valsecchi G. B., Vokrouhlický D., eds, Proc. IAU Symp. 236, Near Earth Objects, Our Celestial Neighbours: Opportunity and Risk. Kluwer, Dordrecht, p. 341
Jones R. L. et al., 2009, Earth Moon Planet, 105, 101
Law N. M. et al., 2009, PASP, 121, 1395
Mignard F., 2010, Advances Space Res., 47, 356
Mignard F. et al., 2007, Earth Moon Planet, 101, 97
Mikkola S., Innanen K., 1994, AJ, 107, 1879
Morais M. H. M., Morbidelli A., 2002, Icarus, 160, 1
Nicholson S. B., 1961, Astron. Soc. Pac. Leaflets, 8, 239
Pilat-Lohinger E., Dvorak R., Burge Ch., 1999, Celest. Mech. Dynamical Astron., 73, 117
Rivkin A. S., Binzel R. P., Howell E. S., Bus S. J., Grier J. A., 2003, Icarus, 165, 349
Scholl H., Marzari F., Tricarico P., 2005, Icarus, 175, 397
Tabachnik S., Evans N. W., 1999, ApJ, 517, L63
Tabachnik S., Evans N. W., 2000a, MNRAS, 319, 63
Tabachnik S., Evans N. W., 2000b, MNRAS, 319, 80
Tanga P., Hestroffer D., Delbo M., Frouard J., Mouret S., Thuillot W., 2008, Planet. Space Sci., 56, 1812
Tedesco E. F., Cellino A., Zappala V., 2005, AJ, 129, 2869
Todd M., Coward D. M., Zadnik M. G., 2012a, Planet. Space Sci., preprint (doi:10.1016/j.pss.2011.11.002)
Todd M., Tanga P., Coward D. M., Zadnik M. G., 2012b, MNRAS, 420, L28
Warner B. D., Harris A. W., Pravec P., 2009, Icarus, 202, 134

This paper has been typeset from a TEX/LATEX file prepared by the author.

Chapter 5

Detection of inner Solar System Trojan Asteroids by Gaia

Todd, M., P. Tanga, D. M. Coward, M. G. Zadnik. 2012. "Detection of inner Solar System Trojan Asteroids by Gaia." *Proceedings of Gaia-FUN-SSO-2 International Workshop, Institut de Mécanique Céleste et de Calcul des Éphémérides, Paris Observatory, France, 19-21 September 2012.*

Detection of inner Solar System Trojan Asteroids by Gaia

M. Todd[1], P. Tanga[2], D.M. Coward[3], M.G. Zadnik[1]

1. Department of Imaging and Applied Physics, Bldg 301, Curtin University, Kent St, Bentley, WA 6102, Australia

2. Laboratoire Lagrange, UMR7293, Université de Nice Sophia-Antipolis, CNRS, Observatoire de la Côte d'Azur (France)

3. School of Physics, M013, The University of Western Australia, 35 Stirling Hwy, Crawley, WA 6009, Australia

Abstract

The Gaia satellite, planned for launch by the European Space Agency (ESA) in 2013, is the next generation astrometry mission following Hipparcos. While mapping the whole sky, the Gaia space mission is expected to discover thousands of Solar System Objects. These will include Near-Earth Asteroids and objects at Solar elongations as low as 45 degrees, which are difficult to observe with ground-based telescopes. We present the results of simulations for the detection of Trojan asteroids in the orbits of Earth and Mars by Gaia.

Introduction

Trojan asteroids share the orbit of a planet and librate about the L4 and L5 Lagrangian points in that planet's orbit. Earlier modelling and simulations for Earth Trojans [3] predict the existence of ~ 17 bodies larger than 100 m, and for Mars Trojans [4, 5, 6] ~ 50 bodies larger than 1 km are predicted. The first discovery of a Trojan asteroid in Earth's orbit (2010 TK7) was announced in 2011 [1], and there are only three known Mars Trojans. Based on those simulations it is possible that more Trojan asteroids exist in the inner Solar System, however detection of such objects by ground-based telescopes are subject to a number of restrictions. This paper describes the results of modelling and simulations for the detection of Trojan asteroids in the orbits of Earth and Mars by the Gaia space mission, which does not share those limitations of ground-based telescopes.

1. Detection by Gaia

By definition, Trojan asteroids are found in the L4 and L5 Lagrangian regions in a planet's orbit. The probable orbits of Earth and Mars Trojans [7, 8] show that peak detection longitudes are consistent with classical Lagrangian points, but that bodies are unlikely to be co-planar as the stable orbits have significant inclinations. The sky area in which these bodies may be located is quite large but this is not a significant problem in the context of Gaia's mission to survey the whole sky.

The apparent magnitude for an Earth Trojan ranges from $V = 17.9$ to $V = 19.5$ [7] and for a Mars Trojan is between $V = 16.2$ to $V = 20.7$ [8], assuming 1 km diameter and an albedo of 0.20, and neglecting atmospheric extinction. This variation is effected by phase angle and distance, with distance being the dominant influence. Since Earth Trojans are co-orbital then these would be brightest when nearest to Earth in their orbits. By comparison the Mars Trojans have greatest brightness at opposition, which is a region outside Gaia's scanning area. The brightness of the Mars Trojans, when within Gaia's scanning area, is $V >\sim 18$.

The limits from the models were used to construct orbits for 20 000 objects each for Earth and Mars Trojans, for simulation of possible detection by Gaia. The instantaneous positions of these are shown in Figure 1.

For the simulated Earth Trojans, 969 orbits never crossed Gaia's field of view. A further 146 had brightnesses $V > 20$, placing them below the detection threshold of $V = 20$. The result of the simulation is that

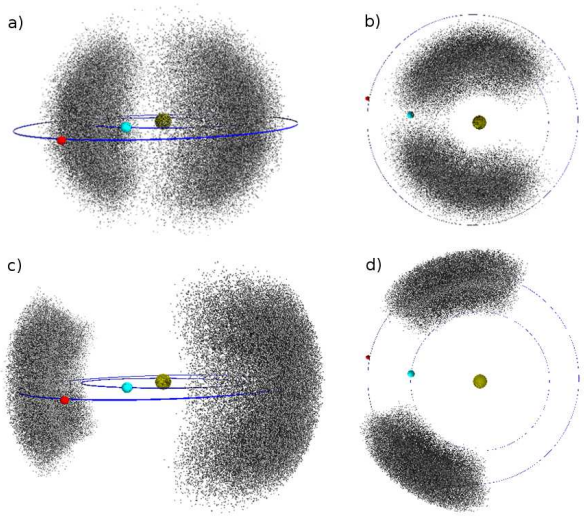

Figure 1: Positions of simulated bodies at JD 2456000.5. a) Distribution of simulated Earth Trojans; b) Projection on the ecliptic plane of the positions of the simulated Earth Trojans; c) Distribution of Mars Trojans; and d) Projection on the ecliptic plane of the positions of the simulated Mars Trojans.

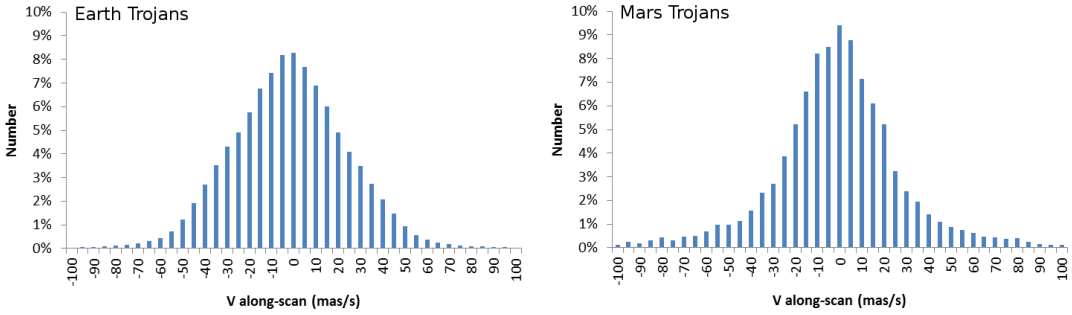

Figure 2: Statistical distribution of the along-scan velocity during observation for the simulated objects.

$\sim$ 94 per cent of objects were detected.

For the simulated Mars Trojans, 142 orbits never crossed Gaia's field of view. In contrast to the detection results for the Earth Trojans, only 2096 were detected with brightness $V < 20$. However 420 of these were detected in only one telescope, which would prevent any orbit calculation and subsequent recovery. The result of the simulation is that $\sim$ 8 per cent of the objects were detected where possible follow-up study could be performed.

In both cases the along-scan velocity is significant. The along-scan velocity for Main Belt asteroids is typically less than 10 mas/s [2] whereas for both Earth Trojans and Mars Trojans along-scan velocities much greater than 10 mas/s is quite common (Figure 2). The length of the window defined for sources $V > 16$ is six pixels (354 mas). For an along-scan drift $>\sim$ 3.5 mas/s a source will travel $>$ 175 mas from the centre of the defined window in the along-scan direction in the $\sim$ 50 seconds it takes to travel the length of the CCD array, with the result that the source drifts outside its window.

In both cases the across-scan velocity is also significant. The across-scan velocity for Main Belt asteroids is typically less than 15 mas/s, whereas the across-scan velocities for Earth and Mars Trojans are much greater (Figure 3). The bimodal distribution of the across-scan velocities for Earth Trojans in Figure 3 is a product of the geometry. The width of the window defined on the CCD is 12 pixels (2124 mas), and so an across-scan drift $>\sim$ 21 mas/s results in the source drifting outside the window. In addition, for across-scan velocity $>$ 195 mas/s, from a mean starting point at the centre of the CCD, the source will

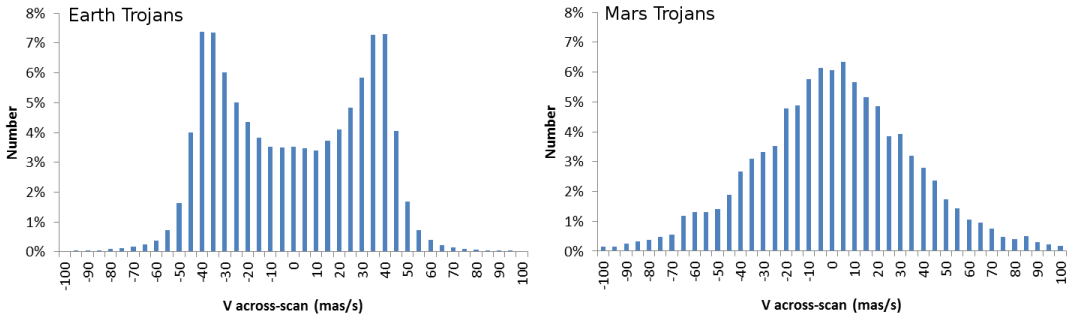

Figure 3: Statistical distribution of the across-scan velocity during observation for the simulated objects.

only be observed in one telescope.
Due to their orbits, the simulated Earth Trojans are observed more frequently than Main Belt whereas the simulated Mars Trojans are observed less frequently. This over-representation of the Earth Trojans in the detection statistics is expected; these are co-orbital and are observed at least once during each scanning cycle. However it is unlikely that there are any Earth Trojans of this size. The known Earth Trojan (2010 TK7) is estimated to have a diameter of ~ 300 m [1], with an apparent magnitude between $V = 20.9$ to $V = 22.7$, and a mean sky motion calculated to be between 25 mas/s to 100 mas/s (see Table 1), making it unlikely to be detected by Gaia. By comparison the three Mars Trojans are much brighter and have a smaller apparent motion, making it probable that they will be detected by Gaia.

Table 1: Inner Solar System Trojan Asteroid magnitudes and mean sky motions.

Designation	Magnitude	Mean Sky Motion (mas/s)
2010 TK7	$20.9 < V < 22.7$	25 - 100
5261 Eureka	$17.1 < V < 19.2$	4.5 - 23.5
1998 VF31	$17.3 < V < 20.1$	6.5 - 35.5
1999 UJ7	$17.4 < V < 19.6$	4.5 - 23.0

Conclusion

The regions where Earth and Mars Trojan asteroids may be found occupy a very large sky area, however Gaia will survey these regions multiple times during its mission. Because of the co-orbital nature of Earth Trojans, that region will be over-observed by comparison with any other field since Gaia will observe that region each scan cycle. In contrast with this, the Mars Trojan region will be observed much less frequently because of the different geometry. For both cases the high along-scan and across-scan velocities may present a problem due to loss of signal as the source will tend to drift out of the window defined on the CCD.
It is unlikely that any Earth Trojans exist which are larger than 2010 TK7. The consequence is that any other Earth Trojans will be too small and hence too faint for Gaia to detect. In the case of the Mars Trojans there is some uncertainty but it is expected that Gaia would detect any additional bodies which are of sizes comparable to those already known. An analysis for the detection of the known Earth and Mars Trojans by Gaia will be forthcoming.

Acknowledgements

MT acknowledges support from the Astronomical Society of Australia, Australian Institute of Physics, and the sponsoring organisations of the Gaia-FUN-SSO2 workshop. MT thanks the SOC/LOC of the Gaia-FUN-SSO2 workshop for providing a fertile environment for discussing Gaia science. DMC is supported by an Australian Research Council Future Fellowship.

References

[1] Connors M., Wiegert P., Veillet C. 2011. Earth's Trojan asteroid, *Nature*, 475, 481.

[2] Mignard F., Tanga P., Todd M. 2011. Observing Earth Trojans with Gaia, GAIA-C4-TN-OCA-FM-051.

[3] Morais M. H. M., Morbidelli A. 2002. The Population of Near-Earth Asteroids in Coorbital Motion with the Earth, *Icarus*, 160, 1.

[4] Tabachnik S., Evans N. W. 1999. Cartography for Martian Trojans, *ApJ*, 517, L63.

[5] Tabachnik S., Evans N. W. 2000. Asteroids in the inner Solar system - I. Existence, *MNRAS*, 319, 63.

[6] Tabachnik S., Evans N. W. 2000. Asteroids in the inner Solar system - II. Observable properties, *MNRAS*, 319, 80.

[7] Todd, M., Tanga, P., Coward, D. M., Zadnik, M. G. 2012. An optimal Earth Trojan asteroid search strategy, *MNRAS*, 420, L28.

[8] Todd, M., Tanga, P., Coward, D. M., Zadnik, M. G. 2012. An optimal Mars Trojan asteroid search strategy, *MNRAS*, 424, 372.

Chapter 6

Predictions for the detection of Earth and Mars Trojan asteroids by the Gaia satellite

Todd, M., P. Tanga, D. M. Coward, M. G. Zadnik. 2014. "Predictions for the detection of Earth and Mars Trojan asteroids by the Gaia satellite." *Monthly Notices of the Royal Astronomical Society* 437 (4): 4019-4026. doi:10.1093/mnras/stt2223.

Monthly Notices of the ROYAL ASTRONOMICAL SOCIETY

MNRAS **437,** 4019–4026 (2014) doi:10.1093/mnras/stt2223
Advance Access publication 2013 December 9

Predictions for the detection of Earth and Mars Trojan asteroids by the *Gaia* satellite

M. Todd,[1]★ P. Tanga,[2] D. M. Coward[3] and M. G. Zadnik[1]

[1]*Department of Imaging and Applied Physics, Bldg 301, Curtin University, Kent St, Bentley, WA 6102, Australia*
[2]*Laboratoire Lagrange, UMR7293, Université de Nice Sophia-Antipolis, CNRS, Observatoire de la Côte d'Azur, BP 4229, F-06304 Nice Cedex 4, France*
[3]*School of Physics, M013, The University of Western Australia, 35 Stirling Hwy, Crawley, WA 6009, Australia*

Accepted 2013 November 13. Received 2013 November 11; in original form 2013 September 26

ABSTRACT

The European Space Agency *Gaia* satellite, planned for launch in late 2013, will perform systematic astrometric observations of the whole sky over a five year period. During this mission, many thousands of Solar System objects down to magnitude $V = 20$ will be observed including near-Earth asteroids and objects at solar elongations as low as 45°, which are difficult to observe with ground-based telescopes. We simulated the detection of Trojan asteroids in the orbits of Earth and Mars by *Gaia*. We find that *Gaia* will not detect the Earth Trojan 2010 TK_7 although it will detect any Earth Trojans with diameters larger than 600 m. We also find that *Gaia* will detect the currently known Mars Trojans and could discover more than 100 new Mars Trojans as small as 400 m in diameter. The results of the *Gaia* mission will test the predictions about the Mars Trojan asteroid population and lead to greater understanding about the evolution of the Solar System.

Key words: methods: numerical – methods: observational – methods: statistical – celestial mechanics – minor planets, asteroids: general – planets and satellites: general.

1 INTRODUCTION

The European Space Agency *Gaia* satellite (http://gaia.esa.int) will be launched in late 2013. *Gaia* will be located near the Earth's L2 Lagrangian point and will survey the whole sky down to magnitude $V = 20$ (Mignard et al. 2007). In the course of its mission, several tens of thousands of asteroids will also be repeatedly observed. Observations of main belt asteroids and near-Earth objects by *Gaia* have been looked at extensively during the past several years in papers such as Mignard et al. (2007) and Tanga & Mignard (2012). However, the sky coverage will also include the regions in the orbits of Earth and Mars where Trojan asteroids are likely to exist (Todd, Coward & Zadnik 2012b; Todd et al. 2012c,d). We anticipate obtaining results from *Gaia* that will include the discovery of new Trojan asteroids.

Trojan asteroids occupy the L4 and L5 Lagrangian regions in a planet's orbit about the Sun. These stable regions exist 60° ahead (L4) and behind (L5) the planet in its orbit and appear to be stable on long time-scales in the *N*-body case of the Solar System (Pilat-Lohinger, Dvorak & Burger 1999; Scholl, Marzari & Tricarico 2005). Studying the Trojans provides insight into the evolution of the Solar System. Several thousand Trojans have been found in the orbit of Jupiter, however, among the terrestrial planets only Earth and Mars are known to have Trojans.

Earth has only one known Trojan (2010 TK_7), discovered through examination of data from the *WISE* satellite (Connors, Wiegert & Veillet 2011), while Mars presently has five known Trojans (Eureka, 1998 VF_{31}, 1999 UJ_7, 2007 NS_2 and 2001 DH_{47}) listed by the Minor Planet Center. Previous modelling (Tabachnik & Evans 1999, 2000a,b) suggests that there may be 10 times this number of Mars Trojans with diameters larger than 1 km, and that there may be several hundreds with diameters larger than 100 m.

Studies of three of the Mars Trojans (Eureka, 1998 VF_{31} and 1999 UJ_7) by Rivkin et al. (2003, 2007) show that these Trojans appear to have separate origins from one another. Rivkin et al. (2007) suggested that the simplest explanation for the origins of Eureka and 1998 VF_{31} is that they formed separately in other parts of the inner Solar System as part of larger bodies and that fragments were trapped in the 1:1 resonance with Mars roughly 3.9 Ga ago; thus, they are most likely to be long-term residents rather than natives.

Previous work (Todd et al. 2012c,d) considered strategies for discovering Earth and Mars Trojans using ground-based telescopes as well as considering the potential benefits of the *Gaia* mission to the discovery of additional Trojans. We subsequently ran simulations to model detection characteristics and detection limits for Earth and Mars Trojans with respect to *Gaia* using a distribution of test particles with a uniform size of 1 km and having Trojan-like orbits (Todd et al. 2012a) and found that these would typically be bright enough

★ E-mail: michael.todd@icrar.org

(mag $V < 20$) but that the relative sky motion may be problematic depending on the observing geometry. In this paper, we use the known Trojans to model the detections of additional Earth and Mars Trojans by *Gaia*. In our simulations, we also included the asteroids 2011 SC_{191}, 2011 SL_{25} and 2011 UN_{63} which have been proposed as Mars Trojans by de la Fuente Marcos & de la Fuente Marcos (2013). We refer to these proposed Trojans hereafter as Trojans for simplicity.

2 MODEL

For our simulations, we used the known orbital elements for the Earth and Mars Trojans. One challenge that we faced is that we cannot be certain when *Gaia* will begin observations. We do not yet know the starting epoch of the observations nor can we predict *Gaia*'s orientation at that epoch. Thus, it is not possible to simulate the real detection sequence. To compensate for this in assessing whether *Gaia* will detect the known Trojans, we cloned the elements to provide 100 test bodies for each of these Trojans. We then modified the cloned elements to compensate for the uncertainty of the starting conditions. Although these orbits would not be stable over a long period the perturbations are trivial over the 5 yr duration of the *Gaia* mission simulation. The modifications are described in Sections 2.1 and bl2.2 for Earth Trojans and Mars Trojans, respectively.

2.1 Earth Trojans

The Earth Trojan 2010 TK_7 is co-orbital with Earth. It resides in the L4 (leading) Lagrangian region and so travels around the Sun ahead of Earth in its orbit. Because it is co-orbital with Earth and hence also with *Gaia*, it was slightly more complex to correct for uncertainties in the starting conditions for the observations by *Gaia* than the Mars Trojans. Starting from the initial position of 2010 TK_7 (Fig. 1a), we created 100 objects by replicating the orbital elements (Table 1) but translating both the ascending node and the mean anomaly. Translating the ascending node spaced the clones of 2010 TK_7 at intervals through 360° such that each clone started from the same ecliptic latitude, effectively rotating the orbit orientation. However, this correction on its own produced a set of false positives because it did not take into account that the 2010 TK_7 is co-orbital

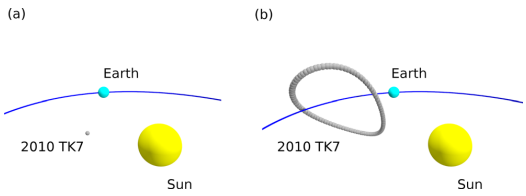

Figure 1. (a) The starting position of Earth's Trojan asteroid, 2010 TK_7, and (b) the starting positions of the clones.

Table 1. Orbital parameters for the Earth Trojan asteroid 2010 TK_7 (semimajor axis a, eccentricity e, inclination i, ascending node Ω, argument of perihelion ω).

Asteroid	a	e	i	Ω	ω
2010 TK_7	1.000 248	0.190 79	20.°882	96.°528	45.°852

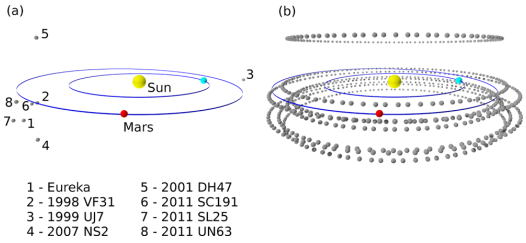

Figure 2. (a) The starting position of the Mars Trojan asteroids, (b) the starting positions of the clones with the ascending node adjusted.

with Earth. Adjusting the mean anomaly in conjunction with the ascending node provided the necessary adjustment to create a set of clones of 2010 TK_7 which were co-orbital with Earth. Since *Gaia*, Earth and 2010 TK_7 are co-orbital, by visualizing the result in a *Gaia*-centric frame, we see the apparent motion of 2010 TK_7 (Fig. 1b). We consider that the drift in position over time as it librates about the L4 point will not significantly affect the results of this simulation given the length of the *Gaia* mission (5 yr) since the period of libration is 395 yr (Connors et al. 2011).

2.2 Mars Trojans

The Mars Trojans are co-orbital with Mars. The observing geometries for an Earth-based instrument, and for *Gaia*, change with time due to the different orbital periods of Earth and Mars (and hence the Mars Trojans). For each of the Mars Trojans we took the initial positions (Fig. 2a) and replicated the orbital elements (Table 2) to create 100 instances of each Trojan. Similarly to the simulation for the Earth Trojan 2010 TK_7, we translated the ascending node of each group of clones to space them at intervals through 360° (Fig. 2b), thereby rotating the orientation of their orbits. However, unlike the Earth Trojan simulation, we did not translate the mean anomaly of the clones as they are not co-orbital with Earth.

3 RESULTS

Gaia will not directly produce images of each source. For these objects, since the brightness is typically at magnitudes below $V = 16$, a window 6 × 6 pixels centred on the source will be assigned when an object is detected. However, if the along-scan motion is greater than 3.5 mas s^{-1} the object will drift out of this window, resulting in a loss of signal. The median absolute along-scan velocity for main belt asteroids is 7 mas s^{-1} (Tanga & Mignard 2012) which is a drift of about half a pixel during a single CCD crossing. A similar case holds for the across-scan motion although the pixel dimensions (59 mas × 177 mas) mean that a drift across-scan up to 10.5 mas s^{-1} will result in the object remaining within the window by the time the object has crossed the CCD array. The absolute across-scan velocity for main belt asteroids is typically less than 15 mas s^{-1} (Tanga & Mignard 2012). Previous results for the detection of Earth and Mars Trojans by *Gaia* (Todd et al. 2012a) found that the along-scan and across-scan velocities for Earth and Mars Trojans are much higher than main belt asteroids. This has the implication that they will frequently drift out of the window during a crossing, resulting in signal degradation.

Table 2. Orbital parameters for the Mars Trojan asteroids (semimajor axis a, eccentricity e, inclination i, ascending node Ω, argument of perihelion ω).

Asteroid	a	e	i	Ω	ω
Eureka	1.523 5160	0.064 6937	20.°282 89	245.°069 53	95.°415 30
1998 VF_{31}	1.524 1558	0.100 3765	31.°297 33	221.°330 11	310.°557 17
1999 UJ_7	1.524 5294	0.039 2950	16.°748 60	347.°387 08	48.°353 02
2007 NS_2	1.523 7155	0.054 0248	18.°621 67	282.°498 88	176.°938 81
2001 DH_{47}	1.523 7644	0.034 7226	24.°399 62	147.°429 10	17.°591 04
2011 SC_{191}	1.523 8022	0.044 1686	18.°744 44	5.°795 90	196.°342 15
2011 SL_{25}	1.523 9213	0.114 4574	21.°496 66	9.°427 31	53.°291 26
2011 UN_{63}	1.523 7402	0.064 5860	20.°362 51	223.°571 38	165.°297 25

3.1 Earth Trojans

After replicating the orbital parameters for 2010 TK_7 (Table 1) and simulating observations by *Gaia*, we plotted the observed positions of the clones relative to Earth (and *Gaia*) (Fig. 3). The solar elongations of these positions range between 44.°6 and 100.°4 (Table 3) and the distance varies between 0.18 au and 0.87 au.

The apparent magnitude of an Earth Trojan with a diameter of 1 km ranges between $V = 17.9$ and $V = 19.5$, assuming an albedo of 0.20 (Todd et al. 2012c). This variation depends on both phase angle and distance, with distance having the greater effect. Our simulation results for the Earth Trojan 2010 TK_7 indicate that it will not be detected by *Gaia* in spite of its proximity to Earth. The Earth Trojan 2010 TK_7 has a diameter of only ∼300 m (Connors et al. 2011). The consequence of this smaller size is that its brightness is correspondingly reduced, ranging from $V = 20.9$ to $V = 22.8$ (Table 3). As a result 2010 TK_7 is always too faint to be detected by *Gaia*.

Using the simulation data to consider the implications for observing a larger Earth Trojan in the same orbit we find that the along-scan (Fig. 4) and across-scan (Fig. 5) velocities are considerably greater than main belt asteroids. The median absolute along-scan velocity of 2010 TK_7 (Fig. 4) is ∼40 mas s^{-1}, almost six times that of the main belt asteroids. A motion along-scan of this magnitude results in the object drifting out of the 6 × 6 pixels window soon after crossing the first CCD in *Gaia*'s focal plane array.

The across-scan motion of 2010 TK_7 (Fig. 5) is also large compared to that of main belt asteroids. The absolute across-scan velocity of main belt asteroids is typically less than 15 mas s^{-1} (Todd et al. 2012a) compared with 40 mas s^{-1} for 2010 TK_7. We also note that the distribution is asymmetric and not the bimodal distribution we observed with the simulated Earth Trojans in Todd et al. (2012a). We attribute this asymmetry to the peculiarity of 2010 TK_7 co-orbiting the Sun in Earth's L4 Lagrangian region.

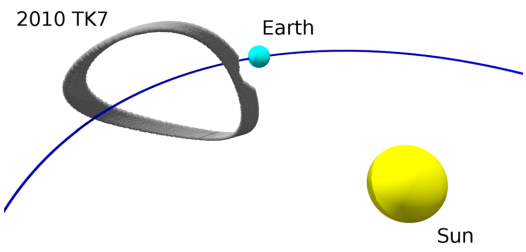

Figure 3. Plotting the positions of the Earth Trojan asteroid 2010 TK_7 clones relative to *Gaia*'s orientation shows that most of the orbits are within the region observable by *Gaia*. There is a small gap where the orbits pass through the unobservable region at solar elongations nearer than 45° from the Sun.

Table 3. Observation statistics for Earth Trojan 2010 TK_7. Note the apparent magnitude of 2010 TK_7 is below *Gaia*'s detection threshold.

Asteroid	Distance from Earth (au)	Solar elongation	Magnitude (V)
2010 TK_7	0.18–0.87	44.°6–100.°4	20.9–22.8

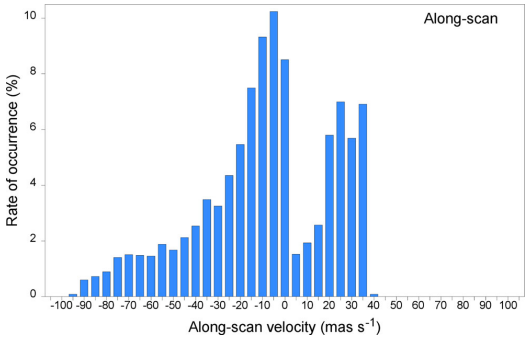

Figure 4. The distribution of the apparent proper (relative to stars) along-scan velocity of Earth's Trojan asteroid, 2010 TK_7. The median absolute velocity is ∼40 mas s^{-1}, about six times greater than that of the main belt asteroids.

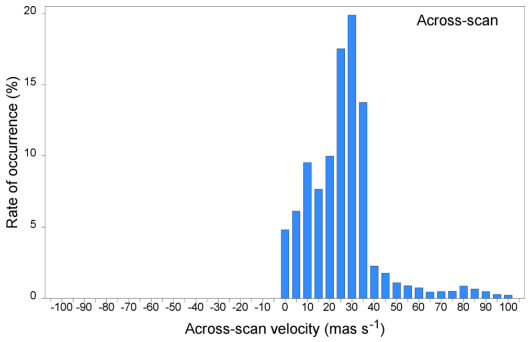

Figure 5. The distribution of the across-scan velocity of Earth's Trojan asteroid, 2010 TK_7. The asymmetry is a result of 2010 TK_7 co-orbiting the Sun in Earth's L4 Lagrangian region.

Given the 106.°5 separation between *Gaia*'s lines of sight, motion in the across-scan direction of 400 mas s^{-1} would result in an object traversing the width of the focal plane array (0.°7) between the first and second observations of the field (Todd et al. 2012d). As the across-scan motion of 2010 TK$_7$ is typically less than 40 mas s^{-1}, we find that a kilometre-scale Earth Trojan in the same orbit as 2010 TK$_7$ would provide enough signal due to its proximity and hence greater apparent brightness to be detected even though it would drift out of the 6 × 6 pixels window soon after crossing the first CCD in *Gaia*'s focal plane array. In this orbit, an object will drift approximately 4 arcmin in the interval between the first and second observations of the field thus making detections on both crossings possible.

The conclusion that can be drawn from this is that if a kilometre-scale Earth Trojan does exist, then *Gaia* will detect it in spite of the signal degradation caused by the high relative drift across the CCD array. There will also be a substantial number of CCD crossings where the relative drift is low enough that *Gaia* will detect any Earth Trojans with diameters larger than ∼600 m.

3.2 Mars Trojans

As with the simulation for the Earth Trojan 2010 TK$_7$, we replicated the orbital parameters for the Mars Trojans (Table 2) and simulated observations by *Gaia*. The three largest Trojans (Eureka, 1998 VF$_{31}$ and 1999 UJ$_7$) were fully detected in our simulations. Of the remaining Trojans, 2007 NS$_2$ had a 98 per cent detection, 2001 DH$_{47}$ had a 43 per cent detection and 2011 SL$_{25}$ had a 9 per cent detection. The Trojans 2011 SC$_{191}$ and 2011 UN$_{63}$ were not detected in our simulations.

The apparent magnitude of a Mars Trojan with a diameter of 1 km and an albedo of 0.20 ranges between $V = 16.2$ at opposition and $V = 20.7$ at a solar elongation of 60° (Todd et al. 2012d). *Gaia* cannot observe at elongations within 45° of opposition, however, the ∼1 km Trojans are bright enough to be detected when they are in *Gaia*'s field of view.

The diameters of the Mars Trojans (Table 4) were calculated using the standard formula (Warner, Harris & Pravec 2009):

$$\log D = 3.1235 - 0.2H - 0.5 \log p_v, \quad (1)$$

where D is diameter in kilometres, H is absolute magnitude and p_v is albedo.

Rivkin et al. (2003) found that Eureka has a visible spectrum consistent with the Sr class in the Bus taxonomy and an infrared spectrum that is consistent with the A class. They also found that 1998 VF$_{31}$ fit closely to Sr or Sa class and that 1999 UJ$_7$ fit to X or T class. Trilling et al. (2007) subsequently observed Eureka and 1998 VF$_{31}$ and determined their albedos to be 0.39 and 0.32, respectively. The other Trojans were assumed to be S class and to have typical albedo values as described in Warner et al. (2009).

Table 4. Calculated diameters of Mars Trojans, assuming S class except where noted.

Asteroid	Abs. mag. (H)	Class	Albedo	Diameter (km)
Eureka	16.1	Sr[a]	0.39[b]	1.28
1998 VF$_{31}$	17.1	Sr[a]	0.32[b]	0.89
1999 UJ$_7$	16.9	X[a]	0.174[c]	1.33
2007 NS$_2$	17.8	S	0.203[c]	0.81
2001 DH$_{47}$	18.7	S	0.203[c]	0.54
2011 SC$_{191}$	19.3	S	0.203[c]	0.41
2011 SL$_{25}$	19.5	S	0.203[c]	0.37
2011 UN$_{63}$	19.7	S	0.203[c]	0.34

[a] Spectral class taken from Rivkin et al. (2003).
[b] Albedo taken from Trilling et al. (2007).
[c] Typical albedo values taken from Warner et al. (2009).

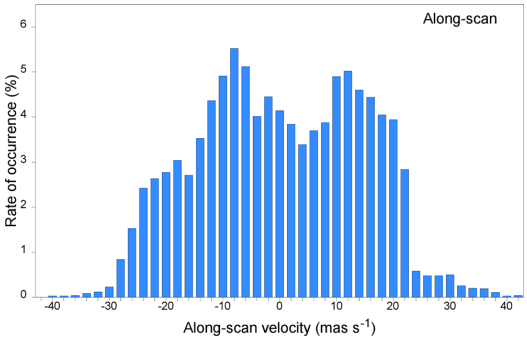

Figure 6. The distribution of the apparent proper (relative to stars) along-scan velocity of the Mars Trojan asteroids. The median absolute velocity is ∼16 mas s^{-1}, about double that of the main belt asteroids.

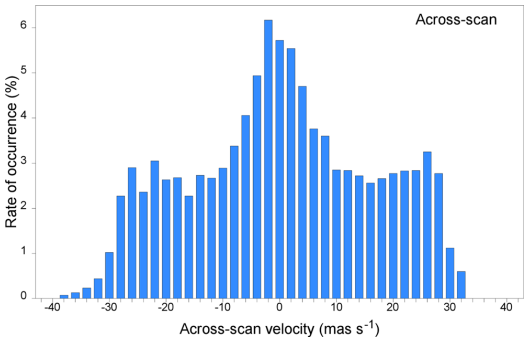

Figure 7. The distribution of the across-scan velocity of Mars Trojan asteroids. The distribution is similar to the across-scan distribution for main belt asteroids.

As with the Earth Trojan 2010 TK$_7$, we found that the along-scan (Fig. 6) and across-scan (Fig. 7) velocities are greater than main belt asteroids. This result was not unexpected since the Mars Trojans are nearer to *Gaia* than the main belt asteroids. Likewise, the velocities were greater for 2010 TK$_7$ than for the Mars Trojans. The median along-scan velocity of the Mars Trojans (Fig. 6) is ∼16 mas s^{-1}, about double that of the main belt asteroids. A motion along-scan of this magnitude results in the object drifting out of the 6 × 6 pixels window after crossing two CCDs in *Gaia*'s focal plane array, resulting in a loss of signal.

The across-scan motion of the Mars Trojans (Fig. 7) is also large compared to that of main belt asteroids but not as large as that of 2010 TK$_7$. The absolute across-scan velocity of the Mars Trojans is typically less than 30 mas s^{-1}, about double that of main belt asteroids. We note that the distribution bears some resemblance to the across-scan distribution for main belt asteroids in Tanga & Mignard (2012).

We find some differences between these simulation results and the expected results for main belt asteroids. It is expected that *Gaia* will make 60–70 observations of each main belt asteroid over the

Table 5. Detection statistics for Mars Trojans. Distance from Earth represents the distance to the object at the nearest observation. Solar elongation represents the minimum angle between the Sun and the object at which an observation was made. Magnitude is the brightest magnitude at which an observation was made. Values for 2011 SC_{191} and 2011 UN_{63} are enclosed in parentheses as these are below *Gaia*'s detection threshold.

Asteroid	Distance from Earth (au)	Solar elongation	Magnitude (V)
Eureka	0.546	48.°9	16.9
1998 VF_{31}	0.459	72.°7	17.4
1999 UJ_7	0.557	74.°5	17.8
2007 NS_2	0.548	100.°2	18.6
2001 DH_{47}	0.557	124.°3	19.6
2011 SC_{191}	(0.536)		(20.1)
2011 SL_{25}	0.448	128.°2	19.8
2011 UN_{63}	(0.500)		(20.3)

5 yr period of its mission (Tanga & Mignard 2012). By comparison the number of observations of the Mars Trojans, except for Eureka, are somewhat fewer. We expect that the number of observations will be linked to the apparent magnitude, which will be a function of distance and phase angle. Tanga & Mignard (2012) found a trend in the relationship between the absolute magnitude of an object and its apparent magnitude when observed by *Gaia*. It was calculated that the *Gaia*'s limit for main belt asteroids is $H \simeq 16 \pm 1$. Based on our simulation results, we have determined that the *Gaia*'s limit for Mars Trojans is $H \simeq 19 \pm 0.5$.

An examination of the positions of the detections relative to Earth (and *Gaia*) shows a link between the brightness and the number of detections. It follows that there is a link between the brightness and the range of elongations over which the Trojans can be detected (Table 5). A result which was initially surprising was the variation in the along-scan and across-scan velocities, however, examination of the results shows that this variation is related to the orbit parameters.

A comparison of the orbits (Table 2) shows that the eccentricity of 1998 VF_{31} and 2011 SL_{25} is $e \simeq 0.1$ and that the other Trojans are $e \simeq 0.05$. It follows that the nearest approach to Earth's orbit and hence the distance from *Gaia* for the nearest detection shows a similar pattern. It can be seen that the distances for 1998 VF_{31} and 2011 SL_{25} are similar to each other, as are the other Trojans (Table 5). We see in the distribution of the along-scan velocity (Fig. 6) that most of the absolute velocities are less than 25 mas s^{-1}. Absolute velocities greater than 25 mas s^{-1} are due to 1998 VF_{31} and 2011 SL_{25} approaching more closely to *Gaia* as a result of the eccentricity of their orbits.

The case is not the same for the across-scan velocity distribution (Fig. 7) although most of the velocities are also less than 25 mas s^{-1}. The distribution of across-scan velocities for most of the Mars Trojans exhibit this profile of a characteristic central peak with a shoulder either side. The maximum and minimum velocity for each Trojan is also consistent with the maximum and minimum velocity in the along-scan direction. However, the across-scan velocity distribution for Eureka is markedly different (Fig. 8) in that we see the across-scan velocities biased towards the maximum and minimum. We postulate that this is due to Eureka being bright enough to be detected at almost all solar elongations and that these detections at the velocity extremes decrease with size and corresponding increase in minimum solar elongation.

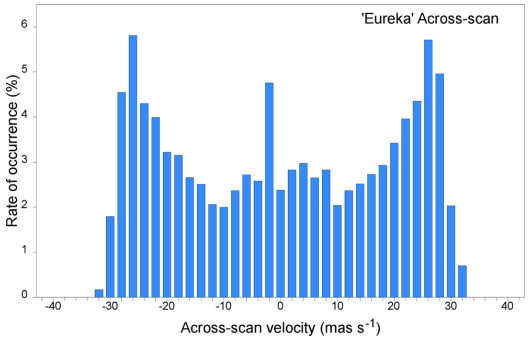

Figure 8. The distribution of the across-scan velocity of Mars Trojan asteroid Eureka.

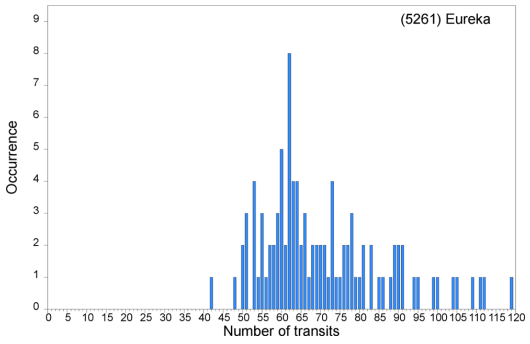

Figure 9. The number of detections of Mars Trojan asteroid Eureka. A maximum occurs at 62 detections.

In our simulations of Eureka, we found that it was fully detected, i.e. all the clones were detected multiple times. Depending on the starting conditions the number of detections of Eureka ranges between 42 and 141 detections with a probability peak at 62 detections (Fig. 9). This number of detections is similar to that expected for main belt asteroids.

Plotting the detections of Eureka relative to Earth and *Gaia* (Fig. 10) shows that observations are made at all solar elongations between about 49° and 135°. At its nearest approach at a

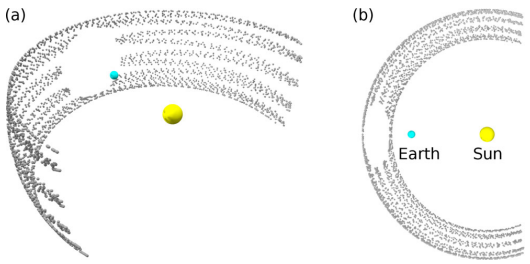

Figure 10. (a) Plotting the detections of Mars Trojan asteroid Eureka relative to *Gaia*'s orientation shows the range of solar elongations at which observations can be made. The height of the region is a result of the orbit inclination. (b) The exclusion of observations at solar elongations closer than 45° to the Sun results in a complementary exclusion zone within 45° of opposition. The apparent thickness of the region is an effect of the projection.

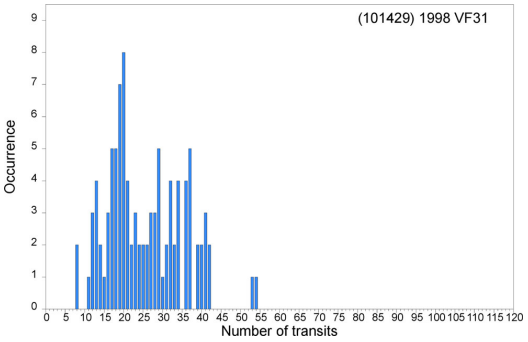

Figure 11. The number of detections of Mars Trojan asteroid 1998 VF_{31}. A maximum occurs at 20 detections.

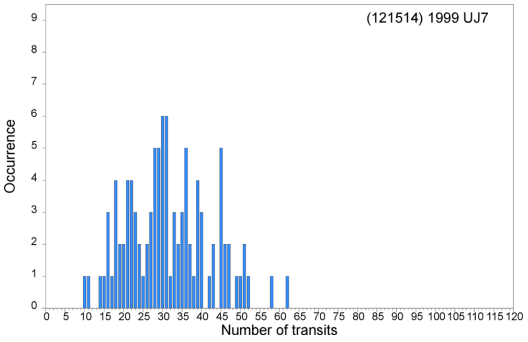

Figure 12. The number of detections of Mars Trojan asteroid 1999 UJ_7. A maximum occurs at 30 detections.

solar elongation of 135° Eureka is ∼0.5 au from Earth and has a brightness of $V \simeq 16.9$. Its farthest detectable distance is at a solar elongation of 48°.9 where its brightness is at *Gaia*'s detection threshold of $V \simeq 20$.

We also found that 1998 VF_{31} and 1999 UJ_7 were fully detected. The results for 1998 VF_{31} and 1999 UJ_7 were quite similar to each other. We found that detections of 1998 VF_{31} ranged between 8 and 54 detections with a probability peak at 20 detections (Fig. 11) and for 1999 UJ_7 ranged between 10 and 62 detections with a peak at 30 detections (Fig. 12).

In our simulations of the remaining Mars Trojans we found that they were not fully detected. We had a 98 per cent success rate with 2007 NS_2 as two of the clones went undetected. The other 98 clones were detected up to 68 times with a probability peak at 15 detections (Fig. 13). For 2001 DH_{47}, only 43 per cent of the clones were detected. The maximum number of detections was 21 and the probability peak was very low at four detections. For 2011 SL_{25}, only 9 per cent of the clones were detected and the maximum number of detections for a single clone was 14 detections. The Trojans 2011 SC_{191} and 2011 UN_{63} were not detected in our simulations as their magnitudes were $V > 20$ at their brightest.

Plotting the detections of 1998 VF_{31}, 1999 UJ_7, 2007 NS_2 and 2001 DH_{47} relative to Earth and *Gaia* (Fig. 14) shows the increasing minimum solar elongations (respectively) at which observations were made (Table 5). It is clear that the range of solar elongations over which *Gaia* will detect a Mars Trojan is related to its size and albedo and hence its range of apparent magnitudes. Eureka is the

Figure 13. The number of detections of Mars Trojan asteroid 2007 NS_2. A maximum occurs at 15 detections.

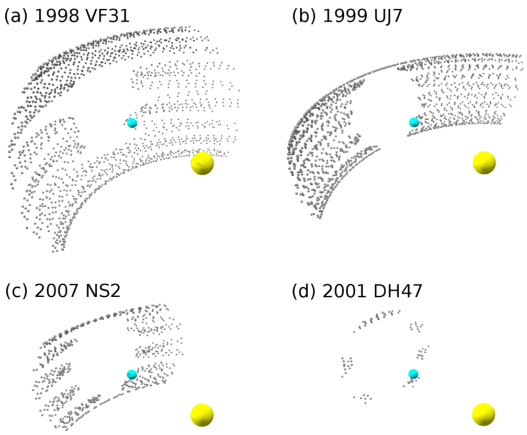

Figure 14. The detections of Mars Trojan asteroids (a) 1998 VF_{31}, (b) 1999 UJ_7, (c) 2007 NS_2 and (d) 2001 DH_{47} relative to *Gaia*'s orientation. The heights of the regions are a result of the orbit inclinations.

brightest of the Mars Trojans and has the largest range of solar elongations at which detections can be made (Fig. 10). The other Mars Trojans are fainter and have smaller regions of detection (Fig. 14). The Trojans 1998 VF_{31} (Fig. 14a) and 1999 UJ_7 (Fig. 14b) are similar in brightness and have similar ranges of solar elongations where they can be detected. With 2007 NS_2 (Fig. 14c) and 2001 DH_{47} (Fig. 14d) we see a reduced range of solar elongations resulting in the detection region being an annulus around the exclusion zone towards opposition. The implication of this is that *Gaia* will only detect smaller Trojans if they pass through this annulus.

From our simulations, we find that the starting conditions and orbit parameters greatly influence the result. We expect that *Gaia* will detect any kilometre-scale Mars Trojans. We can state with a high degree of certainty that *Gaia* will detect Mars Trojans larger than 800 m in diameter. We also consider that *Gaia* will detect Mars Trojans as small as 400 m in diameter. Consequently, we expect that the results of the *Gaia* mission will test the predictions about the Mars Trojan asteroid population and lead to greater understanding about the evolution of the Solar System.

4 SUMMARY

We used the known orbital elements for the Earth and Mars Trojans to simulate detections by the *Gaia* satellite. We cloned the orbital elements to provide 100 test bodies for each of the Trojans and modified them to compensate for the uncertainty of when *Gaia* will begin observations. We found that *Gaia* will not detect the Earth Trojan 2010 TK_7 but consider that it will detect any Earth Trojan with a diameter larger than 600 m. We also found that *Gaia* will detect many of the Mars Trojans and is therefore likely to discover additional Trojans.

4.1 Earth Trojans

Although 2010 TK_7 is very close to Earth and for the most part is within the observable region of sky for *Gaia* (Fig. 3), our simulation results indicate that it will not be detected by *Gaia*. Due to its small size of ∼300 m (Connors et al. 2011), its brightness is low, ranging from $V = 20.9$ to $V = 22.8$ (Table 3). Consequently, 2010 TK_7 is always too faint to be detected by *Gaia*.

We used the simulation results to consider the implications for observing a larger Earth Trojan in the same orbit. The along-scan (Fig. 4) and across-scan (Fig. 5) velocities are considerably greater than main belt asteroids. The median absolute along-scan velocity is $\sim 40\,\mathrm{mas\,s^{-1}}$, almost six times that of the main belt asteroids, and results in the object drifting out of the 6 × 6 pixels window after crossing just one of the CCDs in *Gaia*'s focal plane array. The across-scan motion is typically less than $40\,\mathrm{mas\,s^{-1}}$, about three times higher than main belt asteroids. We note that the distribution of the across-scan motion is asymmetric and not the bimodal distribution we found with the simulated Earth Trojans in Todd et al. (2012a). We attribute this asymmetry to the object residing in Earth's L4 Lagrangian region.

We conclude that, if a kilometre-scale Earth Trojan does exist, then *Gaia* will detect it in spite of the signal degradation caused by the relative drift across the CCD array. We also consider that *Gaia* will detect any Earth Trojan with a diameter larger than ∼600 m as there will be a substantial number of CCD crossings where the relative drift is low enough that the signal degradation will be minimal.

4.2 Mars Trojans

As with the simulation for the Earth Trojan 2010 TK_7, we replicated the orbital parameters for the Mars Trojans (Table 2). The three largest Trojans (Eureka, 1998 VF_{31} and 1999 UJ_7) were fully detected in our simulations. Of the remaining Trojans, 2007 NS_2 had a 98 per cent detection, 2001 DH_{47} had a 43 per cent detection and 2011 SL_{25} had a 9 per cent detection. The Trojans 2011 SC_{191} and 2011 UN_{63} were not detected in our simulations.

As with the Earth Trojan, we found that the along-scan (Fig. 6) and across-scan (Fig. 7) velocities are greater than main belt asteroids. The median along-scan velocity of the Mars Trojans is $\sim 16\,\mathrm{mas\,s^{-1}}$, about double that of the main belt asteroids. A motion along-scan of this magnitude results in the object drifting out of the 6 × 6 pixels window after crossing only two of the CCDs in *Gaia*'s focal plane array. The across-scan motion of the Mars Trojans is typically less than $30\,\mathrm{mas\,s^{-1}}$, also about double that of main belt asteroids. We note that the distribution bears some resemblance to the across-scan distribution for main belt asteroids in Tanga & Mignard (2012).

We found that Eureka, 1998 VF_{31} and 1999 UJ_7 were fully detected, i.e. all of the clones were detected. The number of observations of the Mars Trojans, except for Eureka, will be somewhat fewer than the expected 60–70 observations of each main belt asteroid (Tanga & Mignard 2012) over the 5 yr period of its mission. We found that the number of detections of Eureka is similar to that expected for main belt asteroids. Examining the positions of the detections relative to Earth (and *Gaia*) shows that there is a link between the maximum brightness and hence the range of elongations over which the Trojans can be detected (Table 5).

The results for 1998 VF_{31} and 1999 UJ_7 were quite similar, with probability peaks at 20 and 30 detections, respectively. However, the remaining Mars Trojans were not fully detected. For 2007 NS_2 and 2001 DH_{47}, we found the probability of detection to be 98 and 43 per cent, respectively, with corresponding probability peaks at 15 and four detections. For 2011 SL_{25}, only 9 per cent of the clones were detected. The Trojans 2011 SC_{191} and 2011 UN_{63} were not detected in our simulations as their magnitudes were $V > 20$ at their brightest.

From our simulations, we find that the starting conditions and orbit parameters greatly influence the result in the case of detecting smaller Mars Trojans. Based on our simulation results, we have determined that the *Gaia* limit for the detection of Mars Trojans is $H \simeq 19 \pm 0.5$. We expect that *Gaia* will detect any kilometre-scale Mars Trojans. We can also state with a high degree of certainty that *Gaia* will detect Mars Trojans larger than 800 m in diameter and that *Gaia* may detect Mars Trojans as small as 400 m in diameter.

Past simulations (Tabachnik & Evans 1999, 2000a,b) predict that the number of Mars Trojans with diameters larger than 1 km could be more than 50 and that the number with diameters larger than 100 m could be several hundreds. Assuming a progression of sizes that follows a power law, the number of Mars Trojans that *Gaia* will discover with diameters larger than 800 m will be more than 85, or conservatively more than 55. If we take the conservative view that there are about 30 Mars Trojans which have diameters larger than 1 km then we should expect that *Gaia* will detect between 55 and 140 new Mars Trojans. The results of the *Gaia* mission will test not only the accuracy of these simulation results but also the existing models of the Mars Trojan population and lead to greater understanding about the evolution of the Solar System.

ACKNOWLEDGEMENTS

MT acknowledges support from the Astronomical Society of Australia, the Australian Institute of Physics and the sponsoring organizations of the Gaia-FUN-SSO2 workshop. The work reported on in this publication has been supported by the European Science Foundation (ESF), in the framework of the GREAT Research Networking Programme. MT thanks the SOC/LOC of the Gaia-FUN-SSO2 workshop for providing a fertile environment for discussing *Gaia* science. MT also thanks Heidi Ursula Wallon Pizarro for feedback which helped to improve the manuscript. DMC is supported by an Australian Research Council Future Fellowship.

REFERENCES

Connors M., Wiegert P., Veillet C., 2011, Nature, 475, 481
de la Fuente Marcos C., de la Fuente Marcos R., 2013, MNRAS, 432, L31
Mignard F. et al., 2007, Earth Moon Planets, 101, 97
Pilat-Lohinger E., Dvorak R., Burger C., 1999, Celest. Mech. Dyn. Astron., 73, 117

Rivkin A. S., Binzel R. P., Howell E. S., Bus S. J., Grier J. A., 2003, Icarus, 165, 349
Rivkin A. S., Trilling D. E., Thomas C. A., DeMeo F., Spahr T. B., Binzel R. P., 2007, Icarus, 192, 434
Scholl H., Marzari F., Tricarico P., 2005, Icarus, 175, 397
Tabachnik S., Evans N. W., 1999, ApJ, 517, L63
Tabachnik S., Evans N. W., 2000a, MNRAS, 319, 63
Tabachnik S., Evans N. W., 2000b, MNRAS, 319, 80
Tanga P., Mignard F., 2012, Planet. Space Sci., 73, 5
Todd M., Tanga P., Coward D. M., Zadnik M. G., 2012a, preprint (arXiv:1212.0268)
Todd M., Coward D. M., Zadnik M. G., 2012b, Planet. Space Sci., 73, 39
Todd M., Tanga P., Coward D. M., Zadnik M. G., 2012c, MNRAS, 420, L28
Todd M., Tanga P., Coward D. M., Zadnik M. G., 2012d, MNRAS, 424, 372
Trilling D. E., Rivkin A. S., Stansberry J. A., Spahr T. B., Crudo R. A., Davies J. K., 2007, Icarus, 192, 442
Warner B. D., Harris A. W., Pravec P., 2009, Icarus, 202, 134

This paper has been typeset from a TEX/LATEX file prepared by the author.

Chapter 7

Australian participation in the Gaia Follow-Up Network for Solar System Objects

Todd, M., D. M. Coward, P. Tanga, W. Thuillot. 2013. "Australian participation in the Gaia Follow-Up Network for Solar System Objects." *Publications of the Astronomical Society of Australia* 30: 14-18. doi:10.1017/pasa.2012.014.

Publications of the Astronomical Society of Australia (PASA), Vol. 30, e014, 5 pages.

doi:10.1017/pasa.2012.014

Australian Participation in the *Gaia* Follow-up Network for Solar System Objects

M. Todd[1,5], D. M. Coward[2], P. Tanga[3] and W. Thuillot[4]

[1]Department of Imaging and Applied Physics, Bldg 301, Curtin University of Technology, Kent St, Bentley, WA 6102, Australia
[2]School of Physics, M013, The University of Western Australia, 35 Stirling Hwy, Crawley, WA 6009, Australia
[3]UMR 6202 Cassiopée, University of Nice-Sophia Antipolis, CNRS, Observatoire de la Côte d'Azur, BP 4229, 06304 Nice Cedex 4, France
[4]IMCCE, Observatoire de Paris, CNRS, UPMC, Univ. Lille 1, 77 avenue Denfert-Rochereau, 75014 Paris, France
[5]Corresponding author. Email: michael.todd@icrar.org

(Received June 28, 2012; Accepted August 29, 2012; Online Publication January 24, 2013)

Abstract

The *Gaia* satellite, planned for launch by the European Space Agency (ESA) in 2013, is the next-generation astrometry mission following *Hipparcos*. *Gaia*'s primary science goal is to determine the kinematics, chemical structure, and evolution of the Milky Way Galaxy. In addition to this core science goal, the *Gaia* space mission is expected to discover thousands of Solar System objects. Because of orbital constraints, *Gaia* will only have a limited opportunity for astrometric follow-up of these discoveries. In 2010, the *Gaia* Data Processing and Analysis Consortium (DPAC) initiated a program to identify ground-based optical telescopes for a *Gaia* follow-up network for Solar System Objects to perform the following critical tasks: confirmation of discovery, identification of body, object tracking to constrain orbits. To date, this network comprises 37 observing sites (representing 53 instruments). The Zadko Telescope, located in Western Australia, was highlighted as an important network node because of its southern location, longitude, and automated scheduling system. We describe the first follow-up tests using the fast moving Potentially Hazardous Asteroid 2005 YU55 as the target.

Keywords: instrumentation: miscellaneous – minor planets, asteroids: general – telescopes

1 INTRODUCTION

The European Space Agency (ESA) *Gaia* mission, scheduled for launch in spring 2013, is a space-based all-sky survey. The *Gaia* spacecraft will provide astrometry, photometry, and spectroscopy for point-like sources down to $V \sim 20$. *Gaia*'s science data comprise absolute astrometry, broad-band photometry, and low-resolution spectro-photometry. During its 5-year mission, *Gaia* will survey about 1 billion stars and 300 000 Solar System objects (SSOs), of which the majority will be main-belt asteroids. It will also survey about 500 000 point-like extragalactic sources and ∼1 million faint galaxies. The astrometric precision for the mission will be better than 10 μas for stars brighter than $V \sim 13$ and about 25 μas for stars $V \sim 15$. *Gaia* will initially build on, and then surpass, the results of the *Hipparcos* mission of about 20 years ago (Mignard 2011). Such an observational effort has been compared to mapping the human genome, for the amount of collected data and for the impact that it will have on all branches of astronomy and astrophysics.

In addition to the above core science goal, the *Gaia* space mission will discover exotic transient objects in large numbers. Many thousands of transients will be discovered including exoplanets and supernovae. Tens of thousands of brown and white dwarfs will be identified spectroscopically and, within our Solar System, some hundreds of thousands of minor planets will be observed. Of particular interest will be the numbers of unusual minor planets such as minor planets which have high inclinations, so that they are normally outside the regions of the sky routinely surveyed by near-Earth asteroid (NEA) program and inner Solar System Trojan asteroids.

Because *Gaia*'s primary mission is to perform a space-based all-sky survey, it is not designed to conduct any targeted follow-up studies. *Gaia* will be constrained by its orbit and by its design to survey the sky as completely as possible (Mignard et al. 2007). For these reasons, and because of the expected vast number of discoveries of transient phenomena, *Gaia* will not be able to either confirm or perform detailed studies of the discoveries.

1.1 *Gaia* Follow-up Network

During its 5-year mission, *Gaia* will observe many new SSOs. One feature of *Gaia* observations is the ability to image

Figure 1. The global distribution of observing stations participating in the *Gaia* FUN-SSO. The distribution is biased towards northern latitudes and European longitudes. Blue markers are the current observing stations, red markers are existing facilities which have expressed interest but are not confirmed, and yellow markers are planned future facilities.

at rather low solar elongation (45°), enabling detections of Earth-crossing asteroids (Atens) and inner-Earth asteroids (IEAs), and discoveries of new NEAs at larger solar elongation. In performing an all-sky survey, *Gaia* will necessarily survey regions of the sky away from the regions targeted by NEA programs. This holds the potential to discover asteroids with high orbital inclinations and Trojan asteroids in the stable Lagrangian regions in the orbits of the planets in the inner Solar System (Todd et al. 2011, 2012a, 2012b).

In such cases, due to the motion of the objects and limiting magnitude, the scanning law of *Gaia* will restrict the orbit determination to be constrained on a very small number of astrometric measurements. This implies that only a ground-based optical network can obtain accurate orbital modelling, based on enough astrometric measurements. This is the primary objective of the *Gaia* Follow-up Network for Solar System Objects (FUN-SSO).

In addition to the improvement in accuracy of the astrometric data used for orbital modelling of specific objects, some rare and peculiar SSOs such as asteroids with cometary activity could be studied (Tanga et al. 2008). Due to the limitations of *Gaia*'s observing method, a ground-based follow-up network will be crucial for studying the physical characteristics of these objects.

In order to be effective in acquiring high-quality follow-up imaging following an alert by the *Gaia* data processing system, the network must have a large geographical coverage. This is why several observing stations have been invited for participation in this project. In 2010, the *Gaia* Data Processing and Analysis Consortium (DPAC) initiated a programme to identify optical telescopes for a *Gaia* follow-up network for SSOs to perform the following critical tasks: confirmation of alert, identification of transient, continuous monitoring, and tracking. At the *Gaia* Follow-up Network Meeting in Paris 2010, the Zadko Telescope was highlighted as an important contribution to this network, because of its longitude and robotic operation. To date, the network comprises 37 observing sites (representing 53 instruments) (cf. Figure 1).

SSOs and stars are not differentiated on board but are treated the same way. Each source brighter than $V = 20$ is identified by the star mapper on the CCD array. A window is defined for each identified source for accumulation of charge as it crosses the CCD. An automated data reduction pipeline (implemented by the science consortium, DPAC) is run over all sources. Those which are found to move (from one epoch to the other, essentially) or are extended are sent to a specific branch of the pipeline which applies a specialised data reduction including identification and processing of SSOs. Most of the SSOs that *Gaia* will observe will be known, so they will be simply identified by comparison to ephemeris derived from the complete Minor Planet Center (MPC) catalogue. The remaining objects which are moving and not identified are classed as new asteroid candidates. For these, a tentative orbit is computed for ground-based recovery and an alert will be issued to the *Gaia*-FUN-SSO network.

PASA, 30, e014 (2013)
doi:10.1017/pasa.2012.014

Alerts from the *Gaia* data processing system will be received between 24 and 48 h after detection. Problems may arise for observations of peculiar objects: fast moving objects, faint objects, and NEAs close to Earth with strong parallaxes. Hence, small and less sensitive telescopes (<0.6 m) can be useful but more sensitive instruments (>1 m) will be essential. Furthermore, fully robotic telescopes are proved as ideal for observations triggered by an alert. Among the telescopes in the *Gaia*-FUN-SSO network, five are robotic telescopes.[1]

2 THE ZADKO TELESCOPE

The Zadko Telescope[2] is a 1-m f/4 Cassegrain telescope, built by DFM Engineering, Inc.,[3] and is situated in the state of Western Australia at longitude 115°42′49′′ E, latitude 31°21′24′′ S, and at an altitude of 47 m above sea level (67 km north of Perth).

It is an equatorial, fork-mounted telescope with a primary mirror clear aperture of 1 007.0 mm, and a system focal length of 4 038.6 mm. Its fast optics have a low f-ratio, coupled with a flat, wide field of view (maximum possible FoV ≈1°).

The core science theme of the Zadko Telescope is the discovery and study of transients (Coward et al. 2010). The facility was robotised in 2010, employing an observatory control system developed for the Téléscopes à Action Rapide pour les Objets Transitoires (TAROT). It can acquire photometric data autonomously on gamma-ray bursts (GRBs) and Galactic transients following alerts by the *Swift* satellite and other external triggers. In addition to the follow-up of GRB triggers, the Zadko Telescope is used for the follow-up of exoplanet discoveries, follow-up imaging of Astronomy with a Neutrino Telescope and Abyss environmental RESearch (ANTARES) alerts, follow-up imaging of Laser Interferometer Gravitational Wave Observatory (LIGO)/Virgo gravitational wave alerts, and SSOs. Some Zadko Telescope observations are as follows.

- Zadko measures the light curve of GRB 101024 only 200 s after satellite trigger, revealing unexplained optical light-curve features (Gendre et al. 2011).
- In 2009, a minor planet pilot search programme resulted in the discovery of 13 uncatalogued SSOs. Further studies resulted in four of these being linked to 'orphan' observations in the MPC database.
- Fourteen follow-ups of *Swift* satellite GRB triggers with NASA Gamma-ray Coordinates Network notices.
- The TAROT + Zadko network successfully images sky positions triggered by LIGO for the detection of possible optical counterparts to gravitational wave candidates (LIGO Scientific Collaboration et al. 2012).
- GRBs 090205 and 090516, with respective redshifts of 4.3 and 4.1, are among the most distant optical transients imaged by an Australian telescope.

[1] See http://www.imcce.fr/gaia-fun-sso/ for an updated list.
[2] http://www.zt.science.uwa.edu.au
[3] http://www.dfmengineering.com

Table 1. Zadko Telescope Asteroid Discovery and Follow-up Statistics

Year	Detections	No. of Objects Linkages	Link Span (opp. s/years)
2009	13	4	4/10
2010	4	1	3/5
2011	6	1	5/5
2012	1	1	2/6

For *Gaia* to achieve astrometric accuracy on scales of a few tens of microarcseconds, its reference frame must be well defined. By using the optical positions of quasi-stellar objects (QSOs), assuming that QSOs have no peculiar transverse motion, then any observed proper motion will reveal the global rotation of the *Gaia* sphere. Along with the robotic TAROT telescopes in France and Chile, the Zadko Telescope has been observing selected QSOs since mid-2011 to assist in constructing the initial catalogue for establishing *Gaia*'s reference frame.

The Zadko Telescope observatory is being upgraded in 2012. The observatory building is being replaced with a new observatory optimised for automated rapid response imaging of transients and SSOs. Furthermore, a new instrument and imaging package with spectroscopic capability, funded by the Australian Research Council, will be installed in 2012 and 2013.

The capability of the Zadko Telescope to detect faint objects to $m \approx 21.5$ and its robotic scheduling system enables it to perform optimal targeted follow-up observations. Since 2010, routine examination of selected image sets where the cadence has facilitated detection of moving objects has resulted in the detection of 11 additional uncatalogued SSOs. Follow-up studies have enabled three of these to be linked to earlier detections in the MPC database. In some cases, these linkages have been made between apparitions at several previous oppositions over a period of years up to a decade (see Table 1).

3 PRELIMINARY *Gaia* FUN-SSO TESTING

In 2011 November, observations were made of the Potentially Hazardous Asteroid (PHA) 2005 YU55. On 8 November, this object passed within 325 000 km of Earth.[4] Observing this target so soon after its fly-by of Earth meant that its position was rapidly changing (see Figure 2). An observation of this target demonstrated the capability of the Zadko Telescope to accurately point and acquire images of a relatively fast-moving object. On the first night of the observation, the sky motion was ∼4 arcsec min^{-1}. By comparison, main-belt asteroid sky motions are typically smaller than 0.5 arcsec min^{-1}.

The Zadko Telescope made observations of 2005 YU55 over a period spanning 11 nights, from 11 to 21 November.

[4] www.jpl.nasa.gov/news/news.cfm?release=2011-332

PASA, 30, e014 (2013)
doi:10.1017/pasa.2012.014

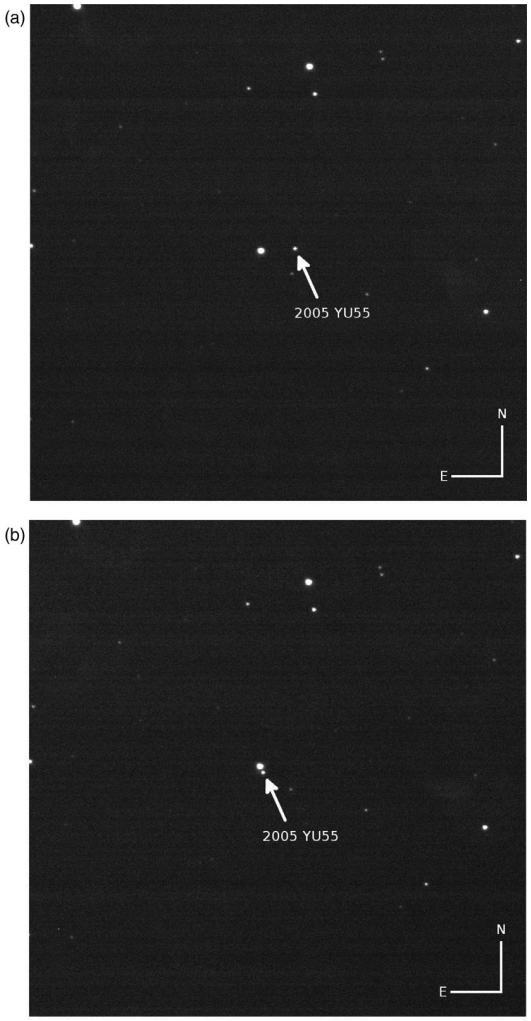

Figure 2. Zadko Telescope images of PHA 2005 YU55. Exp: 60 s, field centre: 02h20m49s6 +17d06m47s, scale: 11.5 ×11.5 arcmin, date: 2011-11-12.60964 (a) and 2011-11-12.62607 (b).

This was the third-longest observational coverage of 14 participating telescopes, and was the only contribution from a Southern Hemisphere telescope. The Zadko Telescope was used to obtain 42 images of PHA 2005 YU55 in 2011 November, of which 21 were used for astrometry. The images and measurements were delivered to the *Gaia* FUN-SSO working group, which reported the collective results from participating instruments to the MPC. During this time, the target faded dramatically (from 13.7 to 18.1 in the Sloan Digital Sky Survey (SDSS) *r* filter).

The residual error between the reported (observed) position and the position calculated by the *Gaia* FUN-SSO working group was calculated by taking ∼3 600 observations between 2005 December and 2011 December and fitting a numerical model of the asteroid motion. The model takes into account perturbations from all eight major planets and Pluto and the relativistic effect of the Sun. The mean residual was determined to be 0.30 arcsec, and for the Zadko Telescope was typically better than 0.20 arcsec in both right ascension and declination. The first measurement from each night, with residuals ($O - C$ values), is given in Table 2, and shows the change in brightness and sky motion over that period.

In 2012 February, observations were planned for asteroids 99942 Apophis and 1996 FG3. Apophis was selected since it will have a very close approach in 2029 and new astrometry would be useful to obtain more accurate ephemerides. New data can also be used to improve our knowledge of the Yarkovsky effect on its trajectory. 1996 FG3 was selected as it is the main target of the proposed Marco Polo-R space mission which will provide a sample return. Better knowledge of its orbital characteristics will help with the success of the mission. Although no data were obtained for these because of observing constraints, the targets were successfully logged into the robotic scheduler as a test.

4 SUMMARY

During its 5-year mission, *Gaia* will discover new SSOs, including IEAs and Earth-crossers (Atens), and new NEAs at larger solar elongations. Because the scanning law of *Gaia* will restrict the orbit determination to a very small number of astrometric measurements, only a ground-based optical network can obtain accurate orbital modelling, based on enough astrometric measurements. This is the primary objective of the *Gaia* FUN-SSO.

In 2010, the *Gaia* DPAC initiated a programme to identify ground-based optical telescopes for the *Gaia* FUN-SSO. The main criteria for the network are facilities that are ideally robotic, or can be re-scheduled to give priority to a *Gaia* alert. The Zadko Telescope was identified as a potentially important contributor to the network because of its robotic operation, sensitivity, and location. It will be used for validation of new SSOs, astrometry, and photometry of these targets.

In 2011, the *Gaia* FUN-SSO working group initiated an observing campaign of SSOs, with the main goal to test the capability of the network node facilities. Simulated *Gaia* alerts were distributed to the network (initially by email) providing ephemerides for the follow-up imaging of real targets. We tested the Zadko Telescope capability for participating in the observing campaign of PHA 2005 YU55 in late 2011. Of the 37 observing stations in the network, 11 were able to participate and provide useful astrometric data. The Zadko Telescope contributed the third-longest observational coverage from 14 participating telescopes and was the only contribution from a Southern Hemisphere telescope. The data from the observations showed that the Zadko Telescope scheduling system worked successfully, with accurate telescope

PASA, 30, e014 (2013)
doi:10.1017/pasa.2012.014

Table 2. Selection of 2005 YU55 Observations Made by the Zadko Telescope Showing the Change in Brightness and Sky Motion Over the Period. The $O - C$ Values Are the Differences from the Calculated Positions

				Sky Motion (arcsec min^{-1})		$O - C$ (arcsec)	
Date (UT)	RA	Decl.	Mag.	α	δ	$\alpha\cos(\delta)$	δ
2011 11 11.60593	02 13 56.45	+17 24 22.7	13.7	+4.1	−0.9	−0.43	−0.10
2011 11 12.60797	02 20 47.59	+17 06 54.4	14.2	+1.9	−0.5	−0.20	−0.09
2011 11 15.60574	02 29 03.05	+16 45 08.8	16.1	+0.3	−0.1	0.05	−0.12
2011 11 16.60259	02 30 24.47	+16 41 42.2	16.3	+0.2	−0.09	0.01	0.04
2011 11 19.59546	02 33 06.84	+16 35 40.7	17.7	+0.03	−0.03	−0.00	−0.13
2011 11 21.59059	02 34 22.04	+16 33 47.7	18.3	+0.02	−0.02	0.50	−0.02

pointings, and positional data that were used for astrometry with an uncertainty of about 0.2 arcsec. Testing of the networks ability to constrain orbits of SSOs will continue until the launch of *Gaia*.

Following upgrades to the Zadko Telescope observatory in 2012 and 2013, the telescope will resume operation for several optical transient projects. These improvements will also provide scope for participation in additional projects, including the follow-up of exoplanet candidates. Furthermore, an image processing pipeline for automated identification and analysis of optical transients is in development and planned for implementation in 2013.

ACKNOWLEDGMENTS

D. M. Coward is supported by an Australian Research Council Future Fellowship. The Zadko Telescope was made possible by a philanthropic donation to the University of Western Australia by the Zadko family. M. Todd and D. Coward acknowledge support received from the European Science Foundation (ESF) for the activity entitled 'Gaia Research for European Astronomy Training'.

REFERENCES

Coward, D. M., et al. 2010, PASA, 27, 331
Gendre, B., Stratta, G., Laas-Bourez, M., Coward, D. M., Klotz, A., Cutini, S., Boër, M., & Stockdale, C. 2011, A&A, 530, A74
LIGO Scientific Collaboration, et al. 2012, A&A, 539, A124
Mignard, F. 2011, Adv. Space Res., 47, 356
Mignard, F., et al. 2007, EM&P, 101, 97
Tanga, P., Hestroffer, D., Delbò, M., Frouard, J., Mouret, S., & Thuillot, W. 2008, P&SS, 56, 1812
Todd, M., Coward, D. M., & Zadnik, M. G. 2011, arXiv:1111.2427
Todd, M., Tanga, P., Coward, D. M., & Zadnik, M. G. 2012a, MNRAS, 420, L28
Todd, M., Tanga, P., Coward, D. M., & Zadnik, M. G. 2012b, MNRAS, 424, 372

Chapter 8

HEIDI: An Automated Process for the Identification and Extraction of Photometric Light Curves from Astronomical Images

Todd, M., H. U. Wallon Pizarro, P. Tanga, D. M. Coward, M. G. Zadnik. 2014. "HEIDI: An Automated Process for the Identification and Extraction of Photometric Light Curves from Astronomical Images." *Monthly Notices of the Royal Astronomical Society* (submitted). `arXiv:1401.2593` [astro-ph.IM]

Mon. Not. R. Astron. Soc. **000**, 1–7 () Printed 14 January 2014 (MN LATEX style file v2.2)

HEIDI: An Automated Process for the Identification and Extraction of Photometric Light Curves from Astronomical Images

M. Todd[1⋆], H. U. Wallon Pizarro[2], P. Tanga[3], D. M. Coward[4] and M. G. Zadnik[1]
[1]*Department of Imaging and Applied Physics, Bldg 301, Curtin University, Kent St, Bentley, WA 6102, Australia*
[2]*IBM Research - Australia, 1060 Hay St, West Perth, WA 6005, Australia*
[3]*Laboratoire Lagrange, UMR7293, Université de Nice Sophia-Antipolis, CNRS, Observatoire de la Côte d'Azur, BP 4229, 06304 Nice Cedex 4, France*
[4]*School of Physics, M013, The University of Western Australia, 35 Stirling Hwy, Crawley, WA 6009, Australia*

ABSTRACT

The production of photometric light curves from astronomical images is a very time-consuming task, taking several hours or even days. Larger data sets improve the resolution of the light curve, however, the time requirement scales with data volume. The data analysis is often made more difficult by factors such as a lack of suitable calibration sources and the need to correct for variations in observing conditions from one image to another. Often these variations are unpredictable and corrections are based on experience and intuition.

The High Efficiency Image Detection & Identification (HEIDI) pipeline software rapidly processes sets of astronomical images, taking only a few minutes. HEIDI automatically selects multiple sources for calibrating the images using a selection algorithm that provides a reliable means of correcting for variations between images in a time series. The algorithm takes into account that some sources may intrinsically vary on short time scales and excludes these from being used as calibration sources. HEIDI processes a set of images from an entire night of observation, analyses the variations in brightness of the target objects and produces a light curve all in a matter of minutes.

HEIDI has been tested on three different time series of 50 images each of asteroid 939 Isberga and has produced consistent high quality photometric light curves in a fraction of the usual processing time. The software can also be used for other transient sources, e.g. gamma-ray burst optical afterglows, Gaia transient candidates.

HEIDI is implemented in the programming language Python and processes time series astronomical images in FITS format with minimal user interaction. HEIDI processes up to 1000 images per run in the standard configuration. This limit can be easily increased, with the only real limit being system capacity, e.g. disk space, memory. HEIDI is not telescope-dependent and will process images even in the case that no telescope specifications are provided. HEIDI has been tested on various Linux systems and Linux virtual machines. HEIDI is very portable and extremely versatile with minimal hardware requirements.

Key words: methods: analytical – methods: data analysis – methods: numerical – techniques: image processing – techniques: photometric – astrometry

1 INTRODUCTION

The process of analysing a time series of astronomical images to measure the variations in brightness of an object over time and to calibrate those variations against reference sources is a very time-consuming task. An accurate understanding of the variation in brightness of an object over time, i.e. its photometric light curve, allows modelling of key characteristics of the object (e.g. the shape of an asteroid, the type of a supernova or gamma-ray burst optical afterglow).

The measurement process often varies only little depending on the type of object, whether it is an asteroid

⋆ E-mail: michael.todd@icrar.org (MT)

tumbling through space, a supernova or the rapidly fading optical afterglow from a gamma-ray burst. The process usually involves examining the images in the time series for at least one suitable reference source in order to calibrate the brightness. Some processes require the reference sources to have particular characteristics, e.g. a specific spectral class or magnitude. Other processes may need sources that have been identified as a photometric standard. If more than one calibration source is available, the precision can be improved enormously; however, this is also much more time-expensive. The process must be repeated for each image and corrections made from one image to another. These corrections can incorporate predictable adjustments such as extinction due to changing air mass. In addition, often the corrections that need to be made in order to obtain a consistent light curve are variable, non-uniform and unpredictable, and are based on experience and intuition.

The ability to quickly analyse a set of images and to produce a high quality light curve is particularly valuable on automated telescopes, e.g. the fully robotic Zadko Telescope in Gingin, Western Australia (Coward et al. 2010). Participation in programmes like the prompt follow-up of gamma-ray burst alerts for the detection of transient optical emissions as part of the Télescope à Action Rapide pour les Objets Transitoires (TAROT) network (Klotz et al. 2008) and the Gaia Follow-Up Network for Solar System Objects (Gaia-FUN-SSO, http://www.imcce.fr/gaia-fun-sso) (Todd et al. 2013) results in the creation of data sets containing transient sources that need rapid analysis.

We have developed a High Efficiency Image Detection & Identification (HEIDI) pipeline software for processing images and analysing the variations in brightness of optical transients. We take the approach that all sources in an image are potential reference sources. The variations in the brightness of the sources in each image of a time series are assessed automatically. Corrections are made to compensate for these variations while also taking into account that some sources may intrinsically vary on short time scales (e.g. short period variable stars). To facilitate production of photometric light curves Solar System objects are identified automatically during the image processing. As a result the automated analysis of an image set and the production of a calibrated light curve is achieved in a matter of minutes. HEIDI thus fulfils an emerging need for the rapid analysis of time series image data.

2 DESCRIPTION OF THE AUTOMATED PIPELINE SOFTWARE HEIDI

HEIDI is implemented in the programming language Python (http://www.python.org) for Linux platforms. It processes astronomical images in FITS format and requires only a minimal amount of user-supplied detail. It can also be installed on Linux virtual machines. This makes the software extremely versatile.

Preprocessing tasks such as astrometric calibration and image alignment are accomplished using existing applications as described in §2.1. The main functions of identification and selection of calibration sources, identification of targets and production of light curves are accomplished using newly developed Python code as described in §2.2 and §2.3. HEIDI has been benchmarked on a Pentium class system and a virtual machine, i.e. low-performance, low-cost systems.

2.1 Astrometric calibration and image alignment

The first step in the image analysis process is to perform the astrometric calibration. The amount of information contained in FITS image headers depends heavily on the system in place at the observing site. While an integrated system would typically produce FITS images which include calibration information in the image headers, some sites may not even include the pointing information. We have therefore adopted a standard approach of uploading one image from the set to the astrometry.net server in order to obtain a new astrometric calibration (Lang et al. 2010). By using the blind astrometric calibration system provided by astrometry.net, HEIDI thus removes any reliance on the images having already had astrometric calibrations or having to verify the pointing information, orientation or scale.

After obtaining the astrometric calibration, HEIDI assumes that all the images in the time series have the same pointing and updates the FITS image headers. The World Coordinate System (WCS) information from astrometry.net is included in the headers of the updated FITS images. The images are then processed through SExtractor (Bertin & Arnouts 1996) in order to build a catalogue of all objects found in the image set. The SExtractor catalogue is subsequently processed through SCAMP (Bertin 2006) which produces image headers that are ready to be used by SWarp (Bertin et al. 2002). SWarp aligns the images and includes the appropriate header information from any translation or rotation applied by SWarp during the alignment process. Most of the processing time is taken up with the SExtractor-SCAMP-SWarp workflow. On a single-CPU Pentium-class system, the astrometric calibration and image alignment stage for a set of 50 images takes about 10 min (vs. 1.25 min for the automated production of the photometric light curve by HEIDI, §2.2, §2.3).

2.2 Correlation of sources

In the correlation stage the images from the astrometric calibration and alignment stage are reprocessed through SExtractor to produce catalogues of all the sources that have been detected across the entire image set. These catalogues are correlated by HEIDI to identify the sources which are common to every image in the time series. These common sources are the candidate reference sources for the photometric calibration of the image set.

HEIDI calculates the natural logarithm of the flux value for each candidate source as a representation of relative (instrumental) magnitude. We refer to the natural logarithm of the flux hereafter simply as log flux. Examination of the log flux value for each candidate source may show some variation across the image set. HEIDI tests the log flux variation of each candidate source and rejects sources as candidates if the variation is greater than a predetermined threshold. An examination of the log flux values for the candidate sources

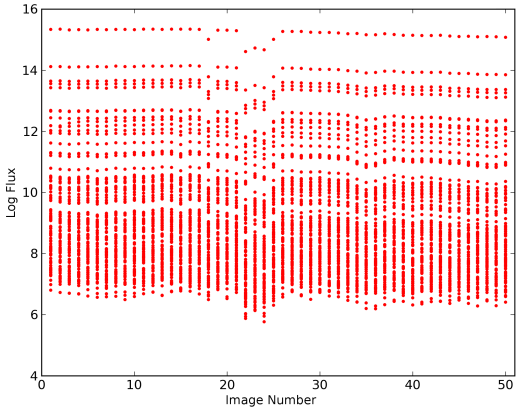

Figure 1. The selected stars from observations of asteroid 939 Isberga show a variation in the log flux values across the time series. As this variation appears to affect every source in a consistent manner it can be analysed and a correction applied.

in a time series of 50 images for asteroid 939 Isberga[1] shows a variation common to all candidate sources (Figure 1). As this variation appears to affect every source in a consistent manner, we conclude that this variation can be analysed and corrected.

For a given time series of N images, HEIDI finds all sources that are common to all N images in that time series. These M sources are selected as candidates for photometric calibration and are tested for variability over the time series.

STEP 1: For the N images and M sources, HEIDI reads the flux values ϕ_{ki}, $k \in \{1,\ldots,N\}$, $i \in \{1,\ldots,M\}$ from the SExtractor catalogues and calculates the natural logarithm of the flux. We will denote the natural logarithm of the flux as φ_{ki}, $k \in \{1,\ldots,N\}$, $i \in \{1,\ldots,M\}$ and refer to it hereafter as log flux. The initial log flux set is hence $\left(\varphi_{ki}\right)_{\substack{k\in\{1,\ldots,N\}\\ i\in\{1,\ldots,M\}}}$, $\varphi_{ki} = \ln\phi_{ki}$ and contains $N \cdot M$ values.

STEP 2: For each image $k \in \{1,\ldots,N\}$ in the time series, HEIDI calculates M log flux means: For each source $i \in \{1,\ldots,M\}$, the source i is excluded (denoted by $\tilde{i}$) and the log flux mean of the remaining sources $j \in \{1,\ldots,M\} \setminus \{i\}$ is determined:

$$\begin{aligned}\langle\varphi_{k\tilde{i}}\rangle &= \langle\varphi_{kj}\rangle_{j\in\{1,\ldots,M\}\setminus\{i\}}\\ &= \frac{1}{M-1}\sum_{\substack{j=1\\ j\neq i}}^{M}\varphi_{kj}, \quad k\in\{1,\ldots,N\}.\end{aligned} \tag{1}$$

STEP 3: HEIDI determines the global maximum of the log flux:

$$\varphi_{max} = \max_{k,i}\varphi_{ki} = \max_{\substack{k\in\{1,\ldots,N\}\\ i\in\{1,\ldots,M\}}}\varphi_{ki}. \tag{2}$$

[1] Three time series of 50 images each were taken by the first author (M. Todd) in November 2011 at the Zadko Telescope in Gingin, Western Australia.

For all $k \in \{1,\ldots,N\}$, $i \in \{1,\ldots,M\}$ the difference between the global maximum log flux φ_{max} and the log flux means $\langle\varphi_{k\tilde{i}}\rangle$ (determined in STEP 2) are calculated:

$$\begin{aligned}\Delta\varphi_{ki} = \varphi_{max} - \langle\varphi_{k\tilde{i}}\rangle\,,\\ k\in\{1,\ldots,N\}, i\in\{1,\ldots,M\}.\end{aligned} \tag{3}$$

This will be our correction factor.

STEP 4: To smooth out the variations across the image set, the log flux values φ_{ki}, $k \in \{1,\ldots,N\}$, $i \in \{1,\ldots,M\}$ are adjusted, yielding an adjusted log flux set:

$$\begin{aligned}\left(\varphi^*_{ki}\right)_{\substack{k\in\{1,\ldots,N\}\\ i\in\{1,\ldots,M\}}}, \varphi^*_{ki} = \varphi_{ki} + \Delta\varphi_{ki},\\ k\in\{1,\ldots,N\}, i\in\{1,\ldots,M\}.\end{aligned} \tag{4}$$

STEP 5: For each source $i \in \{1,\ldots,M\}$ HEIDI determines the adjusted log flux mean, the maximum adjusted log flux and the minimum adjusted log flux of this source across all N images:

$$\langle\varphi^*_{ki}\rangle_{k\in\{1,\ldots,N\}} = \frac{1}{N}\sum_{k=1}^{N}\varphi^*_{ki}, \quad i\in\{1,\ldots,M\}, \tag{5}$$

$$\max_k\varphi^*_{ki} = \max_{k\in\{1,\ldots,N\}}\varphi^*_{ki}, \quad i\in\{1,\ldots,M\}, \tag{6}$$

$$\min_k\varphi^*_{ki} = \min_{k\in\{1,\ldots,N\}}\varphi^*_{ki}, \quad i\in\{1,\ldots,M\}. \tag{7}$$

STEP 6: For each source $i \in \{1,\ldots,M\}$ HEIDI tests whether the deviation of the adjusted log flux values $\left(\varphi^*_{ki}\right)_{\substack{k\in\{1,\ldots,N\}\\ i\in\{1,\ldots,M\}}}$ from the adjusted log flux mean $\langle\varphi^*_{ki}\rangle_{k\in\{1,\ldots,N\}}$ is within a predetermined tolerance *tol*. This test rejects sources that are varying in brightness on short time scales (e.g. short period variable stars) or are otherwise not varying in accordance with the other candidates in the set (e.g. edge effects or vignetting). Only sources that pass this test will remain in the candidate list:

$$\begin{aligned}&|\max_k\varphi^*_{ki} - \langle\varphi^*_{ki}\rangle_{k\in\{1,\ldots,N\}}| \leqslant tol \quad \wedge\\ &|\min_k\varphi^*_{ki} - \langle\varphi^*_{ki}\rangle_{k\in\{1,\ldots,N\}}| \leqslant tol, \quad i\in\{1,\ldots,M\}.\end{aligned} \tag{8}$$

Sources that do not pass this test will be excluded from the candidate list. If X is the number of excluded sources then the reduced candidate list consists of $M - X$ candidates. This concludes the first pass and reduces the original candidate list $\left(\varphi_{ki}\right)_{\substack{k\in\{1,\ldots,N\}\\ i\in\{1,\ldots,M\}}}$ to $\left(\varphi'_{ki}\right)_{\substack{k\in\{1,\ldots,N\}\\ i\in\{1,\ldots,M\}\setminus\{i_1,\ldots,i_X\}}}$:

$$\begin{aligned}\left(\varphi'_{ki}\right)_{\substack{k\in\{1,\ldots,N\}\\ i\in\{1,\ldots,M\}\setminus\{i_1,\ldots,i_X\}}} =\\ \left(\varphi_{ki}\right)_{\substack{k\in\{1,\ldots,N\}\\ i\in\{1,\ldots,M\}}} \setminus \left(\varphi_{ki}\right)_{\substack{k\in\{1,\ldots,N\}\\ i\in\{i_1,\ldots,i_X\}}},\\ \{i_1,\ldots,i_X\}\subseteq\{1,\ldots,M\}.\end{aligned} \tag{9}$$

STEP 7: Repeat STEP 2 to STEP 6 for the reduced candidate list $\left(\varphi'_{ki}\right)_{\substack{k\in\{1,\ldots,N\}\\ i\in\{1,\ldots,M\}\setminus\{i_1,\ldots,i_X\}}}$.

This process of filtering variable sources is applied iteratively. The tolerance *tol* for the deviation test of the log flux (STEP 6) is 0.5, 0.2 and 0.1 for the first, second and third

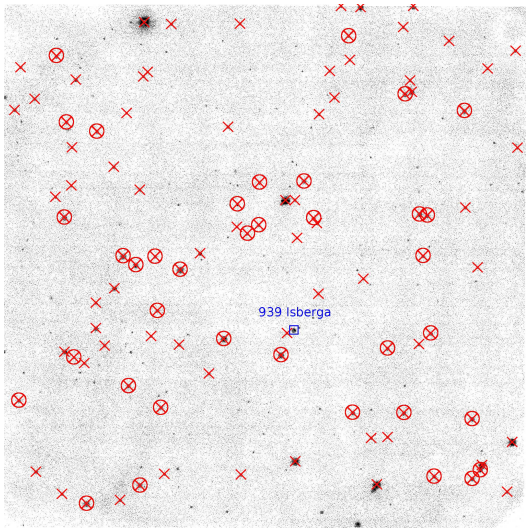

Figure 2. Sample image from the time series for asteroid 939 Isberga. This image is centred on right ascension $01^h\ 08^m\ 32.58^s$, declination $+11°\ 45'\ 48.43''$ (J2000) and has a field of view of ≈ 20x20 arcmin. Sources that are common to all images in the time series are indicated by a cross (×). These sources are tested for their suitability to be used as calibration sources. Circles (⊗) indicate those sources that have been selected as calibration sources. The position of the target, asteroid 939 Isberga is indicated by a square (□).

pass, respectively. We found that additional iterations with finer tolerances do not significantly improve the result as one reaches the limit of measurement precision. The candidate stars that survive this filtering process are used in the photometric calibration of the image set for producing the light curve for the target as described in §2.3. In addition, the candidates that fail the test are recorded for further study.

Figure 2 shows a sample image from a time series of $N = 50$ images for asteroid 939 Isberga. This image contains exactly $M = 100$ sources that are common to all images in the time series, marked with a cross (×). These sources are selected as candidate sources and are tested for their suitability for use as calibration sources. Circles (⊗) indicate the reduced set of 37 sources that were found to be suitable for use as calibration sources by HEIDI. The position of the target, asteroid 939 Isberga is indicated by a square (□).

On a single-CPU Pentium-class system the correlation stage for a time series of 50 images takes only about 1 min.

2.3 Identification of target sources and production of the light curves

HEIDI has been designed to facilitate the production of photometric light curves for Solar System objects (target sources). Following the selection of calibration sources as described in §2.2, the target sources are identified and selected. HEIDI uses the Institut de Mécanique Céleste et de Calcul des Éphémérides (IMCCE) Sky Body Tracker (SkyBoT) Cone-Search and Resolver services (Berthier et al. 2006) to quickly identify the known Solar System objects in the time series, our target sources. HEIDI processes the time series very quickly: For a set of 50 images it takes HEIDI only approximately 15 s to identify one target source, to test for its presence in the image set, to compile the list of the corresponding flux values and to produce the photometric light curve for this object, i.e. ≈ 0.3 s per object per image. As a consequence we have implemented HEIDI to produce light curves for all of the objects found in the time series rather than just the primary target.

The IMCCE SkyBoT Cone-Search service identifies which Solar System objects lie within a specified field of view at a given epoch: HEIDI calls the Cone-Search service and obtains a list of the objects that may be found in the time series by providing the centre coordinates in right ascension and declination and the epoch of observation.

For each object returned by the Cone-Search service, HEIDI calls the IMCCE SkyBoT Resolver service to obtain accurate coordinates: HEIDI provides the name of the object and the epoch for the first image in the time series to the Resolver service. If known, HEIDI also provides the International Astronomical Union (IAU) Observatory Code for the site at which the images were recorded. The Resolver service then returns accurate coordinates for the specified object. If the IAU Observatory Code is provided then the Resolver service returns coordinates in the topocentric frame, otherwise the coordinates are given for the geocentric frame.

To determine the object coordinates in the remaining images of the time series, HEIDI finds the record for each object in the IAU Minor Planet Center Orbit (MPCORB) database (http://www.minorplanetcenter.net). The coordinates for each object are computed from the orbital elements in the MPCORB database on a per-image basis across the time series. These computations are much faster than obtaining coordinates from the Resolver service. It takes only a fraction of a second to calculate the coordinates for an object for all images in the time series, compared with several seconds per image when retrieved from the Resolver service. However, due to rounding errors in the computation, the coordinates provided by the Resolver service may be more accurate than the ones computed by HEIDI. HEIDI will thus determine the difference between the coordinates provided by the Resolver service and the ones computed locally and apply this offset as a correction to all computed coordinates across all images.

The respective coordinates in each image of the time series are then tested to determine the presence of the target sources. To minimise false detections without introducing false non-detections, this is done in a two-step process: In a first step, an area of 10 x 10 pixels around the coordinates of the target is tested for the presence of a source; if no source is found, the area is expanded to 15 x 15 pixels and the test repeated. It is not possible to determine whether a failure to detect a target source is due to the faintness of the object or an error in the position calculation. We thus assume that the primary target for the measurement and production of a light curve has a well-known orbit and also a good signal-to-noise ratio in the time series.

If the object is detected in the images of the time series, the log flux of the object is recorded for each image. Plotting the log flux of the object and the log flux of the calibration sources without correcting for the variations between images

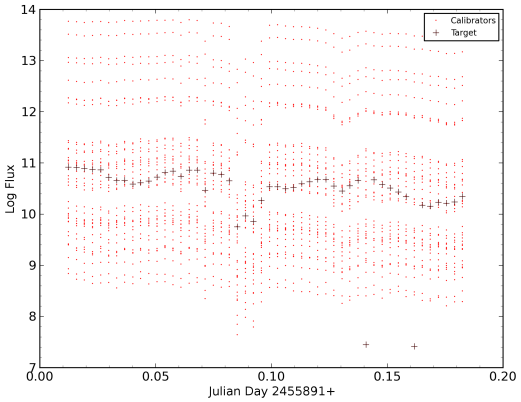

Figure 3. Uncorrected log flux measurements from calibration sources (·) and target (+) in the time series for asteroid 939 Isberga. The calibration sources can clearly be seen to vary in accordance with each other. The target, asteroid 939 Isberga, follows a similar trend. The light curve is not readily apparent.

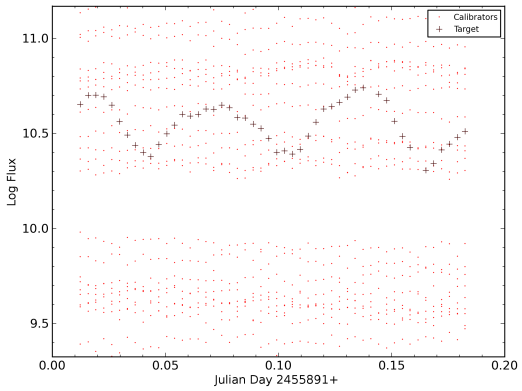

Figure 4. Corrected log flux measurements for calibration sources (·) and target (+) in the time series for asteroid 939 Isberga. The variation in the calibration sources is minimal ($<\pm 0.05$). The light curve of the target is clearly apparent.

in the time series does not give a clear indication of the light curve of an object. Figure 3 shows the uncorrected log flux measurements from calibration sources and the target in a time series for asteroid 939 Isberga.

The log flux mean of the calibration sources identified in §2.2 is calculated for each image (similar to Equation 1 but this time over the entire candidate source set):

$$\langle \varphi_{ki} \rangle_{i\in\{1,\ldots,M\}} = \frac{1}{M}\sum_{i=1}^{M}\varphi_{ki}, \quad k \in \{1,\ldots,N\}. \tag{10}$$

The global log flux mean is also determined:

$$\begin{aligned}\langle \varphi_{ki} \rangle_{\substack{k\in\{1,\ldots,N\}\\ i\in\{1,\ldots,M\}}} &= \frac{1}{NM}\sum_{k=1}^{N}\sum_{i=1}^{M}\varphi_{ki} \\ &\overset{Eq.10}{=} \frac{1}{N}\sum_{k=1}^{N}\langle \varphi_{ki} \rangle_{i\in\{1,\ldots,M\}}.\end{aligned} \tag{11}$$

This is used for reference and correction of variations across the time series.

For each image $k \in \{1,\ldots,N\}$ in the time series, the log flux values of the calibration sources are adjusted by adding the difference between the global log flux mean and the log flux mean for that image. For all $k \in \{1,\ldots,N\}$, $i \in \{1,\ldots,M\}$ the difference between the global log flux mean $\langle \varphi_{ki} \rangle_{\substack{k\in\{1,\ldots,N\}\\ i\in\{1,\ldots,M\}}}$ and the log flux mean $\langle \varphi_{ki} \rangle_{i\in\{1,\ldots,M\}}$ is calculated:

$$\begin{aligned}\Delta\varphi_k = \langle \varphi_{ki} \rangle_{\substack{k\in\{1,\ldots,N\}\\ i\in\{1,\ldots,M\}}} - \langle \varphi_{ki} \rangle_{i\in\{1,\ldots,M\}}, \\ k \in \{1,\ldots,N\}.\end{aligned} \tag{12}$$

For each image $k \in \{1,\ldots,N\}$ in the time series, the log flux value of the target object φ_{kt}, $k \in \{1,\ldots,N\}$ (where t denotes the target source) is adjusted by the same correction factor $\Delta\varphi_k$. To smooth out the background variations across the image set, the log flux values φ_{kt}, $k \in \{1,\ldots,N\}$ for the target object t are adjusted:

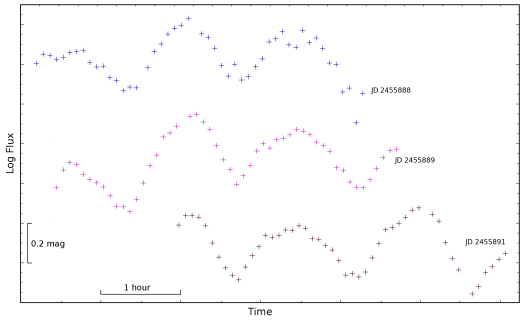

Figure 5. The light curves produced by HEIDI for asteroid 939 Isberga using time series that were obtained on three separate dates show the consistency of the results. It can be easily seen that the three curves follow a very similar pattern. A primary periodicity consistent with the expected rotation period of 2.9173 h is evident.

$$\varphi^*_{kt} = \varphi_{kt} + \Delta\varphi_k, \quad k \in \{1,\ldots,N\}. \tag{13}$$

Applying this correction to the time series for asteroid 939 Isberga shows a light curve that is readily apparent (Figure 4). This light curve for asteroid 939 Isberga produced by HEIDI clearly shows a primary period consistent with the expected rotation period of 2.9173 h (0.12155 d) (Molnar et al. 2008).

The consistency of the results achieved by HEIDI is further demonstrated by extending the analysis to multiple time series for asteroid 939 Isberga that were obtained on three separate dates. The light curves determined by HEIDI for these three time series are shown superimposed in Figure 5. It can be easily seen that the three curves follow a very similar pattern.

These curves can also be overlaid on one another to

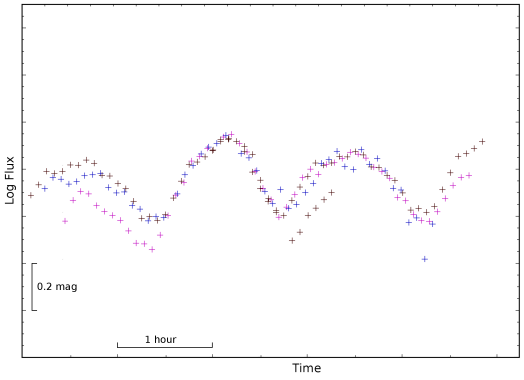

Figure 6. Light curves produced by HEIDI for asteroid 939 Isberga from time series obtained on three separate dates (22, 23 and 25 November 2011) overlaid on one another to show that both the period and the amplitude of each curve is consistent with the period and amplitude of the other curves.

show that both the period and the amplitude are consistent (Figure 6).

3 FUTURE DEVELOPMENTS

The current version (as of November 2013) has good astrometric accuracy but performs only relative photometry, i.e. does not produce calibrated magnitudes. We plan to add the capability for the production of light curves calibrated to a standard photometric system.

The preprocessing tasks of astrometric calibration and image alignment described in §2.1 are independent of the type of object being studied. The candidate sources that are rejected by the filtering process described in §2.2 warrant further study to determine whether they were excluded due to some intrinsic variability. These excluded sources can include non-moving sources that have characteristic light curves, e.g. variable stars, supernovae and gamma-ray burst optical afterglows. In the next version of HEIDI, we will include the ability to also produce photometric light curves for all the excluded objects as a standard function.

Uncertainties on the produced light curves can be inferred from the dispersion of the magnitudes of the calibration sources and will be used to include error bars in the output. If the target source is near, i.e. within 2 to 3 arcsec, a star of similar or greater brightness, it is possible that the star is selected instead of the target source. The next version of HEIDI will include a step to automatically exclude detections in which the position information falls outside a predetermined tolerance. In addition, an algorithm to detect moving objects will be implemented for targets with less accurate position information or unknown targets.

4 CONCLUSIONS

The High Efficiency Image Detection & Identification (HEIDI) pipeline software rapidly processes sets of astronomical images. It is very fast and reliable. HEIDI takes a set of images from a night of observing and produces a light curve in a matter of minutes.

HEIDI is implemented in the programming language Python. It has been tested on various Linux systems and Linux virtual machines. It has minimal hardware requirements and the installation process is relatively straightforward. HEIDI runs in virtual machines without impacting performance and can thus be installed on non-Linux systems (if a Linux virtual machine is available). The High Efficiency Image Detection & Identification (HEIDI) pipeline software we developed has a small footprint yet is very powerful and extremely versatile.

Given programmes like the prompt follow-up of gamma-ray burst alerts for the detection of transient optical emissions and the Gaia Follow-Up Network for Solar System Objects, which require prompt follow-up and rapid analysis of time series data, HEIDI will be very useful and provide a service and a speed that have not been available.

Testing HEIDI on multiple fairly large time series for asteroid 939 Isberga yielded extremely satisfying results. The light curves produced using time series obtained on three separate dates showed consistency with the three curves following a very similar pattern.

HEIDI will be installed at the Zadko Telescope in Gingin, Western Australia. This will allow us to analyse very rapidly all the images in the data archive of the Zadko Telescope and search for interesting variable sources. It will also allow prompt analysis and rapid issuing of results for time critical events such as gamma-ray burst optical afterglow emissions.

The HEIDI package is available from the first author on request.

ACKNOWLEDGMENTS

MT thanks Frédéric Vachier for assistance with photometry. MT thanks Andrew Williams for assistance with processing FITS image files. The work reported on in this publication has been supported by the European Science Foundation (ESF), in the framework of the GREAT Research Networking Programme. DMC is supported by an Australian Research Council Future Fellowship.

REFERENCES

Berthier, J., Vachier, F., Thuillot, W., Fernique, P., Ochsenbein, F., Genova, F., Lainey, V., Arlot, J.-E., 2006, Astronomical Data Analysis Software and Systems XV, 351, 367

Bertin, E., Arnouts, S., 1996, A&AS, 117, 393

Bertin, E., Mellier, Y., Radovich, M., Missonnier, G., Didelon, P., Morin, B., 2002, Astronomical Data Analysis Software and Systems XI, 281, 228

Bertin, E., 2006, Astronomical Data Analysis Software and Systems XV, 351, 112

Coward, D. M., et al., 2010, PASA, 27, 331

Klotz, A., Boër, M., Eysseric, J., Damerdji, Y., Laas-Bourez, M., Pollas, C., Vachier, F., 2008, PASP, 120, 1298

Lang, D., Hogg, D. W., Mierle, K., Blanton, M., Roweis, S., 2010, AJ, 139, 1782

Molnar, L. A., et al., 2008, Minor Planet Bulletin, 35, 9
Todd, M., Coward, D. M., Tanga, P., Thuillot, W., 2013, PASA, 30, 14

Chapter 9

Conclusions and further work

9.1 Conclusions

9.1.1 Introduction

Trojan asteroids (or Trojans) share the orbit of a planet about the Sun and librate around the L4 or L5 Lagrangian points of stability (Section 1.2). Trojans appear to be stable on long timescales, on the order of the age of the Solar System (Pilat-Lohinger, Dvorak, and Burger 1999; Scholl, Marzari, and Tricarico 2005). This raises the question whether Trojans formed with the planets from the Solar nebula or were captured in the Lagrangian regions by gravitational effects. They are thus important Solar System fossils as they provide insight into the evolution of the Solar System.

Since the discovery of the first Trojan asteroid in 1906 (Nicholson 1961) about 6,000 Trojans have been found. The overwhelming majority of these are in the orbit of Jupiter, with only a handful known to exist in the orbits of the other planets. Specifically, as of today there are (Minor Planet Center 2013b):

- 1 Earth Trojan,
- 5 Mars Trojans,
- 5922 Jupiter Trojans,
- 1 Uranus Trojan and
- 9 Neptune Trojans.

Discovery and study of Trojans in the orbits of the inner planets of the Solar System will therefore help constrain models for the distribution and interactions of bodies in the inner Solar System.

Some searches have been conducted for Earth Trojans (Dunbar and Helin 1983; Whiteley and Tholen 1998; Connors et al. 2000) without resulting in a discovery. Dunbar and Helin (1983) analysed 18 photographic plates of the L4 region and estimated that there could not be more than 7.0 ± 3.5 Trojan asteroids with diameters larger than 250 m. Whiteley and Tholen (1998) searched a region covering approximately 0.35 square degrees down to a magnitude of $R = 22.8$ and proposed an upper population limit of fewer than three objects per square degree. Connors et al. (2000) later searched a region covering about 9 square degrees down to a magnitude of $R = 22$ without success. It was not until the examination of data from the WISE satellite by Connors, P. Wiegert, and Veillet (2011) that the first known Earth Trojan (2011 TK_7) was discovered.

Near-Earth asteroid search programmes generally survey areas of sky near the plane of the ecliptic because any orbit must cross the ecliptic irrespective of its inclination (Stokes, J. B. Evans, and Larson 2002). These areas around the ecliptic make up just a small fraction of the regions of stability for Earth Trojans. Orbit simulations (Mikkola and Innanen 1990; Tabachnik and N. W. Evans 2000) suggest that stable Earth Trojan orbits are inclined to the plane of the ecliptic. These stable inclinations range from 10 degrees to 45 degrees. In addition, the Earth–Sun–Trojan geometry requires observations at low altitudes which limits the observing time and restricts the ability to make multiple or follow-up observations. This geometry also results in low apparent motion relative to the background stars as the orbit arc is at an oblique angle to an observer on Earth.

The brightness of the Earth Trojan 2010 TK_7 ranges between an apparent magnitude of $V = 20.9$ and $V = 22.8$ (Todd et al. 2014). It would therefore have been detectable in the searches performed by Whiteley and Tholen (1998) and Connors et al. (2000) had they observed that specific region. The lack of success in earlier searches can be attributed to the observations not covering sufficient sky area in the regions in which Earth Trojans can be found. The largest search area of 9 square degrees by Connors et al. (2000) is only a small fraction (less than 0.7%) of the sky area of between about 1300 and 1500 square degrees described in Todd et al. (2012a) (Chapter 3).

Simulations of the coorbital population predicted 0.65 ± 0.012 objects with diameters larger than 1 km and 16.3 ± 3.0 objects with diameters larger than

100 m (Morais and Morbidelli 2002). The discoveries of the coorbital asteroid 3753 Cruithne (P. A. Wiegert, Innanen, and Mikkola 1997), the horseshoe orbiter 2010 SO_{16} (Christou and Asher 2011) and the L4 Trojan 2010 TK_7 (Connors, P. Wiegert, and Veillet 2011) confirm that objects orbit the Sun in 1:1 mean motion resonance with Earth. It is therefore reasonable to assume that more coorbitals exist than have so far been discovered. The only uncertainties are the number and the sizes of these objects.

Few searches have been conducted for Mars Trojans. The first Mars Trojan (5261 Eureka) was discovered in 1990 during the Mars and Earth-Crossing Asteroid and Comet Survey by E. M. and C. S. Shoemaker at the Palomar Observatory (Bowell et al. 1990). As of today there are five known Mars Trojans. This number represents one-tenth of the predicted population of about 50 Mars Trojans with diameters larger than 1 km, and there may be in excess of 100 Mars Trojans with diameters larger than 100 m (Tabachnik and N. W. Evans 1999, 2000; N. W. Evans and Tabachnik 2000).

Although the predicted numbers of Mars Trojans are much greater than those for Earth Trojans, the lack of discovery of additional Mars Trojans can also be attributed to a lack of observations in the wider regions in which these could exist. Observations are also limited to periods when these regions are visible from Earth. Similar to the modelled Earth Trojan orbits, simulations of Mars Trojan orbits found that stable orbits are inclined to the plane of the ecliptic in the ranges of between 15 and 28 degrees and between 30 and 35 degrees (Scholl, Marzari, and Tricarico 2005). Furthermore, these orbits were found to be stable over the age of the Solar System.

9.1.2 Search strategies for Trojan asteroids in the inner Solar System

Todd, Coward, and Zadnik (2012) (Chapter 2) describe probability distributions for Trojan asteroids in the orbits of Earth and Mars. This paper constrains the regions of highest probability for the existence of Trojans and defines the optimal search areas. This paper also examines strategies for survey telescopes with the aim of optimising observing patterns and cadences to maximise the probability of detecting Earth and Mars Trojans. Various strategies were examined with the conclusion being that the optimal strategy for searching for Earth Trojans is to observe a sub-region of the Earth Trojan field and use Earth's revolution about the Sun to progressively survey that field. This strategy was examined in greater

detail in Todd et al. (2012a) (Chapter 3).

It was also suggested that a similar strategy could be effective in searching the Mars Trojan fields during their passage through opposition. However, it was noted that the changing Earth–Mars geometry over time could have implications for this approach. Further examination of strategies to search for Mars Trojans was made in Todd et al. (2012b) (Chapter 4).

The implications for the detection of Trojans by the *Gaia* satellite and the limitations of *Gaia*'s observing geometry were also considered. As a space-based instrument, *Gaia* does not share the limitations of ground-based telescopes, e.g. atmospheric extinction and local horizon. The primary limitations that were identified for *Gaia* are its limiting magnitude of $V = 20$ and its precession cycle which restricts the range of solar elongations at which it is able to make observations (Mignard et al. 2007). The prospects for detecting Earth and Mars Trojans by *Gaia* were examined further in Todd et al. (2013) (Chapter 5) and Todd et al. (2014) (Chapter 6). It was also noted that *Gaia* detections require follow-up observations from ground-based telescopes and that a follow-up network (Thuillot, Hestroffer, and Tanga 2011) was being developed for this purpose.

9.1.3 An optimal Earth Trojan asteroid search strategy

Todd et al. (2012a) (Chapter 3) developed and expanded the concepts introduced in Todd, Coward, and Zadnik (2012) (Chapter 2), describing a model probability distribution for Earth Trojans. This distribution was used to constrain optimal search areas and imaging cadences for efficient use of telescope time while maximising the probability of detecting Earth Trojans. If the assumption is made that Earth Trojans are approximately evenly distributed between the L4 and L5 regions, then one or the other of these regions can be examined in isolation with the expectation that the other region would yield a similar result. However, there is only a small amount of time available per day where each of these regions can be surveyed due to the Earth–Sun–Trojan geometry. Given these short windows of opportunity where ground-based optical observations can only be made before the morning (L4 region) or after the evening twilight (L5 region), it is advisable that both regions be surveyed.

The regions of highest probability for detection are in the inclination range of between 10 and 45 degrees and the heliocentric longitude ranges of between 30 and 130 degrees (L4) and between 240 and 340 degrees (L5). The geocentric solid angles are about 1,300 square degrees for the L4 region and about 1,500 square

degrees for the L5 region. Surveys of the entire field in a single session are not practical as the geometry does not allow sufficient time. This implies that the conventional approach for detecting asteroids by repeated observations of a field must have cadence times in days rather than hours.

The optimal strategy is to observe a subregion of the Earth Trojan field and use Earth's revolution about the Sun to progressively survey the field as it crosses this subregion. By adopting this approach only a few minutes are required per session, twice per week. These observations can be performed by a survey telescope such as Catalina or Pan-STARRS before or after the primary science mission. Establishing this programme requires continued observations for one year, however, the total time commitment is a few tens of hours spread over the year.

The only known Earth Trojan, 2010 TK_7, would pass through the observed region during its orbit. In addition, considering the existence of the Trojan 2010 TK_7 and the coorbitals 3753 Cruithne and 2010 SO_{16} and the population prediction of Morais and Morbidelli (2002), it is probable that there are no additional large (e.g. larger than 1 km) Earth coorbitals but that there may be several undiscovered objects with diameters larger than 100 m.

A comparison was also made between the *Gaia* satellite and ground-based telescopes. Observations of Earth's L4 and L5 regions by the *Gaia* satellite are not subject to the same constraints as ground-based telescopes, i.e. *Gaia* is not limited by local horizon or airmass. *Gaia* will operate in a continuous scanning mode and hence will image the L4 and L5 regions many times during its five year mission. *Gaia* is only limited by a minimum solar elongation of 45 degrees due to its orbit and in sensitivity to a limiting magnitude of $V = 20$ (Mignard et al. 2007). The prospects for detection of Earth Trojans by *Gaia* were examined further in Todd et al. (2013) (Chapter 5) and Todd et al. (2014) (Chapter 6).

9.1.4 An optimal Mars Trojan asteroid search strategy

Todd et al. (2012b) (Chapter 4) developed and expanded the concepts introduced in Todd, Coward, and Zadnik (2012) (Chapter 2), describing a model probability distribution for Mars Trojans. This distribution was used to constrain optimal search areas and imaging cadences for efficient use of telescope time while maximising the probability of detecting Mars Trojans.

The spatial separation between the L4 and L5 Lagrangian regions allows the L5 (trailing) region to be surveyed while Mars approaches opposition and the L4 (leading) region to be surveyed after Mars has passed opposition. This provides a

period of several months during which each of these regions can be fully surveyed. Even though these regions are visible to an Earth-based observer for most of the night over the period during which the regions are observable, compared with the short windows of opportunity for observing Earth Trojans (Todd et al. 2012a), it is still important to find the optimal strategy for efficient use of telescope time while maximising sky coverage and probability of detection.

Detection of Trojan asteroids by regular and repeated observations of the field can be accomplished using a systematic approach to survey the entire Mars Trojan field during a synodic period. The regions of highest probability for detection are at inclinations less than 35 degrees and the heliocentric longitude ranges of between 40 and 90 degrees (L4) and between 270 and 320 degrees (L5). The geocentric solid angles for these regions vary from about 2,000 square degrees at a solar elongation of 60 degrees to between 11,000 and 17,000 square degrees at opposition. The change in distance between Earth's and Mars' orbit due to Mars' eccentricity results in a wide variation in the sky area when the field is near opposition.

A consequence of the size of the Trojan regions is that when a region is at solar elongations greater than 150 degrees the sky area becomes too large to survey in a single night by any existing wide-field telescope. At solar elongations less than about 150 degrees it would be possible for survey telescopes such as Catalina and the Large Synoptic Survey Telescope (LSST) to survey the entire field. However, by adopting the approach suggested for the Earth Trojan fields of observing a subregion of the Mars Trojan field and progressively surveying the entire field during a synodic period, the amount of time per session is minimised. The amount of time required by this approach is comparable to the time requirement for the Earth Trojan search programme: a few minutes per night at intervals of 3 to 4 days.

A comparison between the *Gaia* satellite and ground-based telescopes for surveys of the Mars L4 and L5 Lagrangian regions was made, similar to the comparison for Earth Trojans in Todd et al. (2012a) (Chapter 3). Although *Gaia*'s orbit prevents observations of these regions when they are at opposition it will survey the regions while they are at solar elongations between 45 and 135 degrees. Consequently it will image these regions multiple times during its mission.

It was considered that *Gaia* will detect Mars Trojans larger than 1 km in diameter provided the lateral motion across the CCD array is less than 0.40 arc-sec/s. The prospects for detection of Mars Trojans by *Gaia* were also examined

in more detail in Todd et al. (2013) (Chapter 5) and Todd et al. (2014) (Chapter 6).

9.1.5 Detection of inner Solar System Trojan Asteroids by Gaia

Todd et al. (2013) (Chapter 5) described initial simulations for the detection of Trojan asteroids in the orbits of Earth and Mars by the *Gaia* satellite. The probability distributions and limits on search areas for Earth and Mars Trojan asteroids from Todd et al. (2012a) (Chapter 3) and Todd et al. (2012b) (Chapter 4), respectively, were used to construct orbits for hypothetical Earth and Mars Trojans. These Trojan-like orbits were used to model the detection characteristics and detection limits with respect to *Gaia* for test bodies with diameters of 1 km and albedos of 0.20.

The Earth and Mars Trojan regions occupy a very large sky area, however, *Gaia* will survey these regions multiple times during its mission. The Earth Trojan regions will be over-observed in comparison to any other field because *Gaia* will observe this region in every scan cycle. In contrast, the Mars Trojan regions will be observed less frequently because of the different geometry. For both cases the along-scan and across-scan velocities are rather high compared with the drift for main belt asteroids. This may present a problem as the source tends to drift out of the window defined on the CCD and may result in signal degradation.

The results for the Earth Trojan simulations are encouraging, with about 94% of the test bodies being detected. However, it was considered unlikely that any Earth Trojans exist which are larger than the known Trojan 2010 TK_7. The consequence is that Earth Trojans will be too small and hence their brightness will be below *Gaia*'s detection threshold.

The results for the Mars Trojans were less positive. While more than 99% of the test bodies crossed *Gaia*'s field of view, most of these were not brighter than the sensitivity limit of $V = 20$. The subset of test bodies that were detected comprised only about 10% of the simulated objects. The implication is that there is some uncertainty about whether *Gaia* can detect Mars Trojans of sizes comparable to those already known.

New simulations were then constructed to determine specifically whether *Gaia* would detect the known Trojans and its potential for discovering new Trojans. These simulations were described in Todd et al. (2014) (Chapter 6).

9.1.6 Predictions for the detection of Earth and Mars Trojan asteroids by the Gaia satellite

Todd et al. (2014) (Chapter 6) elaborated on the initial study presented in Todd et al. (2013) (Chapter 5). This paper investigated the detection of Earth and Mars Trojans by *Gaia* using the known Trojans as a basis for study.

Simulations were constructed using the known Trojans for Earth (2010 TK_7) and Mars (5261 Eureka, 1998 VF_{31}, 1999 UJ_7, 2007 NS_2 and 2001 DH_{47}). The asteroids that were proposed as Mars Trojans by C. de la Fuente Marcos and R. de la Fuente Marcos (2013) (2011 SC_{191}, 2011 SL_{25} and 2011 UN_{63}) were also included in the sample.

The orbital elements for these Trojans were used as a basis for the simulations. The elements were cloned and modified to provide a distributed population due to the uncertainty that existed about when *Gaia* would commence operation.

It was found that *Gaia* will not detect the Earth Trojan 2010 TK_7. Although this Trojan's orbit keeps it very close to Earth and almost always within *Gaia*'s observable region so that it crosses *Gaia*'s field of view almost every scan cycle, it is too faint to be detected by *Gaia* due to its small size (about 300 m (Connors, P. Wiegert, and Veillet 2011)). Consequently the analysis for 2010 TK_7 was extended to determine the *Gaia* detection limit for Earth Trojans.

This analysis included consideration of the along-scan and across-scan drift velocities on *Gaia*'s focal plane array. It was found that these velocities were considerably greater than for main belt asteroids. The median along-scan velocity was about 40 mas/s which is almost six times greater than for main belt asteroids. The across-scan motion was typically less than 40 mas/s which is about three times greater than for main belt asteroids. These velocities would result in a degradation of the signal which would severely impact the likelihood of a positive detection.

An interesting outcome of the velocity analysis is that the distribution of the across-scan motions was asymmetric rather than the bimodal distribution that was found with the simulated Earth Trojans in Todd et al. (2013) (Chapter 5). This asymmetry is attributed to the Trojan residing in Earth's L4 Lagrangian region, whereas the simulated Earth Trojans in Todd et al. (2013) included both (L4 and L5) regions.

The conclusion is that *Gaia* will detect a kilometre-scale Earth Trojan in spite of the signal degradation caused by the relative drift across the CCD array. It was also found that there will be a substantial number of CCD crossings where

the relative drift will be small and thus the signal degradation will be minimal. Consequently it was concluded that the minimum size Earth Trojan that *Gaia* could detect would have a diameter of about 600 m.

The results for the Mars Trojans determined that *Gaia* would detect the currently known Mars Trojans and could discover more than 100 new Mars Trojans as small as 400 m in diameter. The three largest Mars Trojans (5261 Eureka, 1998 VF_{31} and 1999 UJ_7) were fully detected in the simulations and 2001 NS_2 had a 98% detection rate. Of the other Mars Trojans, 2001 DH_{47} was partially detected (43% detection) while 2011 SL_{25} had only a few detections (9%). The Trojans 2011 SC_{191} and 2011 UN_{63} went undetected as these are too faint.

The along-scan and across-scan drift velocities were also greater than for main belt asteroids. The median along-scan velocity was about 16 mas/s, about double the along-scan drift velocity of main belt asteroids. The across-scan velocity was typically less than 30 mas/s, also about double that of main belt asteroids. These velocities would also result in a degradation of the signal but to a lesser extent than for Earth Trojans.

The results indicate that for detecting smaller Mars Trojans the starting conditions and orbit parameters both have a significant impact. It was determined that the *Gaia* limit for detecting Mars Trojans is an absolute magnitude of $H \approx 19 \pm 0.5$ which equates to a diameter of about 400 m. The conclusion is that *Gaia* will detect Mars Trojans with diameters larger than 800 m. It was also considered that *Gaia* could detect Trojans with diameters down to 400 m depending on the starting conditions and the orbit of the Trojan.

From the predictions for the Mars Trojan population (Tabachnik and N. W. Evans 1999, 2000; N. W. Evans and Tabachnik 2000) it was estimated that there may be 70 ± 15 Trojans with diameters greater than 800 m. If these predictions are accurate then it can be expected that *Gaia* will detect between 55 and 140 new Mars Trojans. These simulation predictions and the Mars Trojan population models will be validated by the results of the *Gaia* mission.

9.1.7 Australian participation in the Gaia Follow-Up Network for Solar System Objects

During its five year mission the *Gaia* satellite will survey some hundreds of thousands of Solar System objects down to a magnitude of $V = 20$. Most of these objects will be main belt asteroids, however, it will be the unusual minor planets, such as those with high inclinations and so are normally outside the regions of

sky that are routinely surveyed by near Earth asteroid programmes and the inner Solar System Trojan asteroids that will be of particular interest. Since *Gaia*'s mission is to perform an all-sky survey, its orbit does not allow it to perform targeted follow-up studies (Mignard et al. 2007). Consequently, in 2010, the *Gaia* Data Processing and Analysis Consortium (DPAC) initiated a programme to establish a network of ground-based optical telescopes for performing the tasks of discovery confirmation, identification and tracking of objects.

This network is known as the *Gaia* Follow-Up Network for Solar System Objects (*Gaia* FUN-SSO). The main criteria for telescopes to be included in the network are that they are robotic or that they can be rescheduled to respond to a *Gaia* alert. The Zadko Telescope in Western Australia, described in Todd, Coward, Tanga, et al. (2013) (Chapter 7), has been flagged as an important site because of its location, automated scheduling system and sensitivity.

Located in the Southern Hemisphere in the state of Western Australia at longitude 115°42′49″ E, latitude 31°21′24″ S, the Zadko Telescope is a fully robotic 1-m f/4 Cassegrain telescope. The core science theme of the Zadko Telescope is the study of transients (Coward et al. 2010). Along with the robotic TAROT telescopes in France and Chile, the Zadko Telescope has been observing selected quasi-stellar objects (QSOs) since the middle of 2011 to assist in constructing the initial catalogue for establishing *Gaia*'s reference frame. As a node in the *Gaia* FUN-SSO it will assist in validating new Solar System objects discovered by *Gaia* and provide astrometry and photometry for these targets.

The *Gaia* FUN-SSO working group established a campaign to observe Solar System objects in 2011, with the aim of testing the capabilities of the telescopes in the network. Simulated *Gaia* alerts were distributed to the network, with ephemerides for real targets, for telescopes to perform follow-up observations. Observations were made of the Potentially Hazardous Asteroid (PHA) 2005 YU_{55} as part of the preliminary *Gaia* FUN-SSO testing in November 2011.

The Zadko Telescope contributed one of the longest observing periods of all the participating telescopes. It was also the only Southern Hemisphere telescope to make a contribution. During the observing period ($11 - 21$ November, 2011) the asteroid faded rapidly from magnitude $r = 13.7$ to $r = 18.1$ in the Sloan Digital Sky Survey (SDSS) r filter. The residual astrometric errors for the Zadko Telescope observations are typically better than 0.20 arcsec in both right ascension and declination, compared to the mean residual error for this *Gaia* FUN-SSO test of 0.30 arcsec.

9.1.8 HEIDI: An Automated Process for the Identification and Extraction of Photometric Light Curves from Astronomical Images

The analysis of images to extract astrometric and photometric data is largely a manual process. Where crude photometric measurements are sufficient, e.g. ± 0.5 magnitude, the task is not particularly onerous. However, in the cases where high-precision measurements (± 0.05 magnitude or better) are the primary objective, so that the key characteristics of the object can be modelled, this analysis is a very time-consuming task and can take several hours or even days. Performing such accurate measurements allows the researcher to obtain an accurate understanding of the variation in the brightness of an object over time. This is a necessary step in producing photometric light curves for asteroid rotation measurements and shape modelling, determining the type of a supernova or measuring the decay rate of a gamma-ray burst optical afterglow.

When a higher time resolution is desirable, as in the case of a short rotation period for an asteroid, this results in a larger data set which in turn increases the analysis time. Specific requirements for selecting calibration sources in the images and any corrections needed to compensate for variations in observing conditions during the time series make the analysis more difficult. The High Efficiency Image Detection & Identification (HEIDI) pipeline software, described in Todd, Wallon Pizarro, et al. (2014) (Chapter 8), provides the ability to rapidly process sets of astronomical images.

HEIDI is implemented in the programming language Python, runs on a Linux platform and has minimal hardware requirements. HEIDI processes a time series and produces astrometric and photometric results in a matter of minutes. Taking the approach that all the sources in an image are potential reference sources, HEIDI automatically selects multiple calibration sources. The variations in the brightness of each source are cross-referenced against the variations of the other sources to eliminate those sources which are varying at odds with the other sources. Thus the selection algorithm detects sources that intrinsically vary on short time scales and excludes these from the set of calibration sources. This results in a set of calibration sources that HEIDI then uses to apply corrections to compensate for variations between images in a time series. The automated analysis of an image set and the production of a calibrated light curve is accomplished very quickly.

The HEIDI project originated with the need to obtain photometric light curves

for asteroids and so Solar System objects are automatically identified during the image processing. This ability to quickly analyse a set of images and produce high quality results is particularly valuable on automated or robotic telescopes such as the Zadko Telescope (Coward et al. 2010) where HEIDI is planned to be installed. An increasing number of programmes also require prompt follow-up and rapid analysis of time series data, e.g. the prompt follow-up of gamma-ray burst alerts for the detection of transient optical emissions or the *Gaia* Follow-Up Network for Solar System Objects (Todd, Coward, Tanga, et al. 2013). With potential application to the prompt analysis and rapid issuing of results for programmes such as these, HEIDI addresses a need in providing rapid analysis of time series image data.

9.1.9 Summary

The work presented in this thesis describes probability distributions for Trojan asteroids in the orbits of Earth and Mars. It examines strategies for ground-based telescopes for optimising observing patterns and cadences to maximise the probability of detecting Earth and Mars Trojans and proposes strategies that can be implemented on widefield survey telescopes. Simulations for the detection of Trojan asteroids in the orbits of Earth and Mars by the *Gaia* satellite have been performed. The probabilities for detection by *Gaia* of the known Trojans have been assessed and constraints have been placed on the numbers and sizes of additional Trojans that *Gaia* may discover. The need for follow-up observations of *Gaia* detections and the role of the Zadko Telescope in Western Australia as part of the *Gaia* Follow-Up Network for Solar System Objects have been described. Software has been developed for the rapid analysis of time series data. While this software was initially conceived for producing photometric light curves for asteroid rotation studies, it can also be applied to the prompt analysis and issuing of results for a variety of programmes.

Overall, this work on the detection of Trojan asteroids in the orbits of Earth and Mars not only presents the results of modelling and simulations but offers potential benefits to a variety of optical transient studies such as the optical follow-up of gamma-ray burst alerts or asteroid rotation studies.

9.2 Further Work

9.2.1 Earth coorbital asteroids

This work has focused specifically on Trojan asteroids and has neglected other coorbital asteroids. Earth has other coorbitals apart from the Trojan 2010 TK_7; the asteroids 3753 Cruithne (P. A. Wiegert, Innanen, and Mikkola 1997), 54509 YORP, 2002 AA_{29}, 2001 GO_2 and 2010 SO_{16} (Christou and Asher 2011) are all coorbital but are not in Trojan orbits. Although only 3753 Cruithne is larger than 2010 TK_7 it is possible that *Gaia* may detect other coorbitals which are not in Trojan orbits.

These asteroids can be modelled in the same way as were the known Trojans (Todd et al. 2014). The orbital elements for these can be cloned to construct a population for simulating their detection by *Gaia*. The results of the simulation would provide an indication whether *Gaia* will detect the known coorbitals and determine the detection characteristics and limits for the detection of additional coorbitals. The results from the *Gaia* mission will then help constrain the size of the coorbital population.

9.2.2 Inner Earth Objects

Inner Earth Objects (IEOs) are those bodies with orbits interior to Earth's orbit, i.e. with aphelion distances less than 0.983 au (Earth's perihelion distance). As *Gaia* will observe at solar elongations down to 45 degrees it has been recognised that *Gaia* may detect numbers of these IEOs (Bancelin, Hestroffer, and Thuillot 2012). This prospect bears further investigation.

To date 13 asteroids with aphelion distances that place them in this class have been discovered. Three of these (163693 Atira, 2008 EA_{32} and 2005 TG_{45}) have diameters larger than 1 km, whereas the rest are smaller. While this population of known IEOs is small, the predicted number of IEOs is much larger. Modelling by Zavodny et al. (2008) resulted in predictions of 36 ± 26 IEOs with diameters larger than 1 km and 530 ± 240 IEOs with diameters larger than 250 m.

Any detections of an IEO by *Gaia* would be made when the IEO is near its maximum solar elongation. The rest of the IEO's orbit will be at solar elongations smaller than the 45 degree *Gaia* limit. Given that the known IEOs have some orbit eccentricity (between 0.155 and 0.783), IEOs in general may have only a small orbit arc that is visible to *Gaia*. Constructing a population of IEOs and simulating their detection by *Gaia* would determine the detection characteristics.

This would indicate the size limits for detection by *Gaia*. The results from the *Gaia* mission will then help constrain the size of the IEO population.

9.2.3 HEIDI pipeline software

The HEIDI pipeline software developed as part of this work performs astrometry and relative photometry. The first application of HEIDI was to process image data for identifying short period asteroid rotations. The requirement was to deliver position information and a light curve for time series image data. Since the albedo is usually unknown, the size cannot be directly determined from the brightness. Thus calibrated magnitudes are not essential for asteroid photometry. However, for other applications such as supernova light curves, gamma-ray burst optical afterglows or following up on *Gaia* detections, calibrated magnitudes are indispensable.

The next version of HEIDI will include the capability for providing photometric results calibrated to a standard photometric system. The provision of calibrated photometric results will also include uncertainties. The uncertainties can be inferred from the dispersion of the magnitudes of the calibration sources. These can also be incorporated into the output to provide error bars.

HEIDI automatically selects calibration sources for the time series being analysed. Candidate sources that are rejected by the filtering process are not examined further. This aspect warrants further study as these rejected sources may include interesting objects that have some intrinsic variability. The rejected sources can be recorded and reprocessed to determine whether some regular or systematic variability is evident.

HEIDI automatically identifies the target in each image. If the target is within 2 to 3 arcsec of a star of similar or greater brightness it is possible that the star can be preferentially selected. When the target is non-moving the position tolerance can be easily refined to limit or eliminate such mis-selections. Where the target is moving, as in the case of Solar System objects, the position tolerance can also be refined. However this requires a more selective approach such as fitting a line to the detections before refining the position tolerance. In addition, an algorithm to detect moving objects will be implemented to capture targets where the position information is less accurate. Such an algorithm will also be valuable in finding previously unknown objects, e.g. following up on *Gaia* detections.

HEIDI is planned to be installed at the Zadko Telescope, in Western Australia. The Zadko Telescope participates in various optical transient studies, including

responding to trigger events such as *Gaia* FUN-SSO alerts, or the detection of gamma-ray bursts, gravity waves and neutrino emissions. This will facilitate prompt analysis and rapid dissemination of results. Installing HEIDI at the Zadko Telescope will also allow the images in the data archive to be searched for variable sources and transient events.

Appendix A

Statements of contributions of others

A.1 Statements of contributions of others for "Search strategies for Trojan asteroids in the inner Solar System"

Todd, M., D. M. Coward, M. G. Zadnik. 2012. "Search strategies for Trojan asteroids in the inner Solar System." *Planetary and Space Science* 73 (1): 39-43. doi:10.1016/j.pss.2011.11.002.

27 November 2013

To whom it may concern

I, Prof. David M. Coward, contributed by manuscript editing and project supervision to the paper/publication entitled

Todd, M., D. M. Coward, M. G. Zadnik. 2012. “Search strategies for Trojan asteroids in the inner Solar System.” *Planetary and Space Science* 73 (1): 39-43. doi:10.1016/j.pss.2011.11.002.

undertaken with Michael A. Todd.

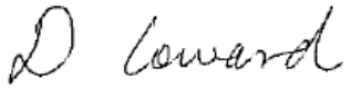

David M. Coward

Michael A. Todd

27 November 2013

To whom it may concern

I, Assoc. Prof. Marjan G. Zadnik, contributed by manuscript editing and project supervision to the paper/publication entitled

Todd, M., D. M. Coward, M. G. Zadnik. 2012. “Search strategies for Trojan asteroids in the inner Solar System.” *Planetary and Space Science* 73 (1): 39-43. doi:10.1016/j.pss.2011.11.002.

undertaken with Michael A. Todd.

Marjan G. Zadnik

Michael A. Todd

A.2 Statements of contributions of others for "An optimal Earth Trojan asteroid search strategy"

Todd, M., P. Tanga, D. M. Coward, M. G. Zadnik. 2012. "An optimal Earth Trojan asteroid search strategy." *Monthly Notices of the Royal Astronomical Society Letters* 420 (1): L28-L32. doi:10.1111/j.1745-3933.2011.01186.x.

27 November 2013

To whom it may concern

I, Paolo Tanga, contributed technical knowledge on the European Space Agency's Gaia mission to the publication entitled

Todd, M., P. Tanga, D. M. Coward, M. G. Zadnik. 2012. "An optimal Earth Trojan asteroid search strategy." *Monthly Notices of the Royal Astronomical Society Letters* 420 (1): L28-L32. doi:10.1111/j.1745-3933.2011.01186.x.

undertaken with Michael A. Todd.

Paolo Tanga

Michael A. Todd

27 November 2013

To whom it may concern

I, Prof. David M. Coward, contributed by manuscript editing and project supervision to the publication entitled

Todd, M., P. Tanga, D. M. Coward, M. G. Zadnik. 2012. “An optimal Earth Trojan asteroid search strategy.” *Monthly Notices of the Royal Astronomical Society Letters* 420 (1): L28-L32. doi:10.1111/j.1745-3933.2011.01186.x.

undertaken with Michael A. Todd.

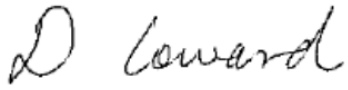

David M. Coward

Michael A. Todd

27 November 2013

To whom it may concern

I, Assoc. Prof. Marjan G. Zadnik, contributed by manuscript editing and project supervision to the publication entitled

Todd, M., P. Tanga, D. M. Coward, M. G. Zadnik. 2012. “An optimal Earth Trojan asteroid search strategy.” *Monthly Notices of the Royal Astronomical Society Letters* 420 (1): L28-L32. doi:10.1111/j.1745-3933.2011.01186.x.

undertaken with Michael A. Todd.

Marjan G. Zadnik

Michael A. Todd

A.3 Statements of contributions of others for "An optimal Mars Trojan asteroid search strategy"

Todd, M., P. Tanga, D. M. Coward, M. G. Zadnik. 2012. "An optimal Mars Trojan asteroid search strategy." *Monthly Notices of the Royal Astronomical Society* 424 (1): 372-376. doi:10.1111/j.1365-2966.2012.21204.x.

27 November 2013

To whom it may concern

I, Paolo Tanga, contributed technical knowledge on the European Space Agency's Gaia mission and simulation results to the publication entitled

Todd, M., P. Tanga, D. M. Coward, M. G. Zadnik. 2012. "An optimal Mars Trojan asteroid search strategy." *Monthly Notices of the Royal Astronomical Society* 424 (1): 372-376. doi:10.1111/j.1365-2966.2012.21204.x.

undertaken with Michael A. Todd.

Paolo Tanga

Michael A. Todd

27 November 2013

To whom it may concern

I, Prof. David M. Coward, contributed by manuscript editing and project supervision to the publication entitled

Todd, M., P. Tanga, D. M. Coward, M. G. Zadnik. 2012. “An optimal Mars Trojan asteroid search strategy.” *Monthly Notices of the Royal Astronomical Society* 424 (1): 372-376. doi:10.1111/j.1365-2966.2012.21204.x.

undertaken with Michael A. Todd.

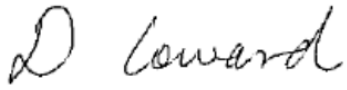

David M. Coward

Michael A. Todd

27 November 2013

To whom it may concern

I, Assoc. Prof. Marjan G. Zadnik, contributed by manuscript editing and project supervision to the paper/publication entitled

Todd, M., P. Tanga, D. M. Coward, M. G. Zadnik. 2012. “An optimal Mars Trojan asteroid search strategy.” *Monthly Notices of the Royal Astronomical Society* 424 (1): 372-376. doi:10.1111/j.1365-2966.2012.21204.x

undertaken with Michael A. Todd.

Marjan G. Zadnik

Michael A. Todd

A.4 Statements of contributions of others for "Detection of inner Solar System Trojan Asteroids by Gaia"

Todd, M., P. Tanga, D. M. Coward, M. G. Zadnik. 2012. "Detection of inner Solar System Trojan Asteroids by Gaia." *Proceedings of Gaia-FUN-SSO-2 International Workshop, Institut de Mécanique Céleste et de Calcul des Éphémérides, Paris Observatory, France, 19-21 September 2012.*

27 November 2013

To whom it may concern

I, Paolo Tanga, contributed technical knowledge on the European Space Agency's Gaia mission and simulation results to the publication entitled

Todd, M., P. Tanga, D. M. Coward, M. G. Zadnik. 2012. "Detection of inner Solar System Trojan Asteroids by Gaia." *Proceedings of Gaia-FUN-SSO-2 International Workshop, Institut de Mécanique Céleste et de Calcul des Éphémérides, Paris Observatory, France, 19-21 September 2012*.

undertaken with Michael A. Todd.

Paolo Tanga

Michael A. Todd

27 November 2013

To whom it may concern

I, Prof. David M. Coward, contributed by manuscript editing and project supervision to the publication entitled

Todd, M., P. Tanga, D. M. Coward, M. G. Zadnik. 2012. “Detection of inner Solar System Trojan Asteroids by Gaia.” *Proceedings of Gaia-FUN-SSO-2 International Workshop, Institut de Mécanique Céleste et de Calcul des Éphémérides, Paris Observatory, France, 19-21 September 2012*.

undertaken with Michael A. Todd.

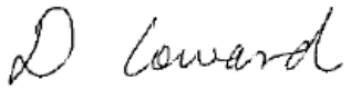

David M. Coward

Michael A. Todd

27 November 2013

To whom it may concern

I, Assoc. Prof. Marjan G. Zadnik, contributed by manuscript editing and project supervision to the publication entitled

Todd, M., P. Tanga, D. M. Coward, M. G. Zadnik. 2012. “Detection of inner Solar System Trojan Asteroids by Gaia.” *Proceedings of Gaia-FUN-SSO-2 International Workshop, Institut de Mécanique Céleste et de Calcul des Éphémérides, Paris Observatory, France, 19-21 September 2012*.

undertaken with Michael A. Todd.

Marjan G. Zadnik

Michael A. Todd

A.5 Statements of contributions of others for "Predictions for the detection of Earth and Mars Trojan asteroids by the Gaia satellite"

Todd, M., P. Tanga, D. M. Coward, M. G. Zadnik. 2014. "Predictions for the detection of Earth and Mars Trojan asteroids by the Gaia satellite." *Monthly Notices of the Royal Astronomical Society* 437 (4): 4019-4026. doi:10.1093/mnras/stt2223.

27 November 2013

To whom it may concern

I, Paolo Tanga, contributed technical knowledge on the European Space Agency's Gaia mission and simulation results to the publication entitled

Todd, M., P. Tanga, D. M. Coward, M. G. Zadnik. 2014. "Predictions for the detection of Earth and Mars Trojan asteroids by the Gaia satellite." *Monthly Notices of the Royal Astronomical Society* 437 (4): 4019-4026. doi:10.1093/mnras/stt2223.

undertaken with Michael A. Todd.

Paolo Tanga

Michael A. Todd

27 November 2013

To whom it may concern

I, Prof. David M. Coward, contributed by manuscript editing and project supervision to the publication entitled

Todd, M., P. Tanga, D. M. Coward, M. G. Zadnik. 2014. “Predictions for the detection of Earth and Mars Trojan asteroids by the Gaia satellite.” *Monthly Notices of the Royal Astronomical Society* 437 (4): 4019-4026. doi:10.1093/mnras/stt2223.

undertaken with Michael A. Todd.

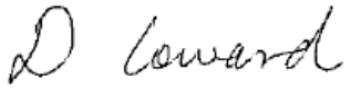

David M. Coward

Michael A. Todd

27 November 2013

To whom it may concern

I, Assoc. Prof. Marjan G. Zadnik, contributed by manuscript editing and project supervision to the publication entitled

Todd, M., P. Tanga, D. M. Coward, M. G. Zadnik. 2014. “Predictions for the detection of Earth and Mars Trojan asteroids by the Gaia satellite.” *Monthly Notices of the Royal Astronomical Society* 437 (4): 4019-4026. doi:10.1093/mnras/stt2223.

undertaken with Michael A. Todd.

Marjan G. Zadnik

Michael A. Todd

A.6 Statements of contributions of others for "Australian participation in the Gaia Follow-Up Network for Solar System Objects"

Todd, M., D. M. Coward, P. Tanga, W. Thuillot. 2013. "Australian participation in the Gaia Follow-Up Network for Solar System Objects." *Publications of the Astronomical Society of Australia* 30: 14-18. doi:10.1017/pasa.2012.014.

27 November 2013

To whom it may concern

I, Prof. David M. Coward, contributed by manuscript editing and project supervision to the publication entitled

Todd, M., D. M. Coward, P. Tanga, W. Thuillot. 2013. “Australian participation in the Gaia Follow-Up Network for Solar System Objects.” *Publications of the Astronomical Society of Australia* 30: 14-18. doi:10.1017/pasa.2012.014.

undertaken with Michael A. Todd.

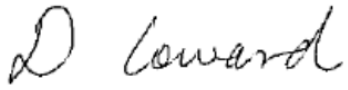

David M. Coward

Michael A. Todd

27 November 2013

To whom it may concern

I, Paolo Tanga, contributed technical knowledge on the European Space Agency's Gaia mission and the Gaia Follow-Up Network for Solar System Objects to the publication entitled

Todd, M., D. M. Coward, P. Tanga, W. Thuillot. 2013. "Australian participation in the Gaia Follow-Up Network for Solar System Objects." *Publications of the Astronomical Society of Australia* 30: 14-18. doi:10.1017/pasa.2012.014.

undertaken with Michael A. Todd.

Paolo Tanga

Michael A. Todd

27 November 2013

To whom it may concern

I, William Thuillot, contributed specific technical knowledge about the Gaia Follow-Up Network for Solar System Objects to the publication entitled

Todd, M., D. M. Coward, P. Tanga, W. Thuillot. 2013. “Australian participation in the Gaia Follow-Up Network for Solar System Objects.” *Publications of the Astronomical Society of Australia* 30: 14-18. doi:10.1017/pasa.2012.014.

undertaken with Michael A. Todd.

William Thuillot

Michael A. Todd

A.7 Statements of contributions of others for "HEIDI: An Automated Process for the Identification and Extraction of Photometric Light Curves from Astronomical Images"

Todd, M., H. U. Wallon Pizarro, P. Tanga, D. M. Coward, and M. G. Zadnik. 2014. HEIDI: An Automated Process for the Identification and Extraction of Photometric Light Curves from Astronomical Images. *Monthly Notices of the Royal Astronomical Society* (submitted). `arXiv:1401.2593` [astro-ph.IM]

27 December 2013

To whom it may concern

I, Heidi Ursula Wallon Pizarro, contributed technical advice for the transcription of software algorithms into mathematical notation in the publication entitled

Todd, M., H. U. Wallon Pizarro, P. Tanga, D. M. Coward, M. G. Zadnik. 2014. “HEIDI: An Automated Process for the Identification and Extraction of Photometric Light Curves from Astronomical Images.” *Monthly Notices of the Royal Astronomical Society* (submitted).

undertaken with Michael A. Todd.

Heidi Ursula Wallon Pizarro

Michael A. Todd

27 December 2013

To whom it may concern

I, Paolo Tanga, contributed technical knowledge on the analysis of astronomical images to the publication entitled

Todd, M., H. U. Wallon Pizarro, P. Tanga, D. M. Coward, M. G. Zadnik. 2014. “HEIDI: An Automated Process for the Identification and Extraction of Photometric Light Curves from Astronomical Images.” *Monthly Notices of the Royal Astronomical Society* (submitted).

undertaken with Michael A. Todd.

Paolo Tanga

Michael A. Todd

27 December 2013

To whom it may concern

I, Prof. David M. Coward, contributed by manuscript editing and project supervision to the publication entitled

Todd, M., H. U. Wallon Pizarro, P. Tanga, D. M. Coward, M. G. Zadnik. 2014. “HEIDI: An Automated Process for the Identification and Extraction of Photometric Light Curves from Astronomical Images.” *Monthly Notices of the Royal Astronomical Society* (submitted).

undertaken with Michael A. Todd.

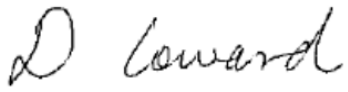

David M. Coward

Michael A. Todd

27 December 2013

To whom it may concern

I, Assoc. Prof. Marjan G. Zadnik, contributed by manuscript editing and project supervision to the publication entitled

Todd, M., H. U. Wallon Pizarro, P. Tanga, D. M. Coward, M. G. Zadnik. 2014. “HEIDI: An Automated Process for the Identification and Extraction of Photometric Light Curves from Astronomical Images.” *Monthly Notices of the Royal Astronomical Society* (submitted).

undertaken with Michael A. Todd.

Marjan G. Zadnik

Michael A. Todd

Appendix B

Copyright forms

B.1 Elsevier journal articles

Copyrights relating to Elsevier journal articles are held by authors. The relevant statement is underlined. The following paper that has been used in this thesis is published in Elsevier journals:

Todd, M., D. M. Coward, M. G. Zadnik. 2012. "Search strategies for Trojan asteroids in the inner Solar System." *Planetary and Space Science* 73 (1): 39-43. doi:10.1016/j.pss.2011.11.002.

How authors can use their own journal articles

Authors can use their articles for a wide range of scholarly, non-commercial purposes as outlined below. These rights apply for all Elsevier authors who publish their article as either a subscription article or an open access article.

We require that all Elsevier authors always include a full acknowledgement and, if appropriate, a link to the final published version hosted on Science Direct.

For open access articles these rights are separate from how readers can reuse your article as defined by the author's choice of Creative Commons user license options.

Authors can use either their accepted author manuscript or final published article for:	
✓	Use at a conference, meeting or for teaching purposes
✓	Internal training by their company
✓	Sharing individual articles with colleagues for their research use* (also known as 'scholarly sharing')
✓	Use in a subsequent compilation of the author's works
✓	Inclusion in a thesis or dissertation
✓	Reuse of portions or extracts from the article in other works
✓	Preparation of derivative works (other than for commercial purposes)

*Please note this excludes any systematic or organized distribution of published articles.

Source: http://www.elsevier.com/journal-authors/author-rights-and-responsibilities

B.2 Oxford University Press journal articles

Copyrights relating to Oxford University Press journal articles are held by authors. The relevant statement is underlined. The following papers that have been used in this thesis are published in Oxford University Press journals:

Todd, M., P. Tanga, D. M. Coward, M. G. Zadnik. 2012. "An optimal Earth Trojan asteroid search strategy." *Monthly Notices of the Royal Astronomical Society Letters* 420 (1): L28-L32. doi:10.1111/j.1745-3933.2011.01186.x.

Todd, M., P. Tanga, D. M. Coward, M. G. Zadnik. 2012. "An optimal Mars Trojan asteroid search strategy." *Monthly Notices of the Royal Astronomical Society* 424 (1): 372-376. doi:10.1111/j.1365-2966.2012.21204.x.

Todd, M., P. Tanga, D. M. Coward, M. G. Zadnik. 2014. "Predictions for the detection of Earth and Mars Trojan asteroids by the Gaia satellite." *Monthly Notices of the Royal Astronomical Society* 437 (4): 4019-4026. doi:10.1093/mnras/stt2223.

Todd, M., H. U. Wallon Pizarro, P. Tanga, D. M. Coward, M. G. Zadnik. 2014. "HEIDI: An Automated Process for the Identification and Extraction of Photometric Light Curves from Astronomical Images." *Monthly Notices of the Royal Astronomical Society* (submitted). arXiv:1401.2593 [astro-ph.IM]

B.3 Cambridge University Press journal articles

Copyright information relating to Cambridge University Press journal articles. The following paper that has been used in this thesis is published in Cambridge University Press journals:

Todd, M., D. M. Coward, P. Tanga, W. Thuillot. 2013. "Australian participation in the Gaia Follow-Up Network for Solar System Objects." *Publications of the Astronomical Society of Australia* 30: 14-18. doi:10.1017/pasa.2012.014.

CAMBRIDGE
UNIVERSITY PRESS

University Printing House
Shaftesbury Road
Cambridge CB2 8BS, UK

www.cambridge.org

Telephone +44 (0)1223 312393
Fax +44 (0)1223 315052
Email information@cambridge.org

Michael Todd

Letter sent as PDF via email:
michael.todd@postgrad.curtin.edu.au

November 25, 2013

Dear Michael Todd

M. Todd, D. M. Coward, P. Tanga and W. Thuillot, "Australian participation in the Gaia Follow-Up Network for Solar System Objects", Publications of the Astronomical Society of Australia, Volume 30, pp 14-18, (2013).

Thank you for your recent permission request to include the above extract(s) in:
your forthcoming PhD thesis, for non-commercial publication.

Non-exclusive permission is granted free of charge for this specific use on the understanding that you have checked that we do not acknowledge another source for this material.

Please ensure full acknowledgement (author, title, publication date, name of journal and Cambridge University Press).

Yours sincerely

Claire Taylor
Publishing Assistant
email ctaylor@cambridge.org

B.4 Institut de Mécanique Céleste et de Calcul des Éphémérides Press articles

 The following paper that has been used in this thesis is published in Institut de Mécanique Céleste et de Calcul des Éphémérides publications:

Todd, M., P. Tanga, D. M. Coward, M. G. Zadnik. 2012. "Detection of inner Solar System Trojan Asteroids by Gaia." *Proceedings of Gaia-FUN-SSO-2 International Workshop, Institut de Mécanique Céleste et de Calcul des Éphémérides, Paris Observatory, France, 19-21 September 2012.*

Bibliography

Ageron, M., I. Al Samarai, C. Akerlof, S. Basa, V. Bertin, M. Boer, J. Brunner, et al. 2012. Search for neutrinos from transient sources with the ANTARES telescope and optical follow-up observations. *Nuclear Instruments and Methods in Physics Research A* 692:184–187. doi:10.1016/j.nima.2011.12.040.

Alan Chamberlain, NASA/JPL-Caltech. 2007. *Asteroid Main-Belt Distribution.* http://ssd.jpl.nasa.gov/?histo_a_ast.

Bancelin, D., D. Hestroffer, and W. Thuillot. 2012. Dynamics of asteroids and near-Earth objects from Gaia astrometry. Planet. Space Sci. 73:21–29. doi:10.1016/j.pss.2012.01.013.

Bessell, M. S., F. Castelli, and B. Plez. 1998. Model atmospheres broad-band colors, bolometric corrections and temperature calibrations for O - M stars. A&A 333:231–250.

Binzel, R. P., A. S. Rivkin, J. S. Stuart, A. W. Harris, S. J. Bus, and T. H. Burbine. 2004. Observed spectral properties of near-Earth objects: results for population distribution, source regions, and space weathering processes. Icarus 170:259–294. doi:10.1016/j.icarus.2004.04.004.

Bonnarel, F., P. Fernique, O. Bienaymé, D. Egret, F. Genova, M. Louys, F. Ochsenbein, M. Wenger, and J. G. Bartlett. 2000. The ALADIN interactive sky atlas. A reference tool for identification of astronomical sources. A&AS 143:33–40. doi:10.1051/aas:2000331.

Bottke, W. F., A. Morbidelli, R. Jedicke, J.-M. Petit, H. F. Levison, P. Michel, and T. S. Metcalfe. 2002. Debiased Orbital and Absolute Magnitude Distribution of the Near-Earth Objects. Icarus 156:399–433. doi:10.1006/icar.2001.6788.

Bowell, E., H. E. Holt, D. H. Levy, K. A. Innanen, S. Mikkola, and E. M. Shoemaker. 1990. 1990 MB: the first Mars Trojan. In *Bulletin of the American Astronomical Society,* 22:1357. Bulletin of the American Astronomical Society.

Boyajian, T. S., H. A. McAlister, G. van Belle, D. R. Gies, T. A. ten Brummelaar, K. von Braun, C. Farrington, et al. 2012. Stellar Diameters and Temperatures. I. Main-sequence A, F, and G Stars. ApJ 746, 101:101. doi:10.1088/0004-637X/746/1/101. arXiv: 1112.3316 [astro-ph.SR].

Branchesi, M., on behalf of the LIGO Scientific Collaboration, the Virgo Collaboration, A. Klotz, and M. Laas-Bourez. 2011. Searching for electromagnetic counterparts of gravitational wave transients. In *Proceedings of the 46th rencontres de moriond and gphys colloquium,* edited by E. Augé, J. Dumarchez, and J. Trân Thanh Vân, 43–46.

Bus, S. J., and R. P. Binzel. 2002. Phase II of the Small Main-Belt Asteroid Spectroscopic Survey. A Feature-Based Taxonomy. Icarus 158:146–177. doi:10.1006/icar.2002.6856.

Christou, A. A., and D. J. Asher. 2011. A long-lived horseshoe companion to the Earth. MNRAS 414:2965–2969. doi:10.1111/j.1365-2966.2011.18595.x. arXiv: 1104.0036 [astro-ph.EP].

Connors, M., C. Veillet, P. Wiegert, K. A. Innanen, and S. Mikkola. 2000. Initial Results of a Survey of Earth's L4 Point for Possible Earth Trojan Asteroids. In *Aas/division for planetary sciences meeting abstracts #32,* 32:1019. Bulletin of the American Astronomical Society. October.

Connors, M., P. Wiegert, and C. Veillet. 2011. Earth's Trojan asteroid. Nature 475:481–483. doi:10.1038/nature10233.

Coward, D. M., M. Todd, T. P. Vaalsta, M. Laas-Bourez, A. Klotz, A. Imerito, L. Yan, et al. 2010. The Zadko Telescope: A Southern Hemisphere Telescope for Optical Transient Searches, Multi-Messenger Astronomy and Education. PASA 27:331–339. doi:10.1071/AS09078. arXiv: 1006.3933 [astro-ph.IM].

de la Fuente Marcos, C., and R. de la Fuente Marcos. 2013. Three new stable L_5 Mars Trojans. MNRAS 432:L31. doi:10.1093/mnrasl/slt028. arXiv: 1303.0124 [astro-ph.EP].

DeMeo, F. E., R. P. Binzel, S. M. Slivan, and S. J. Bus. 2009. An extension of the Bus asteroid taxonomy into the near-infrared. Icarus 202:160–180. doi:10.1016/j.icarus.2009.02.005.

Dunbar, R. S., and E. F. Helin. 1983. Estimation of an Upper Limit on the Earth Trojan Asteroid Population from Schmidt Survey Plates. In *Bulletin of the american astronomical society,* 15:830–830. Bulletin of the American Astronomical Society. June.

Evans, N. W., and S. A. Tabachnik. 2000. Asteroids in the inner Solar system - II. Observable properties. MNRAS 319:80–94. doi:10.1046/j.1365-8711.2000.03761.x. eprint: astro-ph/0005405.

Gray, D. F. 1995. Comparing the Sun with other stars along the temperature coordinate. PASP 107:120–123. doi:10.1086/133525.

Johnson, H. L., and W. W. Morgan. 1953. Fundamental stellar photometry for standards of spectral type on the revised system of the Yerkes spectral atlas. ApJ 117:313. doi:10.1086/145697.

Klotz, A., R. Delmas, D. Marchais, M. Pujol, and C. Jasinski. 2012. The AudeLA software. In *Astronomical society of india conference series,* 7:15. Astronomical Society of India Conference Series.

Landolt, A. U. 1992. UBVRI photometric standard stars in the magnitude range 11.5-16.0 around the celestial equator. AJ 104:340–371. doi:10.1086/116242.

Lineweaver, C. H., and M. Norman. 2010. The Potato Radius: a Lower Minimum Size for Dwarf Planets. In *Proceedings of the 9th Australian Space Science Conference, Sydney, 2009,* edited by W. Short and I. Cairns, 67–78. Australian Space Science Conference Series.

Lithopsian. 2012. *Comparative supernova type light curves.* http://commons.wikimedia.org/wiki/File:Comparative_supernova_type_light_curves.png.

Lupishko, D. F., and T. A. Lupishko. 2001. On the Origins of Earth-Approaching Asteroids. *Solar System Research* 35:227–233.

Lupishko, D. F., M. D. Martino, and R. P. Binzel. 2007. Near-Earth objects as principal impactors of the Earth: Physical properties and sources of origin. In *Iau symposium,* edited by G. B. Valsecchi, D. Vokrouhlický, and A. Milani, 236:251–260. IAU Symposium. May. doi:10.1017/S1743921307003304.

Mainzer, A., T. Grav, J. Masiero, J. Bauer, R. S. McMillan, J. Giorgini, T. Spahr, et al. 2012. Characterizing Subpopulations within the near-Earth Objects with NEOWISE: Preliminary Results. ApJ 752, 110:110. doi:10.1088/0004-637X/752/2/110. arXiv: 1205.3568 [astro-ph.EP].

Mignard, F. 2011. A few metrological aspects of the Gaia mission. *Advances in Space Research* 47:356–364. doi:10.1016/j.asr.2010.05.020.

Mignard, F., A. Cellino, K. Muinonen, P. Tanga, M. Delbò, A. Dell'Oro, M. Granvik, et al. 2007. The Gaia Mission: Expected Applications to Asteroid Science. *Earth Moon and Planets* 101:97–125. doi:10.1007/s11038-007-9221-z.

Mikkola, S., and K. A. Innanen. 1990. Studies on solar system dynamics. II - The stability of earth's Trojans. AJ 100:290–293. doi:10.1086/115514.

———. 1992. A numerical exploration of the evolution of Trojan-type asteroidal orbits. AJ 104:1641–1649. doi:10.1086/116348.

———. 1994. On the stability of Martian Trojans. AJ 107:1879–1884. doi:10.1086/116998.

———. 1995. On the Stability of High Inclination Trojans. *Earth Moon and Planets* 71:195–198. doi:10.1007/BF00612957.

Minor Planet Center. 2013a. *MPC Archive Statistics.* http://www.minorplanetcenter.org/iau/lists/ArchiveStatistics.html. Accessed December 4, 2013.

———. 2013b. *Trojan Minor Planets.* http://www.minorplanetcenter.net/iau/lists/Trojans.html. Accessed December 4, 2013.

Morais, M. H. M., and A. Morbidelli. 2002. The Population of Near-Earth Asteroids in Coorbital Motion with the Earth. Icarus 160:1–9. doi:10.1006/icar.2002.6937.

Morbidelli, A., R. Jedicke, W. F. Bottke, P. Michel, and E. F. Tedesco. 2002. From Magnitudes to Diameters: The Albedo Distribution of Near Earth Objects and the Earth Collision Hazard. Icarus 158:329–342. doi:10.1006/icar.2002.6887.

Murray, C. D., and S. F. Dermott. 1999. *Solar system dynamics.* Cambridge, Cambridge University Press [2000].

NASA/WMAP Science Team. 2012. *Lagrange Points Gravity Field.* http://map.gsfc.nasa.gov/media/990529/index.html.

Nicholson, S. B. 1961. The Trojan Asteroids. *Leaflet of the Astronomical Society of the Pacific* 8:239.

Pilat-Lohinger, E., R. Dvorak, and C. Burger. 1999. Trojans in Stable Chaotic Motion. *Celestial Mechanics and Dynamical Astronomy* 73:117–126. doi:10.1023/A:1008338811969.

Pravec, P., A. W. Harris, P. Kušnirák, A. Galád, and K. Hornoch. 2012. Absolute magnitudes of asteroids and a revision of asteroid albedo estimates from WISE thermal observations. Icarus 221:365–387. doi:10.1016/j.icarus.2012.07.026.

Roy, A. E., and D. Clarke. 2003. *Astronomy: Principles and Practice.* Bristol, Institute of Physics Publishing [2003].

Scholl, H., F. Marzari, and P. Tricarico. 2005. Dynamics of Mars Trojans. Icarus 175:397–408. doi:10.1016/j.icarus.2005.01.018.

Stokes, G. H., J. B. Evans, and S. M. Larson. 2002. Near-Earth Asteroid Search Programs. *Asteroids III:*45–54.

Stuart, J. S., and R. P. Binzel. 2004. Bias-corrected population, size distribution, and impact hazard for the near-Earth objects. Icarus 170:295–311. doi:10.1016/j.icarus.2004.03.018.

Tabachnik, S. A., and N. W. Evans. 1999. Cartography for Martian Trojans. ApJ 517:L63–L66. doi:10.1086/312019. eprint: astro-ph/9904085.

———. 2000. Asteroids in the inner Solar system - I. Existence. MNRAS 319:63–79. doi:10.1046/j.1365-8711.2000.03760.x. eprint: astro-ph/0005400.

Tholen, D. J. 1984. Asteroid taxonomy from cluster analysis of Photometry. PhD diss., Arizona Univ., Tucson.

Thuillot, W., D. Hestroffer, and P. Tanga. 2011. Complementary ground-based observations for Solar System applications. In *Eas publications series,* 45:237–242. EAS Publications Series. February. doi:10.1051/eas/1045040.

Todd, M., D. M. Coward, P. Tanga, and W. Thuillot. 2013. Australian Participation in the Gaia Follow-up Network for Solar System Objects. PASA 30, e014:14. doi:10.1017/pasa.2012.014. arXiv: 1208.5929 [astro-ph.IM].

Todd, M., D. M. Coward, and M. G. Zadnik. 2012. Search strategies for Trojan asteroids in the inner Solar System. Planet. Space Sci. 73:39–43. doi:10.1016/j.pss.2011.11.002. arXiv: 1111.2427 [astro-ph.EP].

Todd, M., P. Tanga, D. M. Coward, and M. G. Zadnik. 2012a. An optimal Earth Trojan asteroid search strategy. MNRAS 420:L28–L32. doi:10.1111/j.1745-3933.2011.01186.x. arXiv: 1111.1127 [astro-ph.EP].

———. 2012b. An optimal Mars Trojan asteroid search strategy. MNRAS 424:372–376. doi:10.1111/j.1365-2966.2012.21204.x. arXiv: 1204.6360 [astro-ph.EP].

———. 2013. Detection of inner Solar System Trojan Asteroids by Gaia. In *Proceedings of GAIA-FUN-SSO 2012: Second "Gaia Follow-up Network for Solar System Objects" Workshop held at IMCCE/Paris Observatory, 2012,* edited by P. Tanga and W. Thuillot, 59–62. April.

———. 2014. Predictions for the detection of Earth and Mars Trojan asteroids by the Gaia satellite. MNRAS 437:4019–4026. doi:10.1093/mnras/stt2223. arXiv: 1311.3372 [astro-ph.EP].

Todd, M., H. U. Wallon Pizarro, P. Tanga, D. M. Coward, and M. G. Zadnik. 2014. HEIDI: An Automated Process for the Identification and Extraction of Photometric Light Curves from Astronomical Images. MNRAS (submitted). arXiv: 1401.2593 [astro-ph.IM].

Warner, B. D., A. W. Harris, and P. Pravec. 2009. The asteroid lightcurve database. Icarus 202:134–146. doi:10.1016/j.icarus.2009.02.003.

Weissman, P. R., and G. W. Wetherill. 1974. Periodic Trojan-type orbits in the Earth-Sun system. AJ 79:404. doi:10.1086/111559.

Whiteley, R. J., and D. J. Tholen. 1998. A CCD Search for Lagrangian Asteroids of the Earth-Sun System. Icarus 136:154–167. doi:10.1006/icar.1998.5995.

Wiegert, P. A., K. A. Innanen, and S. Mikkola. 1997. An asteroidal companion to the Earth. Nature 387:685–686.

Wiegert, P., D. Balam, A. Moss, C. Veillet, M. Connors, and I. Shelton. 2007. Evidence for a Color Dependence in the Size Distribution of Main-Belt Asteroids. AJ 133:1609–1614. doi:10.1086/512128. eprint: astro-ph/0611310.

Zacharias, N., D. G. Monet, S. E. Levine, S. E. Urban, R. Gaume, and G. L. Wycoff. 2004. The Naval Observatory Merged Astrometric Dataset (NOMAD). In *American astronomical society meeting abstracts,* 36:1418. Bulletin of the American Astronomical Society. December.

Zavodny, M., R. Jedicke, E. C. Beshore, F. Bernardi, and S. Larson. 2008. The orbit and size distribution of small Solar System objects orbiting the Sun interior to the Earth's orbit. Icarus 198:284–293. doi:10.1016/j.icarus.2008.05.021.